Master Thesis in Geographical Information Science nr 137

Change of heating fuel consumption patterns produced by the economic crisis in Greece

Panagiotis Patrinos

2021

Department of

Physical Geography and Ecosystem Science

Centre for Geographical Information Systems

Lund University

Panagiotis Patrinos (2021). Change of heating fuel consumption patterns created by the economic crisis in Greece

Master’s degree thesis, 30/ credits in Master in Geographical Information Science
Department of Physical Geography and Ecosystem Science, Lund University

Abstract

The economic crisis in Greece resulted in a change in residential heating fuels utilized, which in turn resulted in a change of air quality over Greater Athens Area. The aim of this study was to investigate the effects of economic crisis in air quality over Attica by examining the change in air pollutants' concentrations before, during, and after the onset of the economic crisis in Greece and to associate this change with the change in fuels used for residential heating.

For this purpose, I analyzed six MODIS L1B datasets with 500m spatial resolution, one for each year studied, MODIS AOT and NDVI products, at 10 km and 500 m spatial resolution respectively. Additionally, I used AQMS measurements and CORINE 2000 Land Cover dataset.

To densify the ground monitoring network, virtual stations were identified according to Narashid et al (2006) criteria. Through OLS regressions, air pollutants' concentration were estimated for the virtual stations and, subsequently, for the whole map of Great Athens Area (GAA) for the chosen time periods.

Subsequently, the association between the change in fuel consumption and the change in pollutant concentrations between the examined periods was performed, based on Kakaras et al (2013) emissions ratios for each fuel utilized in residential heating that indirectly indicate fuel types utilized in the residential heating systems.

Primary results show that during the whole period examined (2007-2012) SO_2 concentrations were increased in most parts of GAA, while NO_2 and PM_{10} were decreased. CO concentrations were stable in most zones of GAA. Where the fuels used for residential heating are concerned, the use of wood and pellet has increased in most urban areas of GAA, while the use of heating oil and natural gas appear to be decreased.

Keywords: Economic Crisis, Air Quality, Satellite Data, Virtual Stations, Regression Analysis, Air pollutants mapping, anthropogenic factors.

Table of Contents

Table of figures

Table of tables

Table of maps

List of abbreviations and acronyms

GAA	Greater Athens Area
MODIS	Moderate Resolution Imaging Spectroradiometer
AOD	Aerosol Optical Depth
AOT	Aerosol optical thickness
CO	Carbon Monoxide
NO2	Nitrogen Dioxide
O3	Ozone
PM	Particulate Matter
SO2	Sulfur dioxide

1. Introduction

1.1. General Introduction

Airborne pollutants are one of the most crucial problems in urban environments and play a significant role in climate change and human life, causing phenomena such as urban heat islands, heat discomfort, agricultural crop loss, problems in respiratory systems (Penttinen, et al., 2001; Saffari A., et al., 2013), cardiovascular diseases (Delfino, Sioutas, & Malik, 2005), neurodevelopmental effects (Morgan, et al., 2011), chronic illnesses and even premature deaths (Al-Saadi, et al., 2005).

The driving factors are human activities and natural pollutant sources (e.g., sea salt, volcanic dust, forest, and grassland fires, etc.). The rapid urbanization growth, which results in industrialization, and the low-quality fuel for household energy consumption, contribute to the degradation of air quality. Moreover, seasonal changes (Chang & Lam, 1997), which include the change in weather conditions such as temperature, wind circulation, humidity, the local topography (through anthropogenic structures and landscaping), and the land use/land cover (LULC) types of the area, (Mozumder, Zhu, & Perinpanayagam, 2012), contribute to the concentration of air pollutants.

During the last decade, the economic crisis has affected the standard of living of the Greek population. The average household income has been reduced year by year. The combination of income reduction, taxation, and the increase in products' prices, forced Greek citizens to adapt their consumption patterns and other aspects of everyday life (Santamouris, et al., 2013).

The global increase of petroleum and natural gas prices has forced the residents to use cheaper heating systems, with their primary choice being firewood, (Saffari A., et al., 2013). This fact leads to air quality change through the increase of air pollutants due to inadequate combustion techniques of firewood (e.g., open chambers, stoves), especially during winter, (Saffari A., et al., 2013), when the heating needs are at their peak. Research conducted between 2000 and 2013, from the Hellenic Statistical Authority (ELSTAT), revealed a significant reduction of heating petroleum consumption.

Multitemporal observation of the air quality conditions over a region is initially implemented through ground-station networks and spatial models, however, the use of such techniques is sometimes ineffective, especially when measurements of in-situ data are few and sparsely distributed, (Basly & Wald, 2000). Measurements of air pollutant concentrations through these

stations cannot cover large areas by utilizing theoretical models (Chitade & Katiyar, 2004), thus change detection is greatly limited to point observations only. The association between air pollutant emissions and the effects of the economic crisis, such as the differentiation in heating system use is unknown. For this reason, the usage of satellite data becomes essential. With the contribution of both ground station and satellite measurements, researchers can monitor and map the air pollution at a global scale and on a daily basis (Wijeratne, 2003).

The aim of this study is to investigate the air pollutant concentrations over the Greater Athens Area (GAA), their intertemporal change in three distinct time periods, and identify change drivers associated with household heating systems. The first period is the years 2007-2008, which is the period before the onset of the economic crisis. The second is the years 2009-2010 that depicts the onset of the economic crisis and, finally, the third period is the years 2011-2012, when the economic crisis has already begun and is intensifying. More specifically, to monitor the change associated with heating systems, winter months need to be examined, as these months represent the time of the year when heating systems are used by most of the population. ELSTAT, in its study on energy consumption in Greek households (2012), defines the months from October to April as winter months.

The remote sensing satellite data that are used for this study were acquired from the MODIS sensor found on Terra and Aqua satellites. The monitoring of air pollution in the study area is implemented by the combination of Aerosol Optical Depth (AOD) values from satellite data, ground measurements, and spatial models, (Engel-Cox, DeFelice, & Falke, 2001), using the methodology developed by Narashid et al. (2006). The association of air pollutant concentrations to the changes triggered by the economic crisis is examined using the “Emission indices by type of fuel and heating technology”. I assumed that (i) the change in the type of fuel used for residential heating systems results in a change in air pollutant emissions and, thus, alters atmospheric pollution concentrations, (ii) the wind does not affect the presentations of the daily conditions captured through the satellite image, as atmospheric movement within a day is relatively negligible (Sifakis, Soulakellis, & Paronis, 1998).

In chapter 1 the general introduction, the motivation, and background information to understand the topic of this thesis and follow the subsequent chapters are presented. This includes (i) the phenomenon of the economic crisis, (ii) the contribution of remote sensing in the mapping of air pollutants concentrations, (iii) details about the air pollutants and their effects to human health and concludes with (iv) a brief introduction to radiative transfer and the retrieval of AOD from space explained. Chapter 2 presents the study area, while Chapter 3 introduces the data and

methodology implemented in this thesis. Chapters 4 and 5 present the results and discussion/conclusion, respectively.

1.1.1. Economic crisis and Energy Consumption

The most crucial socioeconomic problem that Greece faced during the last decade was the financial crisis. The average household income was reduced from 26,221 euros (2009) to 24,900 euros (2010) and later 22,498 euros (2011), (Table 1.1:1, Fig. 1.1:1). "One of the main effects of economic austerity is fuel poverty" (Santamouris, et al., 2013). It affects the economically poor population, and its roots are found in the quality and type of energy consumption that is used and the cost of it. Three main population categories come under the fuel poverty: (i) the population that has difficulty in repaying energy bills, (ii) the generally poor households and (iii) the household that contains vulnerable population groups, such as young children, disabled people, elderly people, etc., (Boardman, 2010).

Table 1.1:1 The household income changes in 9 different income categories, (adapted from Santamouris et al, 2013).

2009 income (1000 of euros)	Income change until 2012 (euros)	% Change relative to average 2009 income in class
0-10	+1682	+26.1
10-20	-1778	-12.7
20-30	-3539	-15.1
30-40	-5056	-15.4
40-50	-5545	-13.2
50-60	-9496	-18.5
60-70	-8615	-14.2
70-80	-21.667	-31.0
80-90	19.400	-23.4

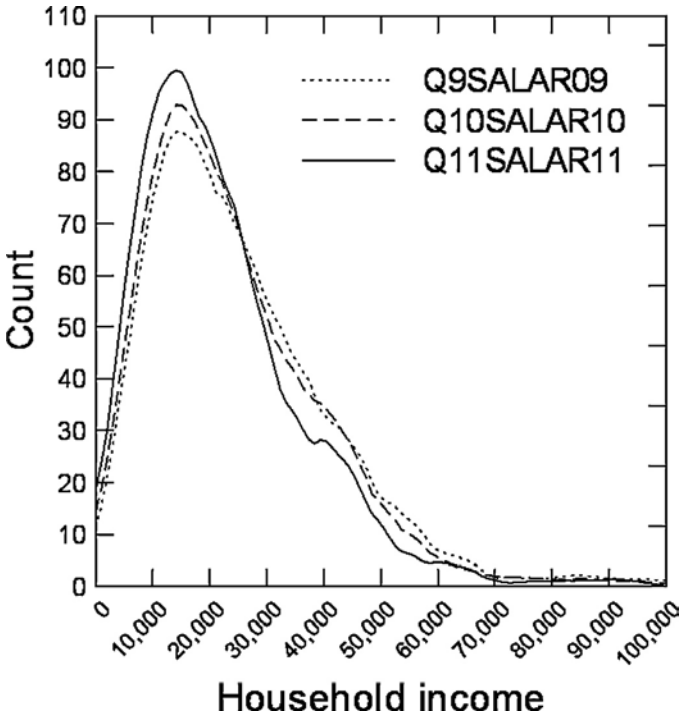

Figure 1.1:1 Changes in the annual household income. Q9SALAR09 is the annual household for 2009, Q10SALAR10 is the household annual income for 2010 and Q11SALAR11 is the annual household income for 2011, (adapted from Santamouris et al, 2013).

Research in annual household energy consumption shows that an average household in Greece consumes 13,994 kWh, of which 81% is used for heating and cooking. Furthermore, the research proved that the three main energy sources that people use are fuel oil (63.7%), electricity (26.8%), and firewood (17.4%), while the primary fuels used for heating are heating petrol (fuel oil) (63.7%), electricity (12.4%) biomass (12.0%) and natural gas (8.7%), (Hellenic Statistical Authority, Energy Consumptiom Survey in Households, 2012).

Santamouris et al (2013) and Boardman (1991, 2001) claimed that an adequate temperature of warmth in a house is usually 21^{o}C for the living area and 18^{o}C for the less occupied rooms. Also, the maintenance of "a good heat quality" depends on the construction quality of the houses. In surveys on energy consumption in Greek households, it was discovered that people with higher incomes live in newer buildings, while the opposite occurs for families with lower incomes. According to the ELSTAT survey (2011), only 50% of the households have thermal insulation and 1 in 10 residents do not know if their building is insulated. Only 28% of the poor portion of the population is living in insulated buildings, while thermal insulation is provided for 70% of people with higher incomes, (Santamouris, et al., 2013). As a result, people with lower incomes need to spend more money on heating.

The instability of the global economy and national taxes have increased the petroleum price and have forced the poor households to alter their house heating energy source to cheaper sources.

Table 1.1:2 The fuel taxes in Greece between 2010 and 2015 (Valavanidis, Vlachogianni, Loridas, & Fiotakis, 2015)

Year	Tax per liter of fuel in euro
2010	1.20 to 1.3
2011	1
2012	1.35
2013	1.3
2014	1
2015	0.8 to 0.85

Table 1.1.2 shows the taxation of fuel in Greece between 2010 and 2015, while table 1.1:3 shows the decrease in fuel consumption from 2010 up to 2014.

Table 1.1:3 The amount of fuel consumption in tons during 2010-2014 in Greece, (Hellenic Petroleum Marketing Companies Association - SEEPE).

	Fuel Consumptions in tons (2010-2014)				
	2010	**2011**	**2012**	**2013**	**2014**
Gasoline unleaded	3,600,750	3,258,255	2,838,592	2,639,477	2,518,478
Gasoline LRP	113,611	66,170	38,968	16,365	4,289
Subtotal	**3,714,361**	**3,324,425**	**2,877,560**	**2,655,842**	**2,522,767**
Heating oil	2,932,033	2,882,583	1,931,716	929,541	971,796
Diesel	2,517,995	2,203,036	2,063,411	2,247,539	2,370,645
Subtotal	**5,450,028**	**5,085,619**	**3,995,127**	**3,177,080**	**3,342,441**
Fuel oil 1500	212,920	176,183	138,922	136,372	146,921
Fuel oil 3500	88,170	79,326	68,257	58,223	64,505
Subtotal	**301,090**	**255,509**	**207,179**	**194,595**	**211,426**
Liquid Gas	294,253	344,682	405,374	425,136	438,890
Kerosene	5,327	6,287	7,353	4,472	3,145
Asphalt	269,012	114,733	99,299	126,194	167,391
Total	**10,034,07**	**9,131,255**	**7,591,892**	**6,583,319**	**6,686,060**

During 2012-2013 the main heating costs increased, while many Greek families have preferred the traditional heating methods, such as fireplaces, wood, and pellet stoves, briquettes, wood chips, and sawdust, (Saffari A., et al., 2013). This solution leads to amplification of the airborne fine particulate matter (smoke haze, PM_{10} and smaller) concentrations, (Florou, M, & Pandis, 2013), which contain several toxic organic compounds, such as methoxyphenyl, (Kjallstrand & Petersson, 2001) and PAHs, (Barregard, et al., 2006), (Tables 1.1:4, 1.1:5).

Table 1.1:4 Comparison between the air pollutant emissions produced by different heating systems.

	Air Pollutants			
Heating Type	CO (ng/J)	NOx (ng/J) [NO_2]	Particulate matter (ng/J)	Unburned hydrocarbons (ng/J)
Natural Gas	8.6	34.4	2.15-6.45	4.3
Petroleum	17.2	68.8	6.02	4.3
Fireplaces	10.750	138.1	357	1.238

Table 1.1:5 CO Emissions by heating source.

Heating source	**CO Emissions [Kg/GJ]**
Petroleum	74
Natural Gas	56
Electricity	243
Wood	110
Biomass	4

Another fact that contributes to air quality degradation is the heat efficiency of each heating type. Petroleum and Natural gas have higher energy efficiency than wood and biomass, which require using higher quantities, (Table 1.1:6), (DEFRA & SMED, 2006).

Table 1.1:6 EER / COP per heating technology, (DEFRA & SMED, 2006).

	Energy Efficiency Ratio (EER) / Coefficient of Performance (COP)
Typical petroleum boiler	0.87
Typical natural gas boiler	0.87
Natural gas Condensation boiler	0.98
Heat pump A	3.00
Heat pump B	2.75
Electrical boiler	1.00
Opened chamber fireplace	0.25
Closed chamber fireplace	0.5
Biomass boiler (Pellet)	0.75

2011 and 2012 were considered cold years in Greece, compared to the normal winter temperature during winter. However, it was found that the energy consumption during these harsh

winters (2011-2012) was 37% less than was foreseen. Low-income households spend almost 67% of their income on electricity, more than higher incomes, whereas the latter have 160% higher energy expenses compared to the first ones. Only 2% of the high-income population was characterized by fuel poverty, while 14% of the low-income population faced this situation, (Santamouris, et al., 2013).

Sardianou (2008) demonstrates that there is a close relationship between the household income, the number of people in the house, the type of the building, the ownership status, and the annual fuel consumption. Table 1.1:7 shows that people living in detached houses consume more energy than people who live in apartments, which indicates higher emissions of air pollutants.

Table 1.1:7 Comparison of the annual environmental effects caused by several types of individual heating, (tons CO/year) *.

	Apartment 100 m^2	**Detached house 100 m^2**
Petroleum	5.43	6.49
Natural Gas	4.14	4.95
Wood	8.2	9.8
Pellets	0.33	0.39
Air condition	17.96	21.46
Electric radiators	17.96	21.46
Heat pumps	2.9	3.5
Heating stoves	7.69	9.29

Average apartment's consumption 100 m^2 200-210 kWh/ m^2/ year and detached house 100m^2 240-250 kWh/ m^2/ year.

Panas (2012) noted that the average energy consumption in Athens' buildings was found to be 29 kWh/m^3, which is higher than what is consumed in other, colder European countries, such as Denmark, Germany, and Netherlands. Two potential reasons are the construction conditions of houses and the fear of seasonal mortality rate. It is argued that the seasonal mortality rate in Greece from 1988 to 1997 was 18%, which was higher compared to other European countries. This correlation becomes stronger in combination with fuel poverty. According to a survey that took place in November 2012, in northern Greece, the largest percentage of interviewees have payment difficulties, their households are energy inefficient, and an intense fear exists about the current economic crisis, (Santamouris, et al., 2013).

One of the main sources of air pollution in Athens is the residential heating systems combustion activities. According to Table 1.1:8, residential combustion has a relatively low impact

to the totals, with the exception of SO_2 (~15%) and PM_{10} (~18%), however during winter months, it makes a significant contribution, (Markakis, Unal, Melas, Yenigun, & Incecik, 2009; Kanakidou, et al., 2011). According to the same table, residential combustion is responsible for 14.9% and 18% of SO_2 and PM_{10} emissions respectively, while being the third major factor for CO emissions.

Table 1.1:8 Anthropogenic emissions in Athens, (adapted from Kanakidou et al, 2011).

	Residential Combustion %	Industry %	Fuel extr. / distribution %	Solvent Use %	Road Transport %	Off-road %	Maritime %	Waste %	Energy %	Totals ktons /year
CO	8.0	3.2	-	-	75.6	13.0	0.2	-	-	473
NO_x	3.1	22.4	-	-	51.0	17.8	3.1	-	2.6	78
SO_2	14.9	29.1	8.4	-	3.2	7.2	11.3	-	25.9	31
NMVOC	3.2	2.1	2.0	13.8	70.6	5.7	0.5	-	2.1	93.2
PM_{10}	18.0	62.7	-	-	13.0	0.8	1.9	3.6	-	21

1.1.2. The contribution of remote sensing in air quality mapping

The ability of mapping air pollutant concentrations, especially in real-time, offers (i) a complete and continuous overview of air quality over the monitored area, (ii) identification of the sources that contribute to the pollution phenomenon and their distribution, (iii) exposes locations that require intervention and measures to decrease pollution levels, (iv) investigates the potential relationships between the land use types in the area and air pollution distribution, and (v) supports the distribution and installation of ground air quality monitoring stations in efficient locations, (Wald & Baleynaud, 1999).

The first efforts of detecting and mapping the air quality in urban areas were realized through networks of ground stations and spatial models in order to investigate the overall conditions. Therefore, the long-term observation of the citizens' exposure to air pollutants, over large geographic regions met some difficulties, such us, the requirement for long-term in situ data, the high cost of equipment, the difficult access in some regions for the installation of the stations, and the need of experienced people with a specific scientific background in order to restore any damages, (Liu, Sarnat, Kilaru, Jacob, & Koutrakis, 2005).

The solution to the aforementioned problems is given by satellite data. Satellite remote sensing applications in combination with in situ data and spatial models can provide (i) possible applications in monitoring air quality in rural and remote locations, such as polar, ocean, and mountainous areas, where no ground stations exist, (Engel-Cox, DeFelice, & Falke, 2001), (ii) knowledge of the repaired measurements or monitoring locations, (iii) estimates of the concentrations even in the troposphere and stratosphere, (iv) assessment of the emission distributions, such as carbon dioxide (CO), nitrogen oxides (NOx), land use types, ozone (O_3), biogenic volatile organic compounds (VOC), (Hidy, et al., 2009) and especially particulate matter (PM), (Engel-Cox, DeFelice, & Falke, 2001), urban haze and analysis of the impact in the urban atmosphere after local fires, dust storms or transport of air pollutants from distant sources and (v) localized pollution forecasting, (Hidy, et al., 2009).

It should be noted that the air quality measurements provided by satellite sensors are in terms of aerosol optical depth (AOD), which is a dimensionless measure of light extinction embodied over the path (the entire vertical depth of the atmosphere or the vertical atmospheric column). The AOD values are ranging from 0 to ~5, with values under 1 categorized as heavy haze. The estimation of air pollutants' concentrations is implemented by the combination of AOD values with ground measurements (e.g., regression analysis), (Engel-Cox, DeFelice, & Falke, 2001).

Many sensors have been launched and many applications have been designed in order to achieve monitoring of air quality using global-scale and regional models (Vijayaraghavan, Snell, & Seigneur, 2008). The need for satellite data is becoming more crucial, as air quality assessment becomes more demanding because of the need to examining more pollutant types and at multiple spatial scales. Mixing satellite products and in situ data can provide maps of model outputs, presenting the quality of the atmospheric column, (Vijayaraghavan, Snell, & Seigneur, 2008).

The main goal of the first applications was to eliminate the atmospheric effect from the satellite data, which was characterized as an error or noise. For that reason, they produced various approaches (e.g. the radiative transfer models), which finally seemed useful for investigating clouds, humidity, ozone, and aerosols, (Kaufman & Sendra, Algorithm for Automatic Atmospheric Corrections to Visible and Near-IR Satellite Imagery, 1998; Kaufman, Fraser, & Ferrare, Satellite Measurements of Large-Scale Air Pollution: Methods, 1990). Their implementation was achieved through existing sensors and by developing others for global monitoring of the climate phenomena. Below, I present a literature review of the combinations of applications and satellite data, for estimating the air quality.

- **Urban air quality**

Researchers used optical sensors (e.g. Landsat and SPOT) to estimate the air quality of an urban area, (Sifakis & Deschamps, 1992; Sifakis, Soulakellis, & Paronis, Quantitative Mapping of Air Pollution Density Using Earth Observations: A New Processing Method and Application to an Urban Area, 1998; Retalis, Cartalis, & Athanassiou, 1999; Sifakis & Soulakellis, Satellite Image Processing for Haze and Aerosol Mapping (SIPHA): Code Description and Presentation of Results, 2000). In particular, they calculated the AOD by the radiometric comparison of a “clear satellite image” with a “polluted image”. This provides the relative air pollution (good correlations with the PM (0.1-3μm) and SO_2), while their combination with ground measurements was used to create particulate matter pollution maps, (Wald & Baleynaud, 1999; Finzi & Lechi, 1991).

- **Regional air quality monitoring**

The assessment of the tropospheric ozone in regional scale is based on the assumption that 90% of the O_3 column is located in the stratosphere and is implemented using the residual analysis, which separates the tropospheric from the stratospheric levels of O_3, (Fishman, Vukovich, Cahoon, & Shipham, 1987; Fishman, Observing Tropospheric Ozone from Space, 2000; Sunwoo, Kotamarthi, & Carmichael, 1992). The primary satellite data that were used for this research originated from TOMS sensor, which measures the total O_3 column; however, this approach was

accurate only under favorable atmospheric conditions. Other studies showed that the O_3 variances from TOMS data were potentially caused by long-scale biomass burning, (Combrink, Diab, Sokolic, & Brunke, 1994). The SCIAMACHY and OMI instruments attempt to solve the errors produced by TOMS data. However, there was one exception in which TOMS data seemed useful; the Asian Brown Cloud case study, because it was a remote location with a lack of in situ data, and thus the satellite remote sensing provided the most reliable information about this phenomenon, (Ramanathan, Crutzen, Kiehl, & Rosenfeld, 2001).

- **Fires, dust storms, and other transboundary events**

Investigating the effects of large fires, dust storms, and volcanic cone emissions with satellite data is less common but easier than the effects of an urban environment in air degradation, however, such kinds of events can contribute to the damage of urban air quality. Various studies have researched the impact of the aforementioned events in people's health by utilizing spatial models that include both satellite data and ground-based measurements, (Cairns, Hao, Alvardo, & Haggerty, 1999; Spichtinger, et al., 2001; Prospero, 1999; Husar, Prospero, & Stowe, 1997). The data used for such kind of studies are MODIS aerosol optical depth, used to evaluate PM levels for transboundary phenomena, (Engel-Cox, DeFelice, & Falke, 2001; Chu, et al., 2003; Wang & Christopher, 2003; Hutchinson, 2003).

1.2. Research objectives

- To determine if air pollutant concentration spatial patterns have changed in the GAA region, during the economic crisis, by utilizing air pollutant concentration maps.
- To determine if the change in air quality over the area of GAA is associated with the change in fuel types utilized for residential heating in the urban zones.

1.3. Theory and Background

1.3.1. Aerosols and Particulate Matter

The suspended gases in the atmosphere are described as aerosols, while the suspended particles are described using the term Particulate Matters and they can be either solid or liquid. These terms, however, are not used for cloud droplets. They are found in both the tropospheric layer (0-12km above the surface of the Earth) as well as in the stratospheric layer (12-40km above the surface of the Earth) of the atmosphere, but their sources and characteristics differ significantly. They have a major impact on our climate and our health (Engel-Cox, Holloman, Coutant, & Hoff, 2004).

According to (Wallace & Hobbs, 2006) particles are considered to be aerosols when they have a diameter from a few nanometers (nm) to hundreds of micrometers (μm). They can be divided into three categories according to their diameter:

- Ultra-Fine Mode: Diameter less than 0.1μm
- Accumulation Mode: Diameter larger than 0.1μm but smaller than 2.5μm
- Coarse Mode: Diameter larger than 2.5μm

Particles with sizes less than 10μm are known as PM_{10}, while particles with sizes less than 2.5μm are referred to as PM2.5 and when sizes are less than 1.0μm they are called PM1.0. At this point, it should be noted that the visible solar radiation is mostly affected by Aerosols with diameters from 0.1μm to 1μm (Saathesh, 2002).

In figure 1.3:1 the size of Particulate Matters is compared with the size of a human hair and a sand grain.

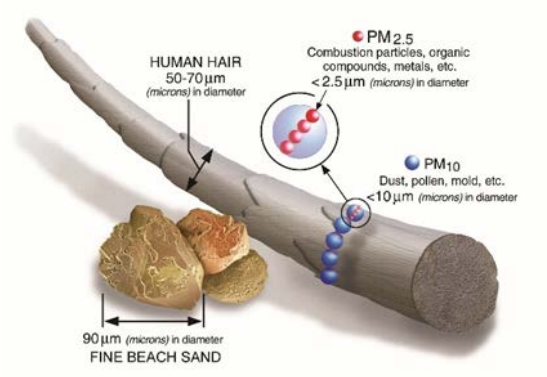

Figure 1.3:1 Size comparisons between PM2.5, PM_{10}, human hair, and a sand grain. (Environmental Protection Agency - EEA).

The Lifetime of the aerosols in the troposphere depends on their size since the bigger their diameter is the more possible it is for the particles to be removed by rainfall (wet removal). Moreover, it is also possible for the particles to fall because of gravity, which is known as Dry Deposition or Sedimentation.

Climatologists also divide aerosols into categories based on their chemical composition. The main categories are sulfates, organic carbon, black carbon, nitrates, mineral dust, and sea salt.

Figure 1.3:2 Sea salt, dust, volcanic ash (Photograph by Katherine Mann, Source: NASA, 2010)

The source of aerosols can be either natural or anthropogenic (EEA, 2016). Approximately 90% of the total aerosol mass in the atmosphere originates from natural sources. More specifically, volcanic eruptions produce sulfates and nitrates, surface wind and sandstorms can transfer dust and wind-driven sea spray causes the transfer of sea salt.

Anthropogenic sources are responsible for 10% of the total aerosol mass in the atmosphere, which originates mainly from the combustion of fossil fuels, metal production, and waste incineration (EEA, 2016). Fossil fuel combustion produces sulfates, biomass burning produces organic and black carbon, while automobiles, incinerators, smelters, and power plants produce mainly sulfates, nitrates, and black carbon. Furthermore, altering land surface by processes such as deforestation, overgrazing, drought, and excessive irrigation can result in the production of dust aerosols. Aerosols can also be produced by cigarettes, cooking stoves, fireplaces, and candles, (NASA, 2010).

Depending on their formation, aerosols are also divided into two categories, primary or secondary. Primary aerosols are those which are directly emitted in the atmosphere as aerosols without additional processes, such as dust and sea salt particles. Secondary aerosols are those which are eventually formed in the atmosphere by oxidation or chemical reactions of precursor gases, such as nitrogen oxides (NO_x) and sulfur dioxide (SO_2), (Hodan & Barnard, 2004; EEA, 2016).

Nitrogen Oxides (NO_2) are produced by the combustion of fossil fuels, power plants, industrial activity, and traffic. Nitrogen Oxides contribute to the formation of Tropospheric Ozone (O_3) and Nitrogen Dioxide (NO_2), which is produced by the oxidation of Nitrogen Monoxide (NO) has serious negative effects on human health. (EEA, 2016)

Sulfur dioxide (SO_2) is emitted during the combustion of sulfur-containing fuels. It can be produced by anthropogenic sources such as industrial activity and household fuel combustion, as well as by natural sources such as volcanic eruptions. It contributes to acid deposition, the effects of which can be severe, including the negative impacts on aquatic ecosystems in rivers and lakes, as well as damage to forests.

Carbon monoxide (CO) and benzene (C_6H_6) are both produced by the incomplete combustion of fossil fuels. Most CO emissions originate from traffic. C_6H_6 emissions are produced by traffic, which is the major source, domestic heating, and oil refining. Emissions from domestic heating are really small except for regions where wood burning accounts for the majority of domestic energy needs.

Particulate Matter (PMs) has many sources and is a complex heterogeneous mixture whose size and chemical composition change spatially and temporally, depending on emission sources and atmospheric and weather conditions. They can be formed as either primary or secondary. Primary Particulate Matters can originate from either natural sources such as volcanic ash, sea salt, and dust, or anthropogenic sources such as domestic heating, waste incineration, fuel combustion for vehicles, and vehicle (tires, brakes) or road wear. Secondary Particulate Matters are produced by the oxidation of SO_2, NO_X, NH_3, and several volatile organic compounds (VOCs), which then form ammonium (NH_{4+}), sulfate (SO_{4-2}), and nitrate (NO_{3-}) compounds. Where human health is concerned, Particulate Matter is one of the most important pollutants that penetrate the respiratory system. Smaller particles, such as $PM_{2.5}$, with a diameter of up to 2.5µm, are considered exceptionally harmful due to their greater ability to penetrate deep into the lungs. (EEA, 2016)

1.3.2. Radiative Transfer Model and Aerosol Optical Thickness

The phrase atmospheric radiative transfer is used to describe the propagation of solar radiation in the atmosphere. Solar radiation propagates through the atmosphere, where it is attenuated by the interaction with suspended particles, gases, and clouds by scattering and absorption.

Scattering refers to the change of the propagation path of the radiation beam in the atmosphere to one or more direction and the angle depends on the wavelength of the incident radiation, the size of the particles, and its refractive index. There are two categories of scattering: Rayleigh scattering where scattering occurs by the interaction with small particles and Mie scattering where scattering occurs by larger particles with a size range close to the wavelength of radiation. Absorption is the process where photons are absorbed by the particles.

The term Aerosol Optical Thickness (AOT), or Aerosol Optical Depth (AOD), is a measure of the atmospheric transparency, refers to the measure of the attenuation of solar radiation due to

scattering and absorption from suspended particles, and it is considered to be one of their most important optical properties, (Saathesh, 2002). In other words, aerosols in the atmosphere can block a part of the sunlight from reaching the ground by absorbing it or scattering it and AOD represents how much sunlight is blocked. It is a dimensionless number that represents the amount of aerosols in the vertical column of the atmosphere over a specific area observed, (National Oceanic and Atmospheric Administration - NOAA).

When a monochromatic light beam, $I_{\lambda 0}$, propagates through the atmosphere, its intensity will be reduced to I_{λ} by the time it reaches the ground. The Beer-Lambert equation gives the intensity of the radiation, from which AOD can be calculated:

$$I_\lambda = I_{\lambda 0} e^{(-m_r \delta_\lambda)}$$

Where:

- m_r: air mass
- δ_λ: Aerosol Optical Depth

For “Deep blue” methodology a value of 0.01 corresponds to an extremely clean atmosphere, and a value of 0.4 would correspond to a very hazy condition. Generally, higher AOD values correspond to higher attenuation of solar radiation and hence it means more aerosols are present in the atmosphere. Table 1.3:1 represents the corresponding atmospheric conditions for specific values of AOD using the “Dark target” methodology (Levy, et al., 2014).

Table 1.3:1 AOD values and atmospheric conditions utilizing the “Dark target” methodology (Levy, et al., 2014).

AOD	Corresponding Condition
0	Clear Sky, Free from Aerosols
0.02	Very clean, usually over isolated areas
0.2	Fairly clean air
0.6	Polluted air
1.5	Heavy smoke/dust event (e.g., volcanic eruption)
>3	The solar disk is obscured

Figure 1.3:4 shows the distribution of aerosols globally, according to their sizes based on MODIS data. The more intense the colors, the thicker the layers of aerosols. Red color indicates the existence of fine (Ultra-fine and Accumulation Mode) particles while yellow indicates the existence of coarse particles. Gray areas correspond to a lack of data.

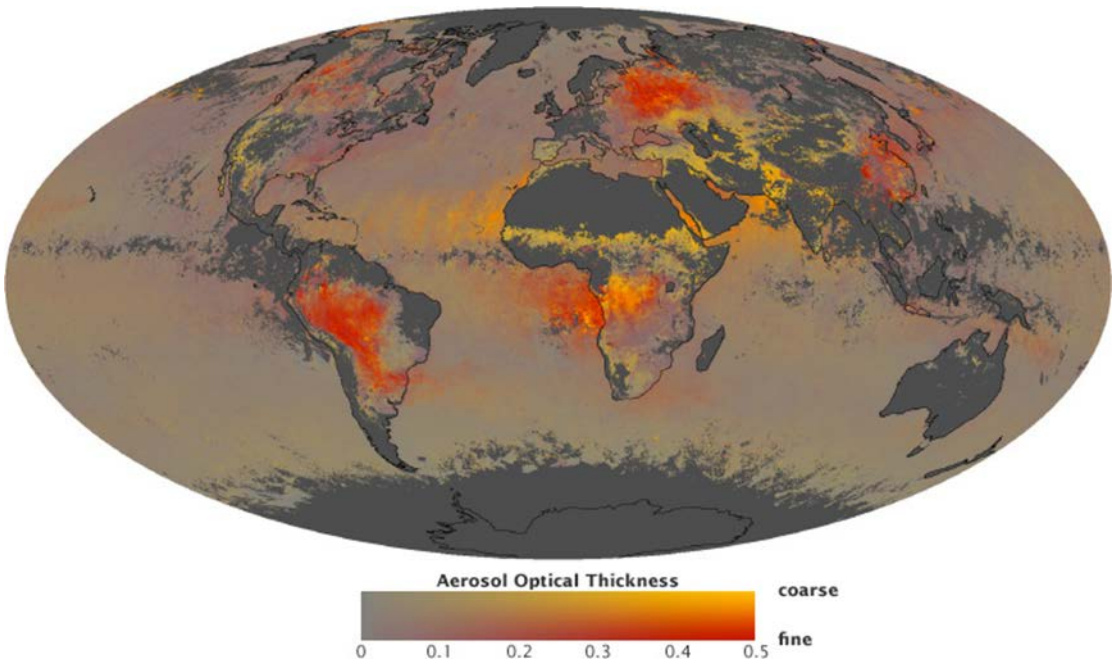

Figure 1.3:3 Global Distribution of aerosols according to their size, based on MODIS data (NASA, 2010)

1.3.3. Moderate Resolution Imaging Spectroradiometer (MODIS)

MODIS (Moderate Resolution Imaging Spectroradiometer) is an important instrument aboard NASA's Terra (EOS AM-1) and Aqua (EOS PM-1) satellites. Terra and Aqua, scan a total area of approximately 2330 km, providing almost complete global coverage in one day. Data in 36 high-resolution spectral channels between 0.415 and 14.235μm are acquired, with a spatial resolution of 250m in bands 1 and 2, 500m in bands 3 to 7, and 1000m in bands 8 to 36. According to Barnes, the radiation measured by MODIS, in high spectral analysis, provides improved and valuable information on the physical structure of the atmosphere and surface of the earth (Barnes, Pagano, & Salomonson, 1998).)

1.3.4. Virtual stations

Although many previous studies have shown that there is a positive relationship between satellite data and air pollution ((Weber, et al., 2001), (Basly & Wald, 2000), (Sifakis & Deschamps, 1992), (Ung, et al., 2001), (Muller, Doll, & Elvidge, 2000), (Wijeratne, 2003), (Narashid & Mord, 2006), a correlation between only a small number of monitoring stations (AQMS) and satellite image measurements is not mathematically convincing (Weber, et al., 2001).

The concept of "virtual stations" is introduced to densify the AQMS stations (Narashid & Mord, 2006). By utilizing the concept of virtual stations, the quantity of points of measurements is increased enabling for the use of interpolation and extrapolation methods in the calculation of pollutants' distribution over the study area (Narashid & Mord, 2006), (Wijeratne, 2003). Virtual stations are satellite image cells that exhibit characteristics similar to the cells that contain a monitoring station. By identifying such cells, we can densify the number of stations utilized in

mathematical models in our analysis, producing more robust statistical results. Identification can be performed with any information available that describes the physical characteristics of the cell, such as satellite image bands, land use maps, etc. Once identified, we can employ statistical methods to compute the estimated concentrations in these cells and utilize them as additional measurement stations in our research.

Each cell of a satellite image can be characterized by various parameters, environmental, morphological and spectral ((Weber, et al., 2001), (Narashid & Mord, 2006), (Wijeratne, 2003), (Ung, et al., 2001), (Narashid & Mohd, 2010)). Each available parameter can be utilized as a dimension that describes each cell of a satellite image. Combined, the dimensions of a cell form a multidimensional vector, which can be understood as an ID that describes the cell (Weber, et al., 2001). The larger the number of dimensions is, the more accurate the identification of satellite image is, as more characteristics of the examined cell are taken under consideration and the differentiation between cells is better. (Narashid & Mohd, 2010) (Ung, et al., 2001)

2. Study Area

The study area that is chosen for this study is the Great Athens Area (GAA), (Map 2:1), with coordinates 37.96^{o} N, 23.71^{o} E, which is located in the southeastern part of the European continent. It accommodates 3,827,624 inhabitants (population census of 2011), who represent 35.35% of the total population of Greece and its urban density is 1,005.13 inhabitants per square kilometer, (Hellenic Statistical Authority, Energy Consumptiom Survey in Households, 2012). The total extent of the area is 3,808 km^2, while the 450 km^2 is characterized as a highly populated area. The typical average air temperature during the winter months is 10^{o}C and during summer months is 26^{o}C. 20 years survey (1984-2004) shows that the average annual wind speed is approximately 3.3 m/s, while in winter it is 3.4 m/s and on summer 3.5 m/s. The mean precipitation amounts to 400 mm/yr. The Urban Heat Island (UHI) effect, causes the temperature increase of the Greek capital's center by 4^{o}C compared to the surrounding areas' temperatures, which leads to heat discomfort, (Kallos, Kassomenos, & Pielke, 1993; Melas, Ziomas, & Zerefos, Boundary layer dynamics in an urban coastal environment under sea breeze conditions, 1995; Kassomenos & Katsoulis, 2006).

The GAA is characterized by a Mediterranean climate, with hot and dry summers and wet and mild winters. In particular, in the Mediterranean climate, the evaporation is intense, with greatly exceeding precipitation and river run-off. This causes a decrease in the mean sea level and salinity to increase, (Demirov & Pinardi, 2002). As a result, the Mediterranean climate is sensitive to air pollution exposure, which is growing due to urban agglomeration, ((IPCC), 2007). Furthermore, it is also more vulnerable to photochemical episodes because they can also occur during the winter.

The air circulation in the GAA is guided by the existence of the physical North and East boundaries, which are the Parnes, Penteli, and Hymettus mountains, with height over 1000 m. In Athens, the predominant wind axis is northeast/southwest, with northeasterly directions, (Melas, Ziomas, & Zerefos, Boundary layer dynamics in an urban coastal environment under sea breeze conditions, 1995). Athens's peninsula is influenced by sea and land breeze circulation phenomena, which occur during the weakening of the synoptic wind. The sea/land breezes develop along the axis of the basin (NE to SW) and Anabatic/katabatic air masses flow from the enclosing mountains. As a result, the ventilation of the basin is poor; the boundary layer is shallow and, probably, it enhances air pollution, (Melas, Ziomas, & Zerefos, Boundary layer dynamics in an urban coastal environment under sea breeze conditions, 1995). In particular, the sea/land breeze system generating in the Saronic Gulf and taking place in the southern part of the Athens peninsula relocates air pollution from the center and favors the air pollutants accumulation in the northern suburbs. Air pollution episodes do not have a seasonal pattern in Athens, but the greatest

percentage of them occurs when the sea-breeze system develops, (Kallos, Kassomenos, & Pielke, 1993).

As it is mentioned before, Athens congregates 35.35% of the total population of the country, mostly on the western part of the Attica peninsula. During the summer months, the wind pattern in the atmospheric boundary layer is highly constant in the northeastern direction. Summer monsoons also occur in GAA, and thus, these phenomena favor good ventilation of the basin and prevent pollution episodes during the summer season, (Kanakidou, et al., 2011). According to Lawrence, et al., (2007), the Athens plume is traveling towards southeast over the East Mediterranean Sea. Finally, the mountain Aigaleo (up to 450m) acts as a natural boundary, preventing most of the transfer of air pollutants released from the industrial area west of the center, in the Thriassion plain, from reaching the center of the city, (Melas D. , Ziomas, Klemm, & Zerefos, 1998).

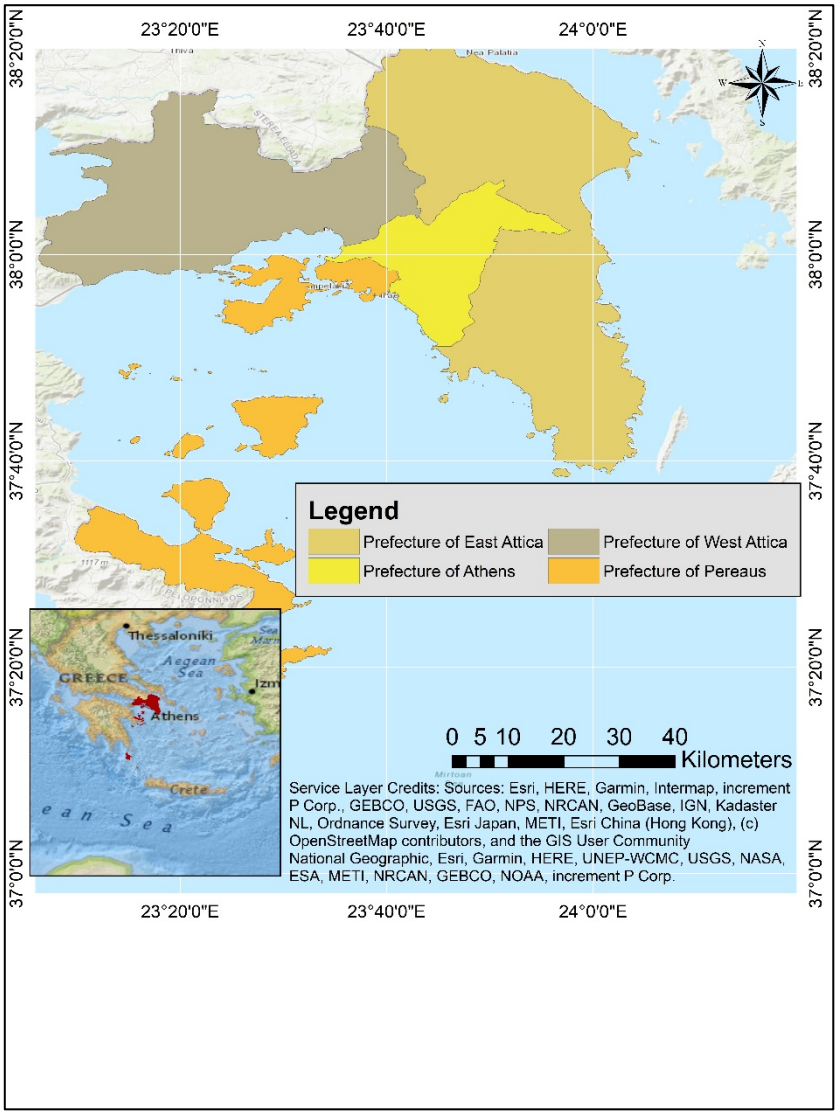

Map 2:1 Map of GAA. The polygons show the segregation of the peninsula into 4 regions (Athens, West Athens, East Athens, and Piraeus).

3. Material and Methods

3.1. Materials

3.1.1. Satellite Data

For this study, I used four products acquired from the MODIS sensor, of Terra satellite.

(i) The **Level 1B Calibrated Earth View products,** (MOD02HKM) at 500m spatial resolution, containing the 250m resolution bands also, resampled to 500m resolution, which were downloaded from NASA's Level 1 and Atmosphere Archive and Distribution System (LAADS) [http://ladsweb.nascom.nasa.gov/data/].

The MODIS Level 1B (L1B) products contain the first 7 spectral bands out of the 36 total spectral bands, which cover the visible, near-infrared, and shortwave infrared regions of the electromagnetic spectrum (EMS), (Table 3.1:1), with measurements derived only during daytime since February 2000, and their data type is 16-bit unsigned integer format. The data are in Geographic projection. It is considered necessary in order to perform any further analysis, to convert the initial values to Radiance values and Surface Reflectance values. MODIS L1B products' filenames begin with MOD02HKM when acquired from Terra, while when acquired from Aqua, filenames begin with MYD02HKM.

(ii) The **Aerosol Optical Thickness (AOT)**, (MOD04_L2) composite products with the coarse spatial resolution of 10km, derived using the Deep Blue algorithm for land surfaces, *(Hsu et al, 2013)*, which were download from NASA's Land Processes Distributed Active Archive Center (LP DAAC) [https://lpdaac.usgs.gov/].

The Aerosol retrieval algorithm utilizes seven spectral bands derived from the calibrated and geolocated L1B products (M?D02 and M?D03)[1] and others to apply cloud and screening procedures. These seven bands are located in 0.66, 0.86, 0.47, 0.55, 1.24, and 1.64 microns of the EMS. Especially, the MODIS Aerosol products provide the aerosol field in the whole atmospheric column, over cloud and snow/ice free surfaces. These products are supplied in 3km spatial resolution (MOD04_K3) and in 10km (MOD04_L2). The data type is 16-bit signed integer format, so the range of their values will be from 32.768 to +32.768. In order to convert these values into the traditional range

[1] Question mark represents the O for Terra satellite and Y for Aqua satellite. NASA's AOT algorithm utilizes data from both satellites to produce the final composite product MOD04_L2 (A., Remer, & Kaufman)

values, the initial data must be divided by 10.000, thus the data will be stored with a float data type format.

(iii) The **Vegetation Index products** (MOD13_A1) composite, with 500m spatial resolution and 16 days temporal resolution, in order to acquire the Normalized Difference Vegetation Index (NDVI) product. They were downloaded from NASA's Land Processes Distributed Active Archive Center (LP DAAC) [https://lpdaac.usgs.gov/].

The 16-day Vegetation Index data are supplied at 250m, 500m, and 0.05-degree spatial resolutions. In addition, there are monthly data with 1km and 0.05-degree resolution. Also, these products have to be divided by 10.000 in order to convert the initial values into the traditional data range, (from -1 to +1).

(iv) The **Geolocation Fields** (MOD03) for all daily orbits, for each 1km of MODIS Instantaneous Field of Views (IFOV). These data give the location and the ancillary information of the intersection of the centers of each IFOV from 10 detectors on the surface of the Earth. A digital elevation model is utilized to model the Earth's surface. The satellite altitude and orbit, the instrument telemetry, and the digital elevation model are the primary inputs. The Geolocation fields include the geodetic latitude, longitude, surface height above the geoid, solar zenith and azimuth angles, satellite zenith and azimuth angles, and a land/sea mask. These data are used to calculate the position of the center of the MODIS data, *(https://modis.gsfc.nasa.gov/data/dataprod/mod03)*.

Table 3.1:1 MODIS Bands after Processing into Reflectance and Brightness/Temperature Files, (adapted from Yale Center for Earth Observation, 2010, [http://www.yale.edu/ceo]). Bands 1 to 19 are in nm. Bands 20 to 36 are in μm.

16 Brightness/Temperature Bands			22 Reflectance or Radiance Bands		
ERMapper		MODIS	ERMapper		MODIS
Band 1	= Band 20	3.660-3.840	Band 1	= Band 1	0.620-0.670
Band 2	= Band 21	3.929-3.989	Band 2	= Band 2	0.841-0.876
Band 3	= Band 22	3.929-3.989	Band 3	= Band 3	0.459-0.479
Band 4	= Band 23	4.020-4.080	Band 4	= Band 4	0.545-0.565
Band 5	= Band 24	4.433-4.498	Band 5	= Band 5	1.230-1.250
Band 6	= Band 25	4.482-4.549	Band 6	= Band 6	1.628-1.652
Band 7	= Band 27	6.535-6.895	Band 7	= Band 7	2.105-2.155
Band 8	= Band 28	7.175-7.475	Band 8	= Band 8	0.405-0.420
Band 9	= Band 29	8.400-8.700	Band 9	= Band 9	0.438-0.448
Band 10	= Band 30	9.580-9.880	Band 10	= Band 10	0.483-0.493
Band 11	= Band 31	10.780-11.280	Band 11	= Band 11	0.526-0.536
Band 12	= Band 32	11.770-12.270	Band 12	= Band 12	0.546-0.556
Band 13	= Band 33	13.185-13.485	Band 13	= Band 13L	0.662-0.672
Band 14	= Band 34	13.485-13.785	Band 14	= Band 13H	0.662-0.672
Band 15	= Band 35	13.785-14.085	Band 15	= Band 14L	0.673-0.683
Band 16	= Band 36	14.085-14.385	Band 16	= Band 14H	0.673-0.683
			Band 17	= Band 15	0.743-0.753
			Band 18	= Band 16	0.862-0.877
			Band 19	= Band 17	0.890-0.920
			Band 20	= Band 18	0.931-0.941
			Band 21	= Band 19	0.915-0.965
			Band 22	= Band 26	1.360-1.390

The selection criteria are mentioned below.

- The products must be cloud-free because cloud cover is an indirect but decisive factor for the research. The existence of cloud cover in the study area prevents the extraction of the DN values of the pixels containing the AQMS. Additionally, the areas where virtual stations can be identified, and the accuracy of the identification is reduced. If AQMS locations are not visible, the available data for the regression analysis accuracy is reduced, which can have a substantial impact on the accuracy and representation of the created model.
- Both L1B and AOT products must be acquired on the same dates and times.
- The Vegetation Index data are acquired on different days because they are derived from the 16-day MODIS products. Although, I chose the dates that were close to those of the aforementioned products.
- All products have to cover the entire region of GAA.
- The selection of the appropriate acquisition dates was achieved based on the daily medians of the air pollutant concentrations, which were received by the Air Quality Monitoring Stations (AQMS).

Table 3.1:2 depicts the selected L1B and AOT datasets and their Geolocation Fields. Table 3.1:3 presents the Vegetation Index data.

Table 3.1:2 The chosen L1B & AOT Satellite data and their Geolocation Fields data

L1B	AOT	Geolocation Fields	Date	Time
MOD02HKM	MOD04_L2	MOD03	17/03/2007	09.45.00
MOD02HKM	MOD04_L2	MOD03	01/04/2008	09.15.00
MOD02HKM	MOD04_L2	MOD03	09/10/2009	09.40.00
MOD02HKM	MOD04_L2	MOD03	19/03/2010	08.45.00
MOD02HKM	MOD04_L2	MOD03	12/03/2011	09.45.00
MOD02HKM	MOD04_L2	MOD03	17/03/2012	08.35.00

Table 3.1:3 The chosen Vegetation Index MODIS data

Vegetation Index	Date	Time
MOD13_A1	22/03/2007	00.00.00
MOD13_A1	06/04/2008	00.00.00
MOD13_A1	30/09/2009	00.00.00
MOD13_A1	22/03/2010	00.00.00
MOD13_A1	06/03/2011	00.00.00
MOD13_A1	21/03/2012	00.00.00

3.1.2. Ground Stations Measurements

In order to investigate the exposure of GAA to the atmospheric pollution, Air Quality Measurements Dataset (AQMS network), (Map 3:1) was obtained from the Ministry of Reconstruction of Production, Environment, and Energy of Greece (YPEKA). Table 3.1:5presents the measured air pollutants as well as the methods of measurement.

All air pollutants are measured continuously throughout a 24-hour period, except for PM, which is measured on a daily basis. The response time of automatic analyzers is about one minute. Using a microprocessor located in each automatic station and connected to automatic analyzers, the average hourly pollutant values are calculated. These values are transferred to the central office

of the Service via a telephone line, and this makes it possible to continuously monitor the levels of air pollution in the area. However, due to malfunctions in measuring equipment, data transmission failures, or other unpredicted factors, data may not be available for all days and periods examined in all the available stations. At the same time, some stations do not measure all pollutant concentrations. PM_{10} concentrations are only measured in 9 out of 16 AQMS available in GAA.

Table 3.1:4 Air pollutants and the methods of measurement, (adapted from [http://www.ypeka.gr])

Air pollutants	Methods of measurement
Carbon Monoxide (CO)	Infrared absorption (NDIR)
Oxides of Nitrogen (NOx)	Chemiluminescence
Sulfur Dioxide (SO_2)	Fluorimetry
Particulate Matters (PM_{10})	Beta radiation absorption, except for Elefsina where Gravimetric analysis is used.

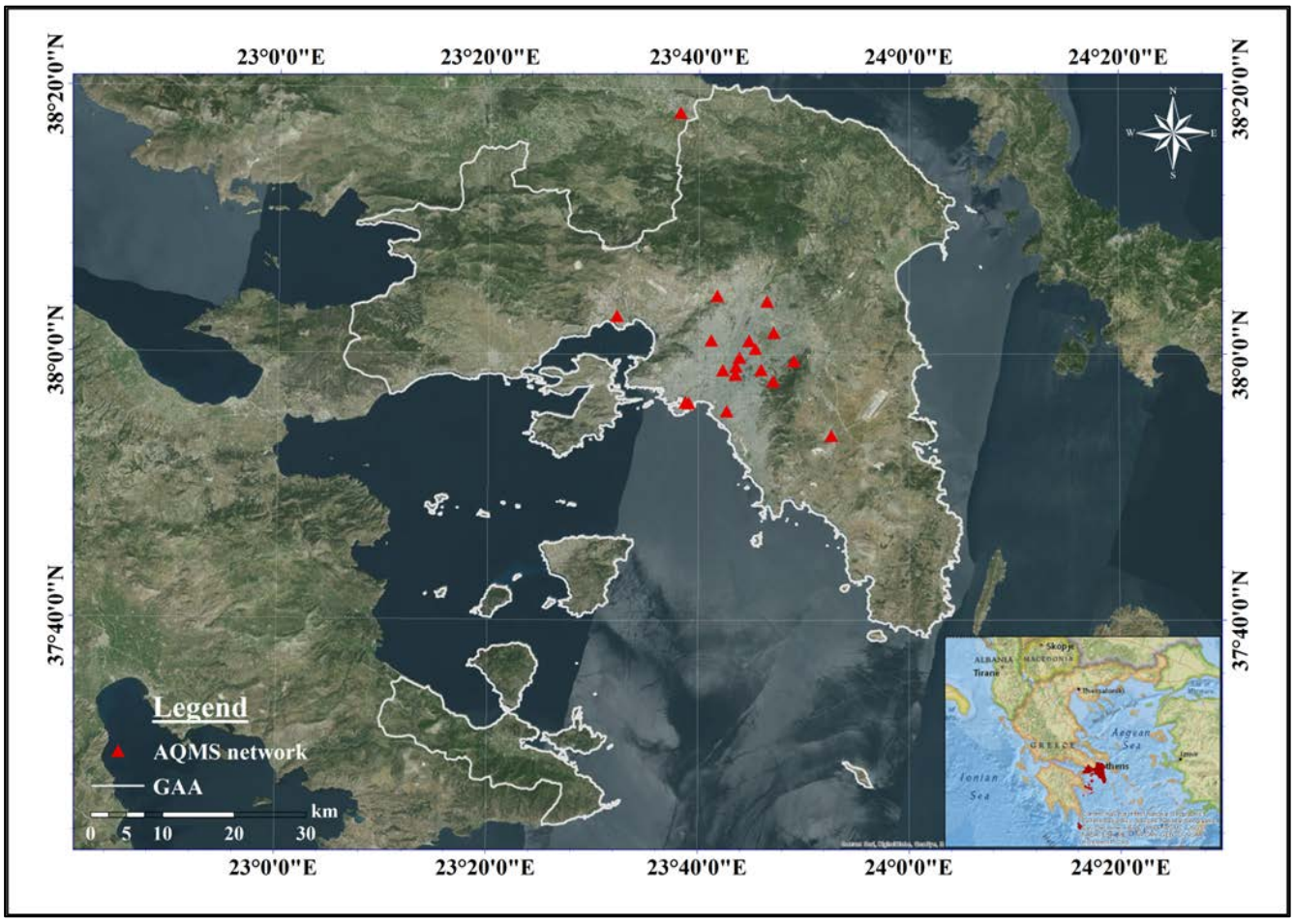

Map 3:1 The locations of the AQMS.

3.1.3. CORINE 2000

The Coordination of Information on the Environment (CORINE) Land Cover map was created for the first time in 1985 (reference of the CLC 1990), while updates have been developed in 2000, 2006, and 2012. It divides the land cover into 44 different classes. The regional phenomena are described by using a Minimum Mapping Unit (MMU) of 25 hectares (ha) and the linear phenomena by a width of 100 m. Except for the land cover mapping, time-series are produced in order to examine land cover changes between years and the difference between the spatial layers that are used, with an MMU of 5 ha. Almost all the European countries participate in the production of the national CLC databases. CLC is implemented by utilizing high-resolution satellite data, national in situ data, semi-automatic approaches, satellite image processing, and GIS procedures.

For this study, I use the CORINE 2000 Land Cover map, as a criterion for the identification of the virtual stations (see chapter 3.2.2). In particular, the CLC 2000 map was developed by using a Landsat-7 ETM image, of a single date, with a geometric accuracy of an MMU of 25 ha. The thematic accuracy was more than 58%.

3.1.4. Heating Systems

- **Emissions Estimations per fuel used in heating systems**

The Laboratory of Steam engines and boilers of the National Technical University of Athens (NTUA) in cooperation with the Chemical Process & Energy Resources Institute (CPERI) estimate the emissions indices per fuel type and per heating technology, according to the available heating systems in Greece. These emissions indices are used to investigate the potential change in energy consumption due to the economic crisis, according to the air pollutants' concentrations change.

Due to the economic crisis and energy conservation, an increase is observed lately in the use of biomass and other alternative energy sources for heating households and hot water production. Except for CO emissions, biomass is also the main source of Nitrogen Oxides (NOx), Sulfur Dioxide (SO_2), Particulate Matters (PM10) and other emissions. Table 3.1.6 describes the emission indices per fuel type and heating technology, (Kakaras et al, 2013). The primary data that were used for the calculation of the indices include the heating technologies, which use minerals or renewable fuels and were recorded by the DEFRA & SMED (2010), while the primary data that refer to heating systems using electrical energy were derived from Karakas et al, (2013).

Table 3.1:5 The Emission indices per fuel type and per heating technology, (adapted from Karakas et al, 2013).

	CO (gr/kWh_{th})	NOx (NO_2) (mg/kWh_{th})	SOx (SO_2) (mg/kWh_{th})	PM_{10} (mg/kWh_{th})
Typical petroleum boiler	0.17	300	48	13.1
Typical natural gas boiler	0.13	90	n/a	2.1
Natural gas Condensation boiler	0.11	80	n/a	1.8
Opened chamber fireplace	58	1152	144	2160
Closed chamber fireplace	29	576	72	1080
Biomass boiler (Pellet)	1.4	312	48	144

- **Heating Petrol Consumption**

Finally, the examination of the change in petrol consumption as a heating fuel is implemented by using the measurements of the petroleum products consumption from 2000 to 2013, recorded by the Ministry of Reconstruction of Production (YPEKA) and the total petroleum consumption for the same period, for the administrative region of Attica, recorded by Hellenic Statistical Authority, (2013).

3.2. Methods

This chapter presents the main processing procedures applied in this thesis. It is divided into four sub-chapters (i) the pre-processing steps, (ii) the identification of virtual stations and the regression analysis, (iii) the interpolation and the air pollutants' concentration mapping, and (iv) the relation of the anthropogenic factors with the air quality and its temporal change.

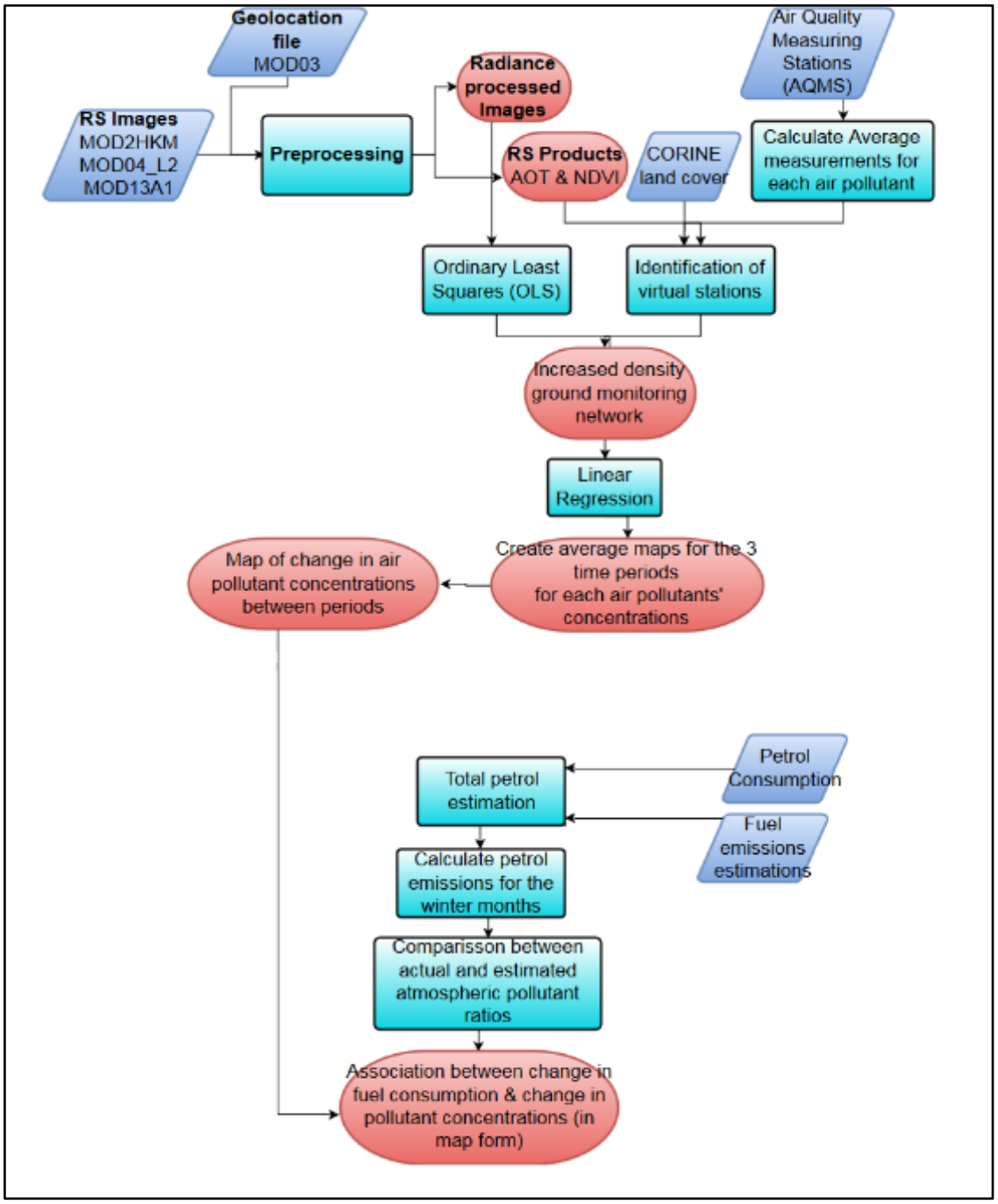

Figure 3.2:1 Flow chart of the applied methodology

3.2.1. Pre-Processing Steps

After importing all the data in ERDAS IMAGINE software, I realized that none had coordinates information. Thus, to project all 3 types of data in UTM 34N, WGS'84 datum, I used an external plugin named MODIS Toolkit, which was downloaded from GitHub (https://github.com/dawhite/MCTK) and installed in ENVI software. This toolkit provided an automated way to project the data, to convert the data in ENVI format (.hdr) for further processing, and to apply the procedure to the whole or part of the extent of the data, which are included in each MODIS product. Moreover, it also automatically imports the wavelengths (in microns) in L1B data.

Continuing, in order to simplify the processing method, I combined the datasets of all years into a single stack, in order to isolate the spatial extent to the area of interest (GAA), by subsetting the images. The procedure was applied to all three types of MODIS data (L1B radiance datasets, AOT, and NDVI).

Furthermore, the median values of each air pollutant concentration for each period examined were calculated for each existing station of the AQMS Network. Also, the median of each spectral band was calculated for each 2-year period.

3.2.2. Identification of Virtual Stations

For the identification of virtual stations, the multi-dimension vector "IDs" of cells without AQMS are compared to the cells with AQMS. The objective is to identify cells whose "IDs" are similar to those of AQMS stations. The larger the number of dimensions utilized in the vector, the easier and more accurate it is to identify cells that are similar to cells containing AQMS.

For my research, the parameters that were available as dimensions for the satellite image's cells' identification ("IDs") were:

- Spectral bands 1, 3, and 4 of MODIS, which are comparable to the visible light bands used in previous researches employing virtual stations ((Weber, et al., 2001), (Wijeratne, 2003), (Ung, et al., 2001), (Narashid & Mohd, 2010))
- AOD and NDVI products of MODIS
- CORINE land cover dataset, comparable to land cover datasets used as dimensions in previous studies ((Narashid & Mohd, 2010), (Wijeratne, 2003), (Narashid & Mord, 2006)).

- For MODIS acquired data, minimum and maximum radiance values for visible bands, NDVI, and AOD in cells where AQMS are located.

- For the CORINE land cover dataset, the category code values in cells where AQMS are located.

The median values of all years of the criteria were calculated and used in conjunction with the category codes from the CORINE land cover dataset. As a result, I created a "multidimensional vector for each point of the image integrating "several items of information", (Weber, et al., 2001). These were then used to finally identify the virtual stations in GAA. To identify the appropriate locations for use as virtual stations the values of cells without an AQMS were compared to the values of cells containing AQMS. The following criteria should be met:

- Similar DN/radiance values for the selected bands (R: 1, G: 4, B: 3), (Narashid & Mord, 2006).
- Similar values for AOD
- Similar values for NDVI
- Similar categories for CORINE Land Cover data. (Weber, et al., 2001)

The initial raw value rasters were reclassified into Boolean rasters (1 and NO DATA values) for each dimension, with value 1 assigned to each cell of the initial raster with a value within the minimum and maximum range of AQMS cells' median values for the specific dimension. For CORINE land cover, the Boolean raster was created through reclassification, by isolating cells with CORINE category codes identical to codes exhibited in AQMS containing cells.

Subsequently, the Boolean rasters were summed together into a new raster representing the similarity of the satellite image cells to those cells containing AQMS. The new raster contained a range of values between 1 to 6, describing the similarity of the examined cell to one of the cells with AQMS stations, while the cells that had no dimension similar were given a NO DATA value

Finally, through reclassifications, a final Boolean raster was created, with values 1 and NO DATA, where only cells with at least four out of six dimensions (over 50% similar dimensions) similar to AQMS cells were selected. The centroid of cells in the final raster with value 1 was extracted using Raster to point tool. These would be the final virtual stations for my study.

3.2.3. Regression Analysis and Verification

Once the virtual stations have been identified, Ordinary Least Squares (OLS) regression analysis was performed between the DN/radiance values of the pixel containing the AQMS from L1B data and the values of individual pollutants' concentrations in these stations, to determine the

relationships between them. The bands utilized in identifying the virtual stations cannot be used in this step. The spectral bands that used for the regression analysis are 2 (0.841-0.876μm), 5 (1.230-1.250μm), 6 (1.628-1.652μm), and 7 (2.105-2.155μm).

Mozumder et al. (2013) test both single and multivariate regression models, while Liu et al. (2005) note that the relationship may not necessarily be linear. The resulting models, describing the relationship between air pollutant concentrations (dependent variable) with the DN/radiance value(s) of the pixel (independent variable), were then used to estimate the air pollutants' concentrations in virtual stations.

Based on observations from a previous study by Haron Narashid and Wan Mohd Naim (2006), utilizing a small number of 6 to 7 AQMS in the regressions' training sets can help in achieving higher correlations between satellite data and AQMS measurements (Narashid & Mord, 2006). As such, 6 AQMS were initially selected as the sample size for the training sets. Where the analysis utilizing 6 AQMS combinations yielded no statistically significant results, 7 AQMS samples were used instead.

Where AQMS had missing data for the pollutant-time period combination, the specific AQMS was not included in the training set. Similarly, AQMS with erroneous data, denoted as -999 in the datasets, were also filtered out in the sampling process.

All possible AQMS combinations were tested. For 6 AQMS samples, a total of 5005 combinations are possible, using the 16 available AQMS in GAA, while for 7 AQMS samples, 6435 possible combinations exist. For PM10 regressions, where the population of AQMS with equipment capable of measuring the pollutant's concentrations is limited to only 9 stations in GAA, only 84 possible combinations exist using 6 AQMS samples. No need for 7 AQMS samples arose for PM10.

The resulting regressions were filtered to exclude the ones that did not yield statistically significant results. From the remaining regressions, those presenting the lowest standard error for each pollutant–time period combination were, then, selected for use in the next steps of my analysis. The ones exhibiting the lowest standard errors for each pollutant-time period combination were finally selected for the next steps of the analysis.

Utilizing the formulae produced by the first regression (table 4.2:1), that utilize only AQMS stations in their samples, values were estimated for each of the seven pollutants examined within my research. Samples of 6 or 7 AQMS were selected for the analysis, as these yielded the smallest p-values in conjunction with low standard errors. The formulae from these regressions were then

utilized with the values from bands 2,5,6, and 7 in virtual stations to estimate the pollutant values in these virtual stations.

The result was a densified air quality monitoring network, which is then used as input for the next steps of the analysis. The regression coefficients can be used as direct measures of sensitivity for the method. RMSE of the proposed method was less than the one achieved through simple interpolation using only the actual AQMS network, (Basly & Wald, 2000).

With both AQMS and virtual stations, the densified network is expected to be better suited in the computation of pollutant concentrations over all the cells of the study area through a second regression analysis, utilizing both AQMS and the newly computed values over virtual stations as the regression's sample. (Wijeratne, 2003)

OLS regression analysis was also chosen for the second regression, using the increased sample, and was applied in order to identify the appropriate equation (beta coefficients) that models the concentration of each pollutant over the whole GAA.

For the verification of the first set of regressions, AQMS that were not selected in the training sets were used in the validation sets used to calculate the average of the accuracy of the resulting formulae. AQMS with missing or incorrect (denoted as -999 in the measurement records) were excluded from the verification sets also.

Each validation set included 7 to 10 AQMS, except for PM10 validations. Here, due to the decreased initial population of AQMS with appropriate measuring equipment, only 3 stations remained for each PM10 –time period combination. The accuracy of the estimation was calculated in each AQMS in the validation set for each pollutant-time period combination. The average accuracy was then computed for each regression formula. The formulas utilized for the validation of the results are:

$$Avg.Pollutant\ accuracy = \frac{\sum_{i=1}^{n}(actual\ value_i - estimated\ value_i)}{n}$$

$$where\ n\ the\ number\ of pollutant - time\ period\ combinations\ utilized$$

$$Avg.Accuracy = Avg.Pollutant\ accuracy - 1$$

In the second regression analysis, both the estimated air pollutant concentrations of the virtual stations and the existing AQMS measurements were used as the dependent variable and the DN/Radiance values of the spectral bands 2, 5, 6, and 7 of the cells containing them were again

used as independent variables, similar to the methodologies employed by previous studies. (Narashid & Mohd, 2010), (Wijeratne, 2003), (Ung, et al., 2001)

3.2.4. Air Pollutants Concentration Mapping

After applying the regression analysis mentioned above, 21 equations, one for each of the seven pollutants for each of the three periods examined, were created representing the concentrations of each pollutant for each time period examined. These 21 equations were then implemented in ArcGIS for each cell, to estimate and map the air pollutant concentrations in the whole extent of GAA.

The implementation of the equations of each air pollutant concentration resulted in three Average Air Pollutant Maps for each pollutant examined, one for each period studied. Again, a total of 21 maps were produced in total, presenting the concentration of air pollutants over GAA.

3.2.5. Relation between Heating Systems and Air Quality

To associate the atmospheric pollutant concentrations with changes in residential heating systems, the pollutant concentrations in the atmosphere need to be compared to pollutant emissions of several types of fuels used in these systems and the petrol consumption. For the emissions produced by these types of fuels, data from the study conducted by Kakaras et al. (2013) titled "Emission indices by type of fuel and heating technology" were used to calculate the ratios between different pollutants for each type of fuel. Through the bibliographic review, it was noted that each fuel has a distinct emission profile (Kakaras, et al., 2013) and thus the ratios between any two pollutants of a fuel used are also distinct. Each fuel type produces a set amount of pollutants in mg/kWh_{th} which means that, for set fuel, the ratio between two pollutants produced during its consumption will not change regardless of the quantity of fuel used. Due to a lack of spatially referenced data on fuel quantities consumed for residential heating in GAA, the ratios can be utilized to determine changes in fuel consumption without having the exact amount of fuel consumed. The same ratios were also calculated for the air pollutant concentrations for each period studied. By comparing the two sets of ratios, it can be determined if a change has occurred in the types of fuels used for residential heating during the onset of the economic crisis in Greece or later. The use of each heating type was estimated only in the urban areas of GAA, which were identified using the CORINE Land Cover data, (Map 3:2).

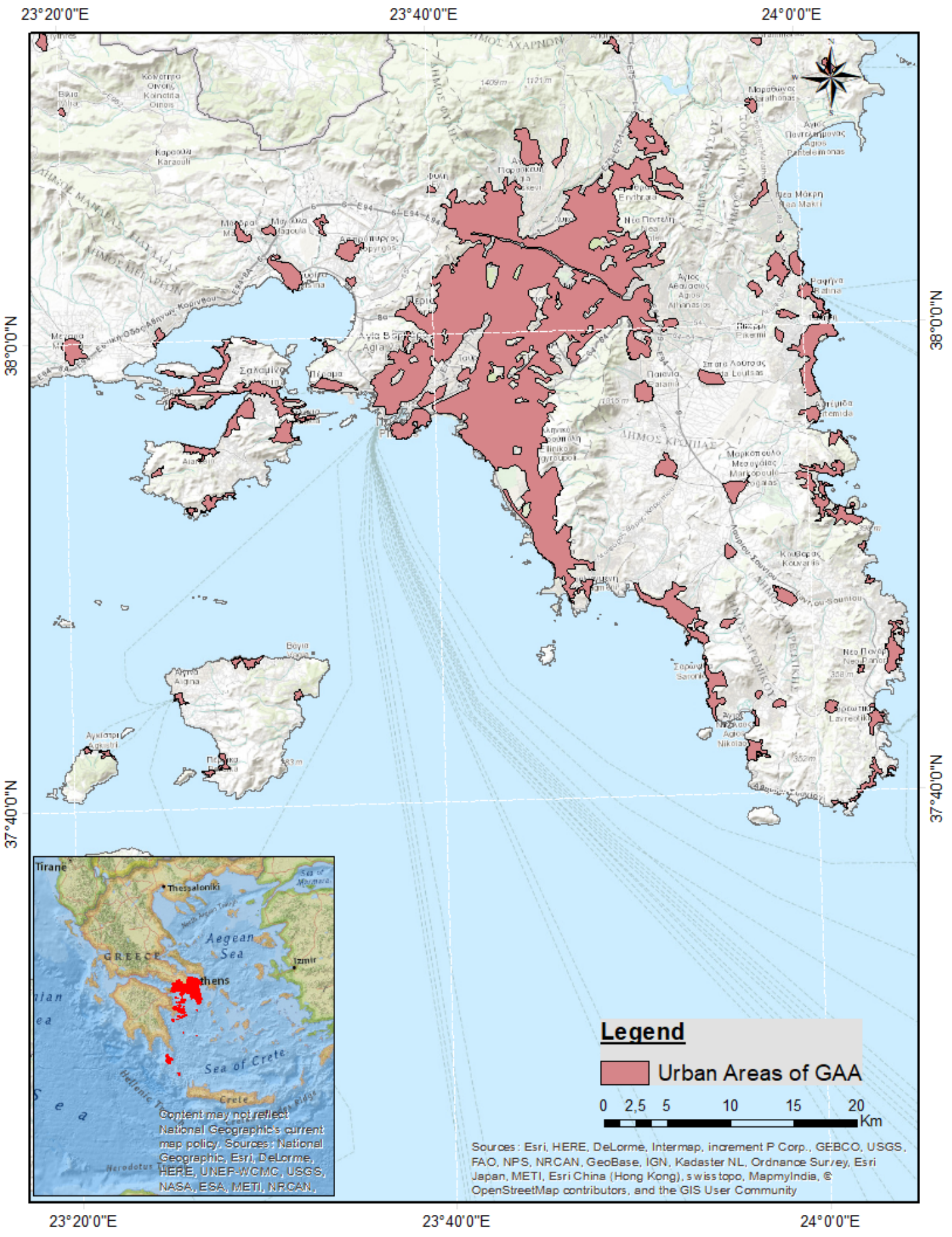

Map 3:2 Map of the urban areas of GAA used for the estimation of the use of each heating type/fuel.

The calculated ratios of each heating type are presented in table 3.2:1. Table 3.2:2 presents the ratios used for the estimation of the use of each heating type.

Table 3.2:1 Ratios for each heating fuel type

(mg/mg for all pollutants ratios except CO that is in gr) – NO_2 is utilized wherever NO_X is referenced

Fuel and Heating Type	CO/NOx	CO/SO_2	CO/PM_{10}
Typical petroleum boiler	0.57	3.54	12.98
Typical natural gas boiler	1.44	N/A	61.90
Natural gas Condensation boiler	1.38	N/A	61.11
Opened chamber fireplace	50.35	402.78	26.85
Closed chamber fireplace	50.35	402.78	26.85
Biomass boiler (Pellet)	4.49	29.17	9.72

Fuel and Heating Type	NOx/CO	NOx/SO_2	NOx/PM_{10}
Typical petroleum boiler	1.76	6.25	22.90
Typical natural gas boiler	0.69	N/A	42.86
Natural gas Condensation boiler	0.723	N/A	44.44
Opened chamber fireplace	0.02	8.00	0.53
Closed chamber fireplace	0.02	8.00	0.53
Biomass boiler (Pellet)	0.22	6.50	2.17

Fuel and Heating Type	SO_2/CO	SO_2/NOx	SO_2/PM_{10}
Typical petroleum boiler	0.28	0.16	3.66
Typical natural gas boiler	N/A	N/A	N/A
Natural gas Condensation boiler	N/A	N/A	N/A
Opened chamber fireplace	0.002	0.13	0.07
Closed chamber fireplace	0.002	0.13	0.07
Biomass boiler (Pellet)	0.03	0.15	0.33

Fuel and Heating Type	PM_{10}/CO	PM_{10}/NOx	PM_{10}/SO_2
Typical petroleum boiler	0.077	0.044	0.273
Typical natural gas boiler	0.016	0.023	N/A
Natural gas Condensation boiler	0.016	0.022	N/A
Opened chamber fireplace	0.037	1.875	15.00
Closed chamber fireplace	0.037	1.875	15.00
Biomass boiler (Pellet)	0.103	0.462	3.00

Table 3.2:2 The chosen ratios for each heating type.

Fuel and Heating Type	Ratios
Typical petroleum boiler	NOx/CO, SO2/CO
Typical natural gas boiler **Natural gas Condensation boiler**	CO/ PM_{10}, NOx/ PM_{10}
Opened chamber fireplace **Closed chamber fireplace** **Biomass boiler (Pellet)**	PM_{10}/ SO_2, PM_{10}/NOx CO/ SO_2, CO/NOx

4. Results

4.1. Virtual station identification

Having all available factors considered, a final raster was created with only cells that have more than 50% of the dimensions of their ID similar to those found in cells with AQMS. The cells were then converted into points. The resulting virtual stations as well as the existing AQMS, are shown in the map (4:1) presented below:

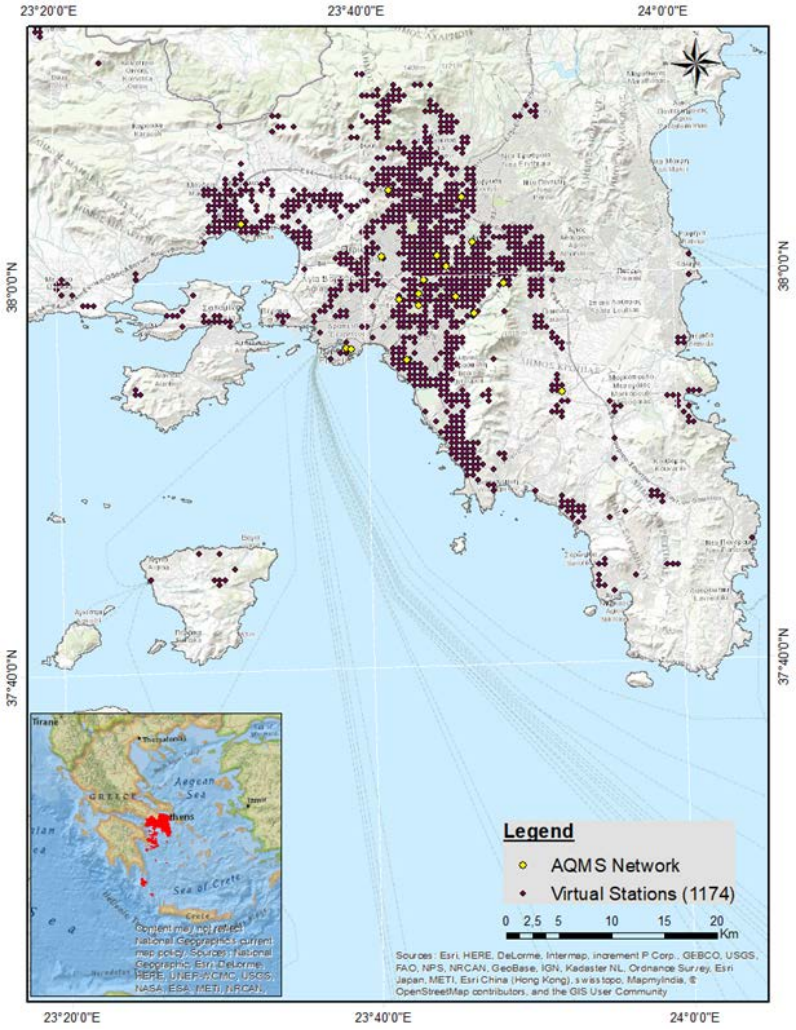

Map 4:1 Map of the virtual stations and the AQMS Network.

4.2. Pollutant estimation regressions and results validation

Following the observations made in the study by Haron Narashid and Wan Mohd (Narashid & Mord, 2006), training sets for the 1st OLS regression were limited to 6 AQMS which seem to produce increased correlations between satellite data and pollutant measurements. All possible AQMS combinations were examined, by creating regressions with all possible combinations of AQMS as described in the methods section (3.2.3), and regression formulae were produced. With the exceptions of CO and NO_2 for the 2011-2012 period, all other pollutant-time period combinations had at least one resulting regression with statistically significant results. For the two pollutants during the 2011-2012 period. 7 AQMS training sets were also examined, which yielded at least one regression with statistically significant results. These results are presented in the following table (Table 4.2:1).

The results show the regression formulas for each pollutant – time period combination, as computed using AQMS training datasets. Except for CO and NO_2 pollutants for the 2010-2011 period where it was required to utilize an additional AQMS in the regression analysis, the remaining regressions utilized 6 AQMS sample sizes to produce the formula that were later utilized in the next steps of the study. Included in the table are the OLS regression formula and its corresponding P-value, Standard Error, Adjusted R^2 (due to utilizing 4 MODIS bands as independent variables), and the sample size utilized in the training dataset.

Finally, utilizing both the virtual stations and AQMS, new regressions were performed to create the final formulae that would be used to create the final pollutant concentration rasters for the analysis [full second OLS regression results are included in appendix A due to large size], as described in the methodology by Ung, et al., (2001), Wijeratne (2003), and Narashid & Mohd, (2010).

Table 4.2:1 1st regression results

Pollutant	Time period	OLS regression formula	P-value	Standard error	R squared adjusted	Sample size
CO	2007-2008	6.234+(-0.313* [Band 2])+(0.206* [Band 5])+(1.630* [Band 6])+(-3.871* [Band 7])	0.005	0.004527	1	6
CO	2009-2010	-5.317+(-0.359* [Band 2])+(0.04* [Band 5])+(4.317* [Band 6])+(-7.925* [Band 7])	0.002	0.009517	1	6
CO	2011-2012	0.851+(-0.245* [Band 2])+(0.2* [Band 5])+(1.152* [Band 6])+(-1.736* [Band 7])	0.001	0.010301	0.998	7
NO2	2007-2008	46.169+(-11.153* [Band 2])+(17.577* [Band 5])+(12.055* [Band 6])+(-6.022* [Band 7])	0.001	0.010480	1	6
NO2	2009-2010	52.604+(3.657* [Band 2])+(-3.531* [Band 5])+(-29.338* [Band 6])+(64.797* [Band 7])	0.009	0.210335	1	6
NO2	2011-2012	78.203+(-13.79* [Band 2])+(5.334* [Band 5])+(75.168* [Band 6])+(-101.57* [Band 7])	0.0001	0.332732	1	7
SO2	2007-2008	38.587+(1.556* [Band 2])+(2.205* [Band 5])+(-27.937* [Band 6])+(46.831* [Band 7])	0.012	0.095474	1	6
SO2	2009-2010	-29.041+(-0.26* [Band 2])+(-0.643* [Band 5])+(16.541* [Band 6])+(-37.965* [Band 7])	0.009	0.064641	1	6
SO2	2011-2012	-7.233+(0.715* [Band 2])+(-1.135* [Band 5])+(1.151* [Band 6])+(-2.988* [Band 7])	0.006	0.008919	1	6
PM10	2007-2008	-35.842+(9.505* [Band 2])+(-4.694* [Band 5])+(-68.314* [Band 6])+(142.966* [Band 7])	0.005	0.072231	1	6
PM10	2009-2010	15.069+(6.703* [Band 2])+(-6.702* [Band 5])+(-29.37* [Band 6])+(55.167* [Band 7])	0.002	0.017492	0.95	6
PM10	2011-2012	27.236+(-9.205* [Band 2])+(1.135* [Band 5])+(68.063* [Band 6])+(-97.644* [Band 7])	0.017	0.173518	0.999	6

To validate the formulas' accuracies for the 1st regression, the AQMS that were not included in the training sets were used for validation. Again, stations with missing or erroneous data were excluded from the process. In the results, the columns presented are the pollutant – time period combination examined, the number of AQMS utilized in the validation dataset, the average pollutant accuracy, and the Average Accuracy. The formulas utilized for the accuracy calculations are presented in the Methods section 3.2.3. The resulting accuracy validation estimates are presented in the following table:

Table 4.2:2 Regression validation results

Pollutant – time period combination	AQMS used count	Average Pollutant accuracy - Percentage from actual	Average accuracy
CO – 07/08	9	144.99%	44.99%
CO – 09/10	10	221.88%	121.88%
CO – 11/12	7	140.04%	40.04%
NO2 – 07/08	9	103.08%	3.08%
NO2 – 09/10	10	106.92%	6.92%
NO2 – 11/12	7	109.62%	9.62%
SO2 – 07/08	10	147.25%	47.25%
SO2 – 09/10	9	143.72%	43.72%
SO2 – 11/12	9	103.69%	3.69%
PM10 – 07/08	3	87.49%	-12.51%
PM10 – 09/10	3	147.81%	47.81%
PM10 – 11/12	3	127.60%	27.60%

As observed in the table, most regressions have errors within acceptable limits of under 50% [(Wijeratne, 2003), (Santamouris M. , 2007), (Sifakis & Deschamps, 1992)] over or under estimation error in calculations and comparable to previous studies of similar nature [(Wijeratne, 2003), (Hidy, et al., 2009), (Basly & Wald, 2000)]. An exception is observed for CO during the 2009–2010 period, where a large overestimation is returned by the regression.

For CO in 2009-2010, the validation shows a large overestimation of pollutant concentrations in the validation set, which is almost double the actual measured concentration in the AQMS, as observed in the table above.

All validations have an acceptable number of AQMS in the validation sets, following the generally acceptable rule of having at least 30% of the overall sample utilized for the validation set. For CO, NO_2, and SO_2 the number of AQMS ranges from 7 to 10. For PM_{10}, due to the limited number of AQMS with equipment capable of measuring this type of pollutant (total population of 9 stations), only 3 AQMS are present in each validation set. However, even the 3 stations satisfy the common ratio between training and validation sets of 70%-30% respectively.

4.3. Average Air Pollutant Mapping

CO highest concentrations (Map 4:2) appear to be generally decreasing between 2007 and 2012, with 2011-2012 (4.28868 mg/m^3) largest concentrations being 34.84% lower than 2007-

2008 (6.5822 mg/m^3) and 76.91% lower than 2009– 2010 (18.5766 mg/m^3) corresponding largest concentrations. During 2009-2010, a large spike in concentrations of CO is observed with the highest concentrations of the period being almost 3 times higher than those of the previous period (2007–2008), dropping rapidly again during the 2011- 2012 period. During all three periods, most of East Attica and Industrialized areas in the south section of West Attica maintain high concentrations throughout 2007-2012. The extent of the industrialized areas with a high concentration in West Attica, however, continuously reduces from 2007–2008 to 2009–2010 and again to 2011–2012. On the contrary, the south section of Central Attica, large areas in the northern limits of the north sections of West and Central Attica, a large area in the limit between West and Central Attica, and the urban area of Megara in the south section of West Attica maintain relatively low concentrations throughout 2007–2012. The coastal areas in East Attica present low concentrations throughout 2007–2012, increasing in extent between 2007-2008 and 2009–2010 and again in 2011–2012. The rest of the north sections of West and Central Attica, Salamina, and Aegina islands (which are parts of the administrative district of Attica) present high concentrations through 2007-2008 that decrease during 2009–2012.

Finally small areas of low concentration in the south section of East Attica during 2007-2008, present high concentrations during 2009-2010 but again having low concentrations and appearing extended during 2011–2012.

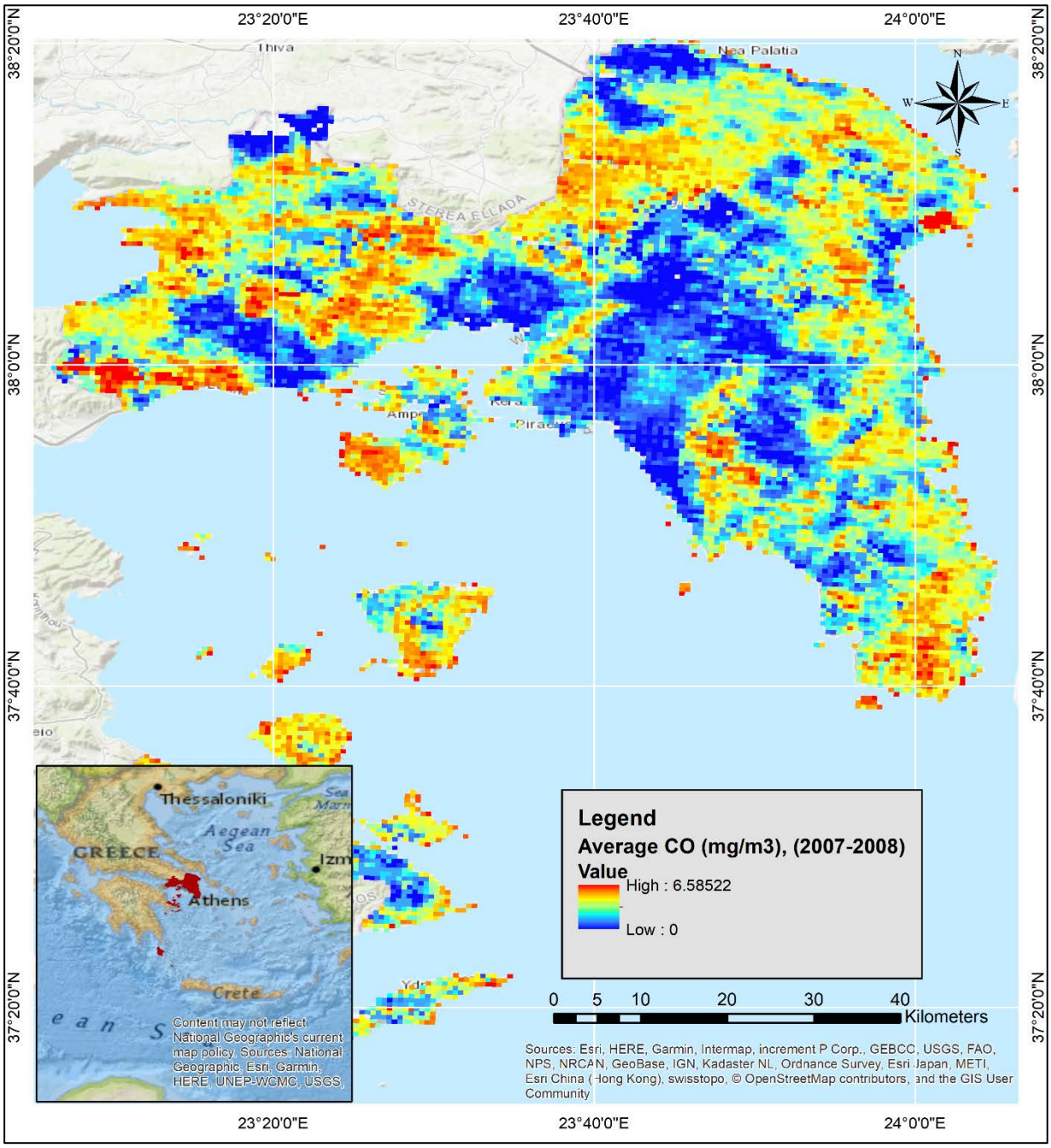

Map 4:2 Average CO (mg/m^3) concentrations in 2007-2008

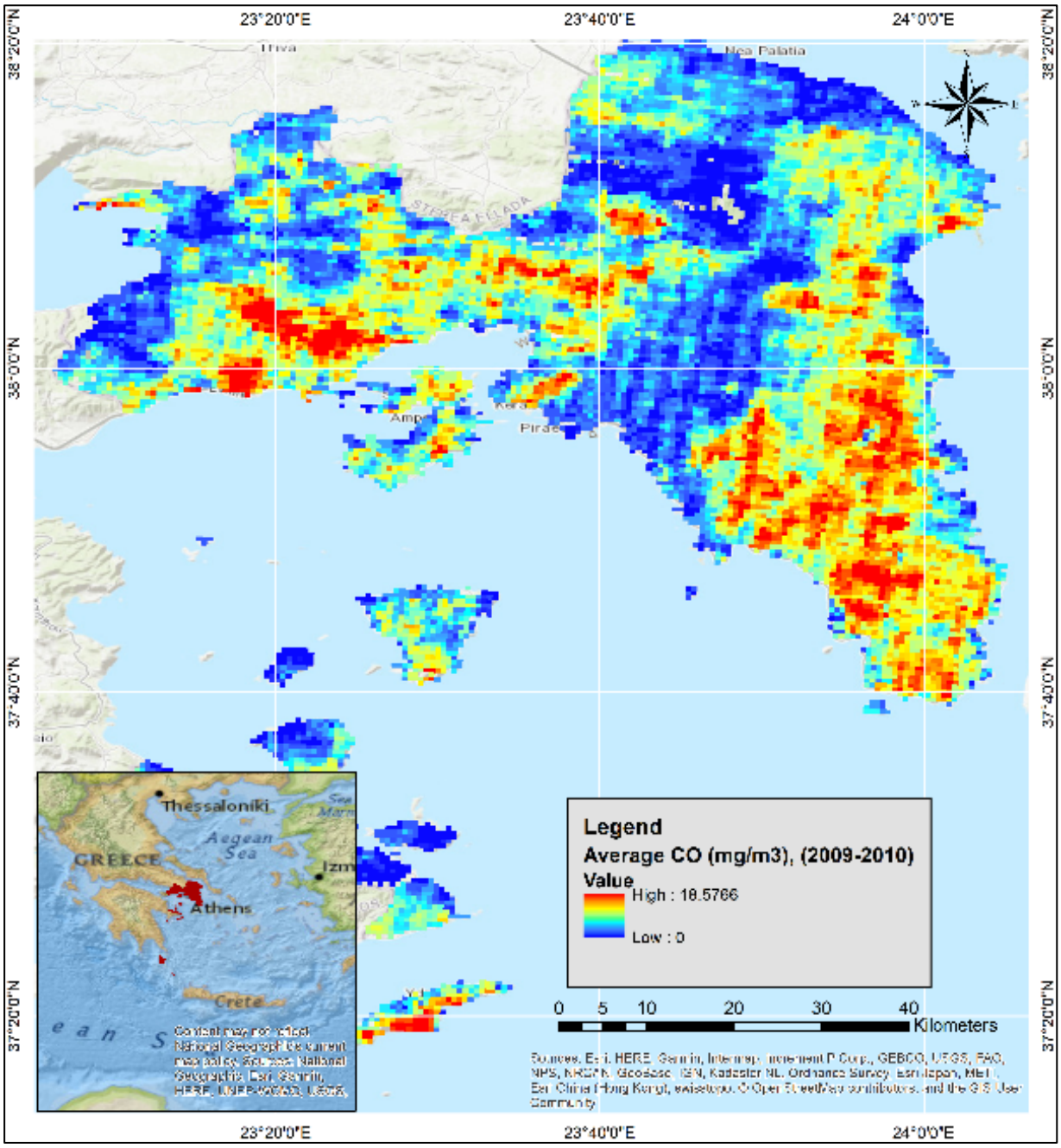

Map 4:3 Average CO (mg/m^3) concentrations in 2009-2010

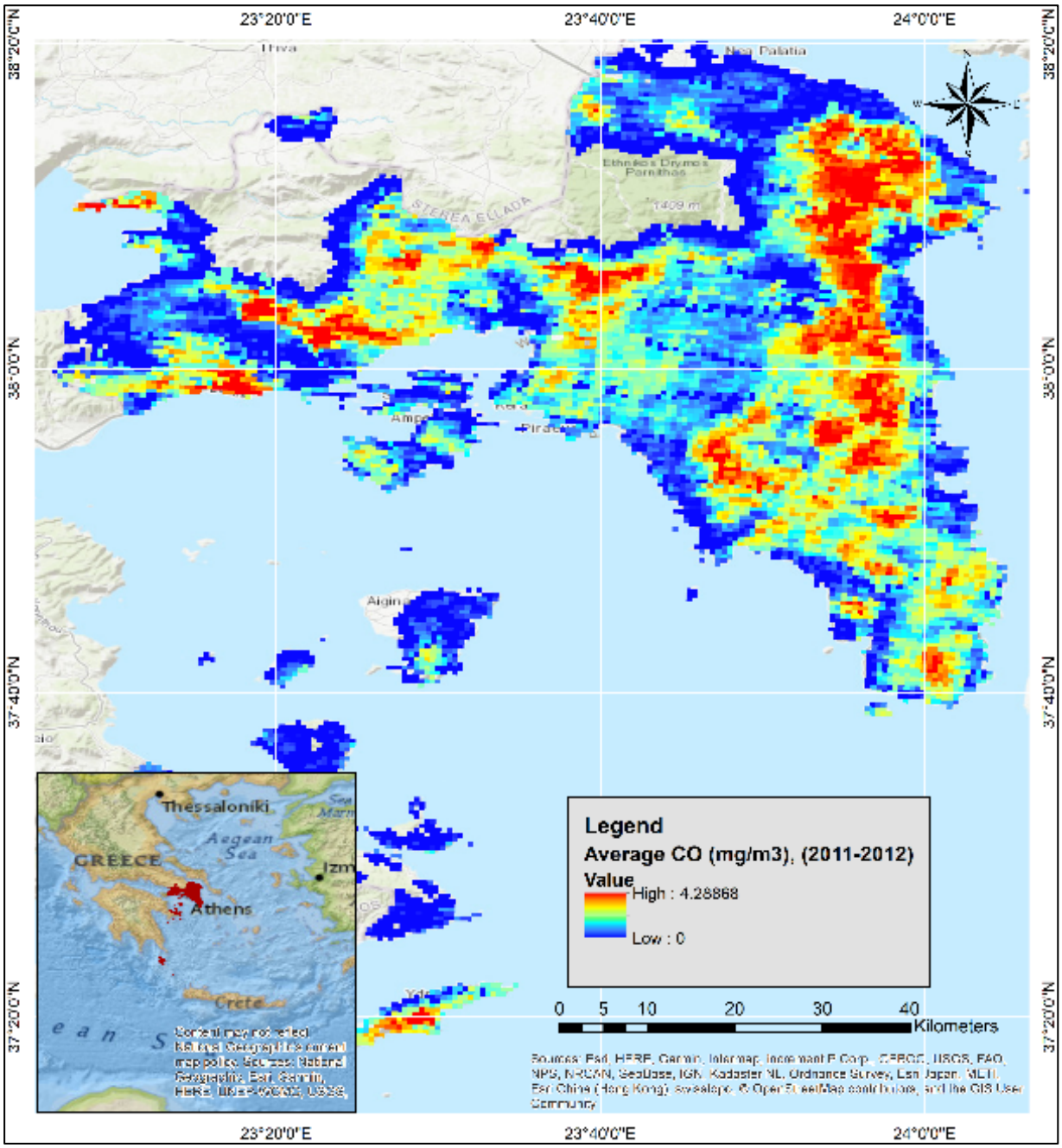

Map 4:4 Average CO (mg/m^3) concentrations in 2011-2012.

Between the first two periods (2007-2008 and 2009–2010), concentrations appear to increase mainly in the industrialized areas and areas adjacent to them (including Megara urban area) in West Attica and the south section of East Attica. Small areas in the north section of all three areas (West, Central, and East) also exhibit smaller increases, similar to the east part of Salamina island and an extensive area between West and Central Attica. Most of the northern sections of West and Central Attica on the other hand, exhibit high decreases of CO concentrations, similar to small, mostly coastal, and isolated areas in the north section of East Attica. The south section of Central Attica presents a mixture of areas with decreases and areas where concentrations of CO are relatively stable.

Between 2009 and 2012, previously observed changes are reversed. Industrialized and urban areas in the south section of West Attica, and almost all the south section of East Attica, which previously showed an increase in concentrations of CO, now show the highest decrease. The range of this decrease is larger than the range of the increase in concentrations during 2007–2012. The area in the West limit of West Attica, which previously showed a decrease, now presents a medium increase similar to Central Attica and most of the coastal areas of East Attica. Both Salamina and Aegina islands show a mixture of stable areas and areas with changes, with no dominant trend. The range of the increase in CO concentrations between the two periods is low and areas with high increases in concentrations are very small and isolated inside larger areas with medium increases in concentrations.

Generally, between 2007 and 2012, most of Attica exhibits an increase in CO concentrations, the range of which is relatively small (2.93 mg/m^3) compared to the ranges of fluctuation between the three periods. The largest increase of CO concentrations is observed in large areas in the southern sections of Central and East Attica and a relatively small area in the north section of East Attica. Urban and industrialized areas of the south section of West Attica and the rest of the south section of Central Attica exhibit relatively medium increases. Most of the north section of West Attica, the area in the western limit of West Attica, and most of the north section of Central Attica exhibit large decreases in CO concentrations. A large area in the southern coastal limit of East Attica also exhibits a mixture of small decreases and stable concentrations. The west part of Salamina island exhibits decreasing concentrations, similar to the coastal areas of Aegina Island, while the east part does not present a dominant trend, similar to the central area of Aegina Island.

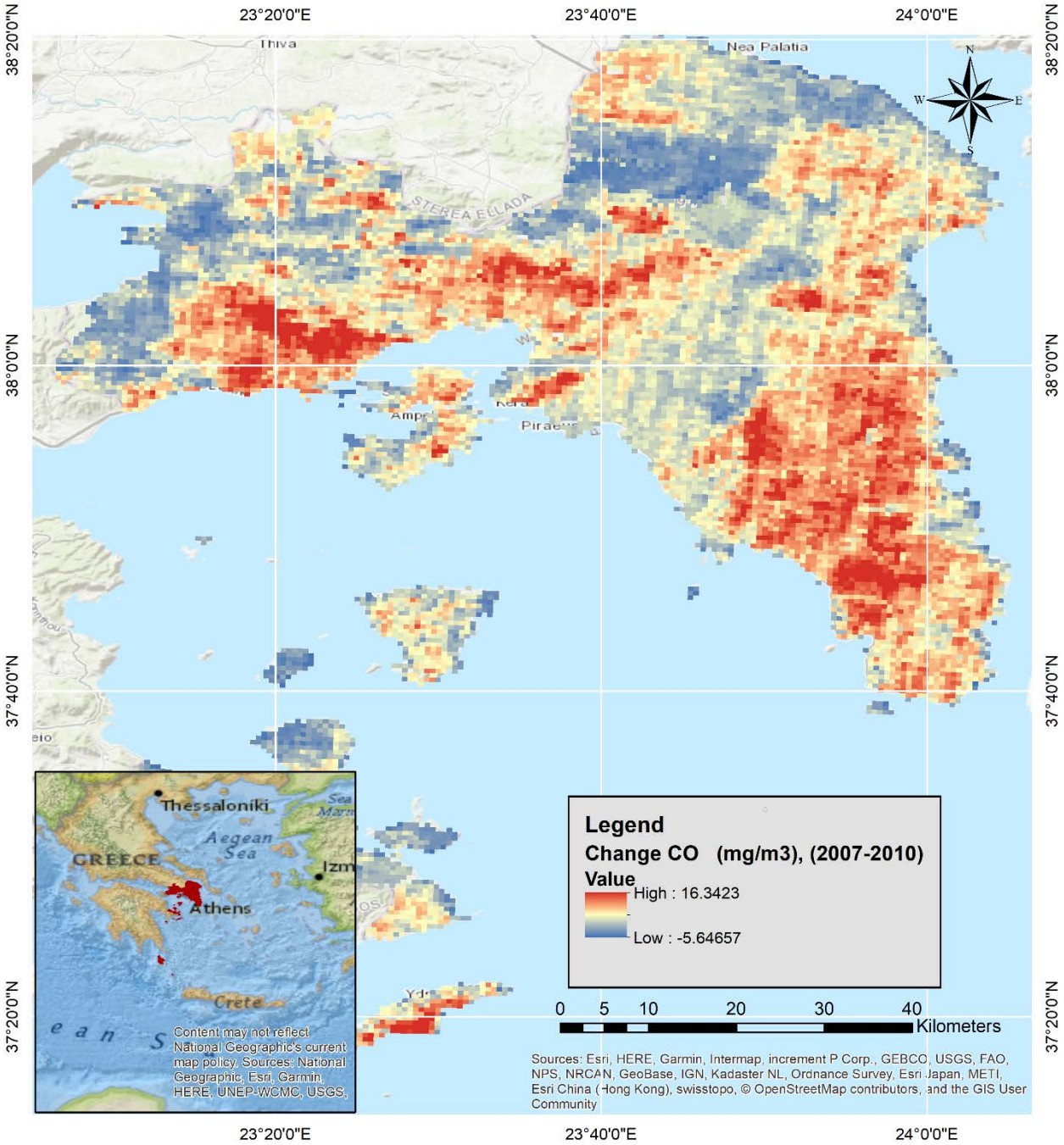

Map 4:5 Change in CO (mg/m^3) concentrations in 2007-2010.

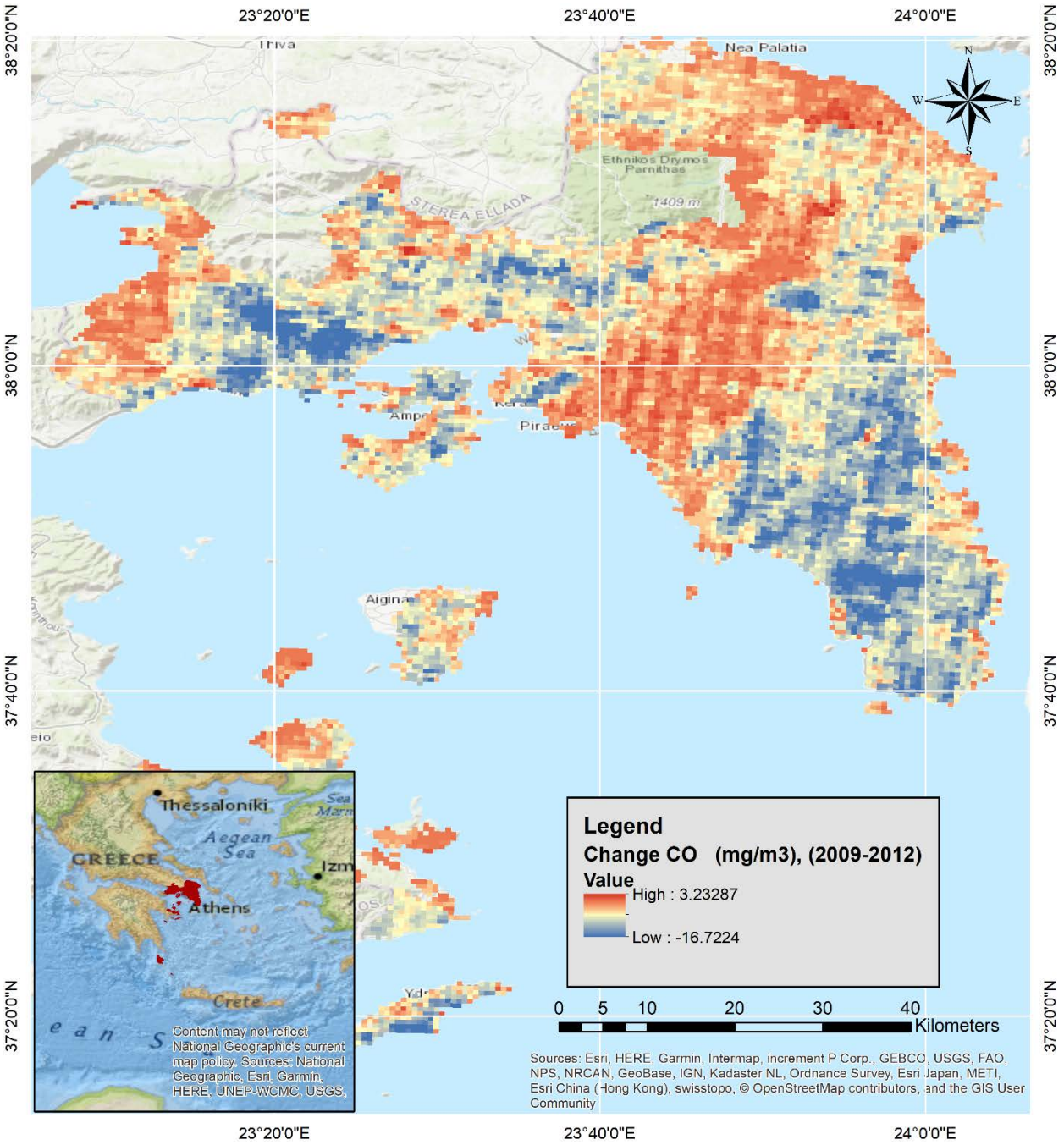

Map 4:6 Change in CO (mg/m^3) concentrations in 2009-2012

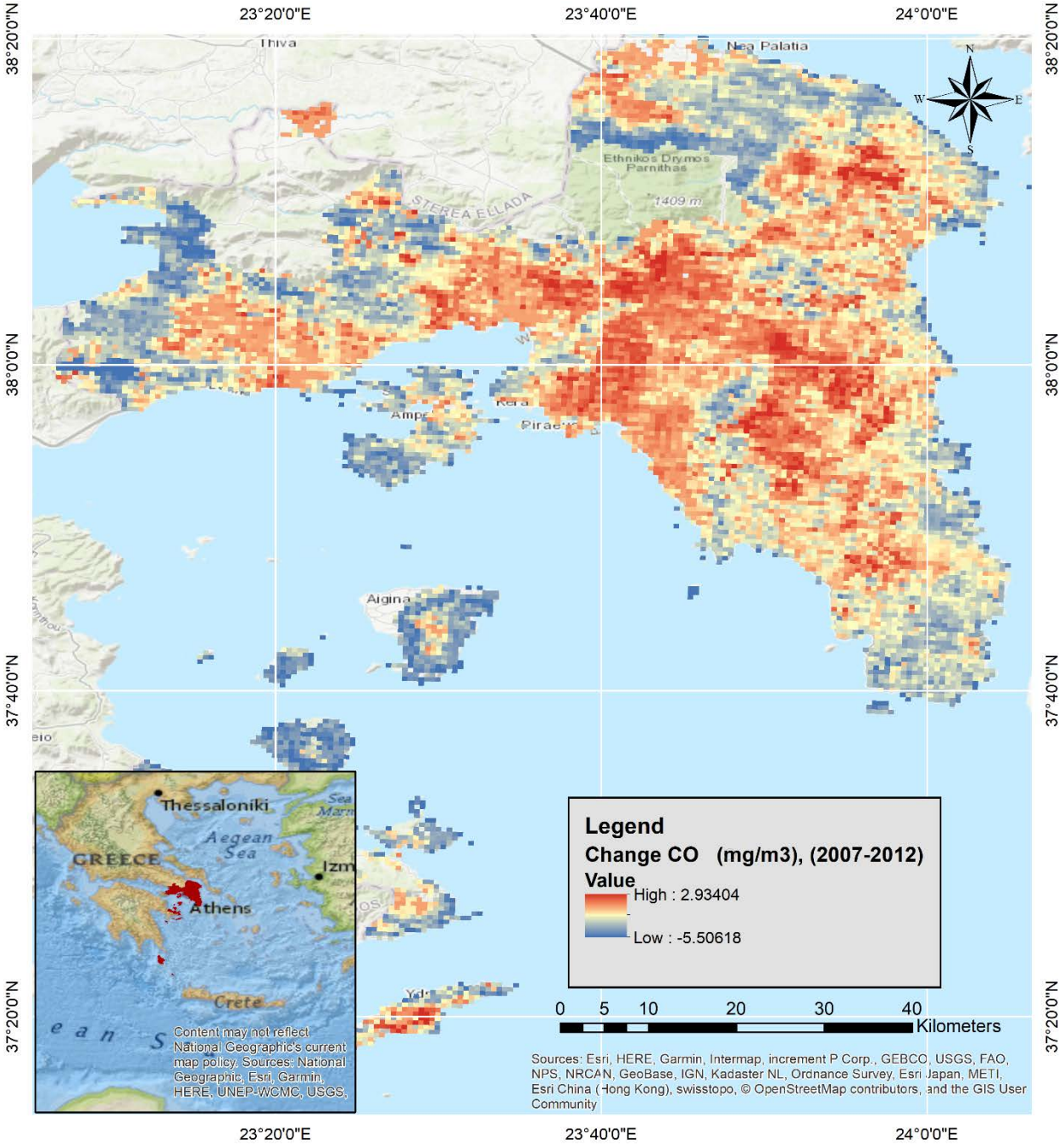

Map 4:7 Change in CO (mg/m^3) concentrations in 2007-2012

NO_2 highest concentrations appear to be generally increasing between 2007 and 2012, with 2011-2012 largest concentrations being 27.5% larger than the corresponding concentrations during 2007-2008. During all three periods, industrialized areas in the south section of West Attica have among the highest observed concentrations, similar to small areas in the south section of East Attica. On the other hand, a large area in the north section and the urban area of Megara in the south section of West Attica, most of the south section and all the north section of Central Attica and extended coastal regions of East Attica present some of the lowest NO_2 concentrations during the three periods.

During 2007-2008, most of the north section and extended areas of the south section of East Attica present low concentrations. A large area in the southwest coastal region of Central Attica exhibits average concentrations for the period.

During 2009-2010, a spike is observed in NO_2 concentrations, with high concentration areas extending substantially in size, mainly in East Attica where most of the north section and almost all the south section present very high concentrations.

In 2011-2012, the north section of East Attica maintains the high concentrations of NO_2 observed during the previous period. The rest of Attica exhibits concentration distributions similar to those observed during 2007-2008, however high and low concentration areas are better defined and segregated. Additionally, the industrialized areas with high concentrations in West Attica seem to reduce slightly in size, as does the average-concentrations area observed in the southwest coastal region of Central Attica's south section.

Aegina and Salamina islands show no dominant trend during both 2007-2008 and 2009-2010. The concentrations' spike of 2009-2010 is still evident, however, with a small increase in the size of areas on the islands with high concentrations. During 2011-2012, both islands present mainly low concentrations with small areas of average concentrations in their southern parts.

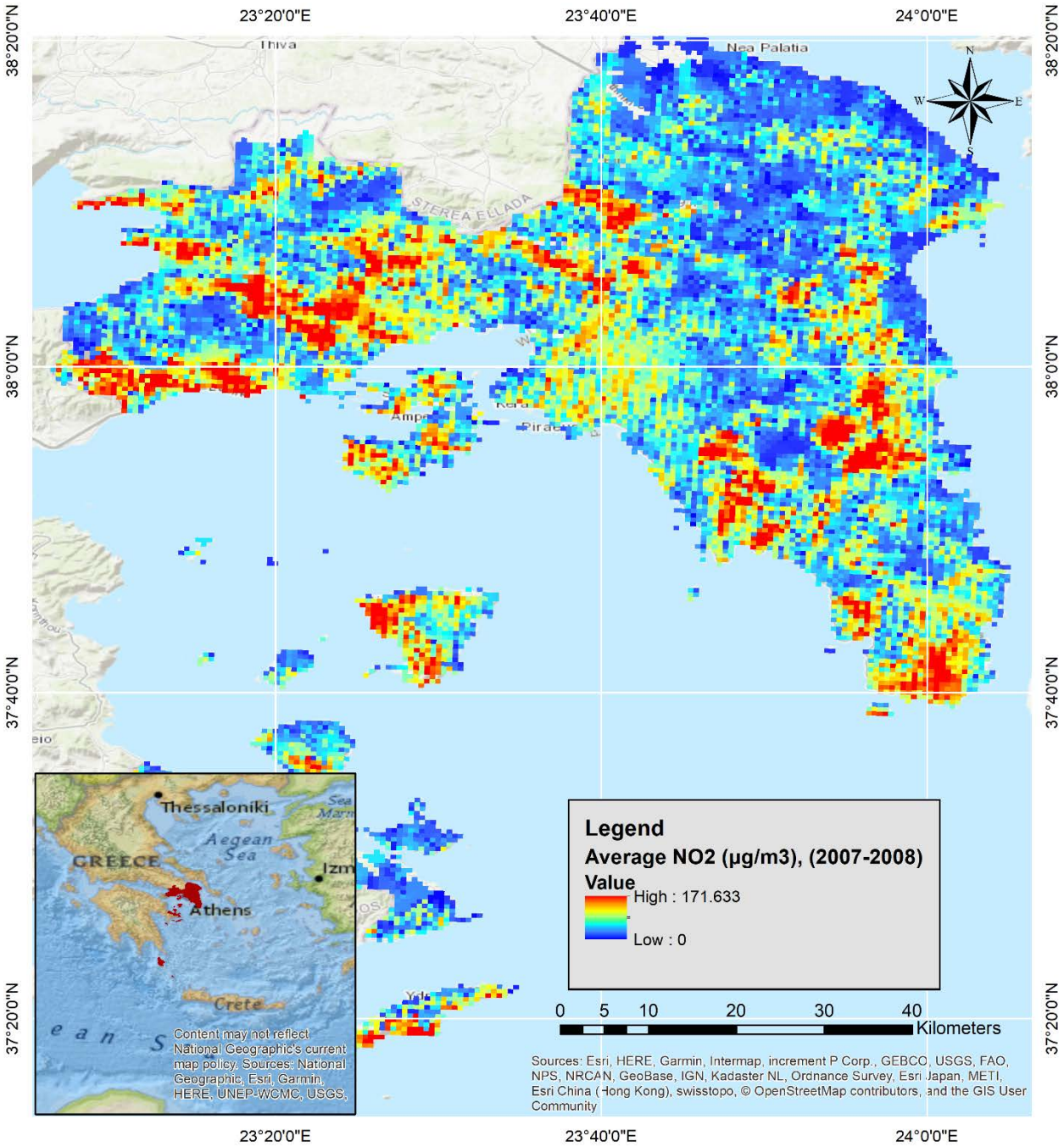

Map 4:8 Average NO_2 (µg/m^3) concentrations in 2007-2008

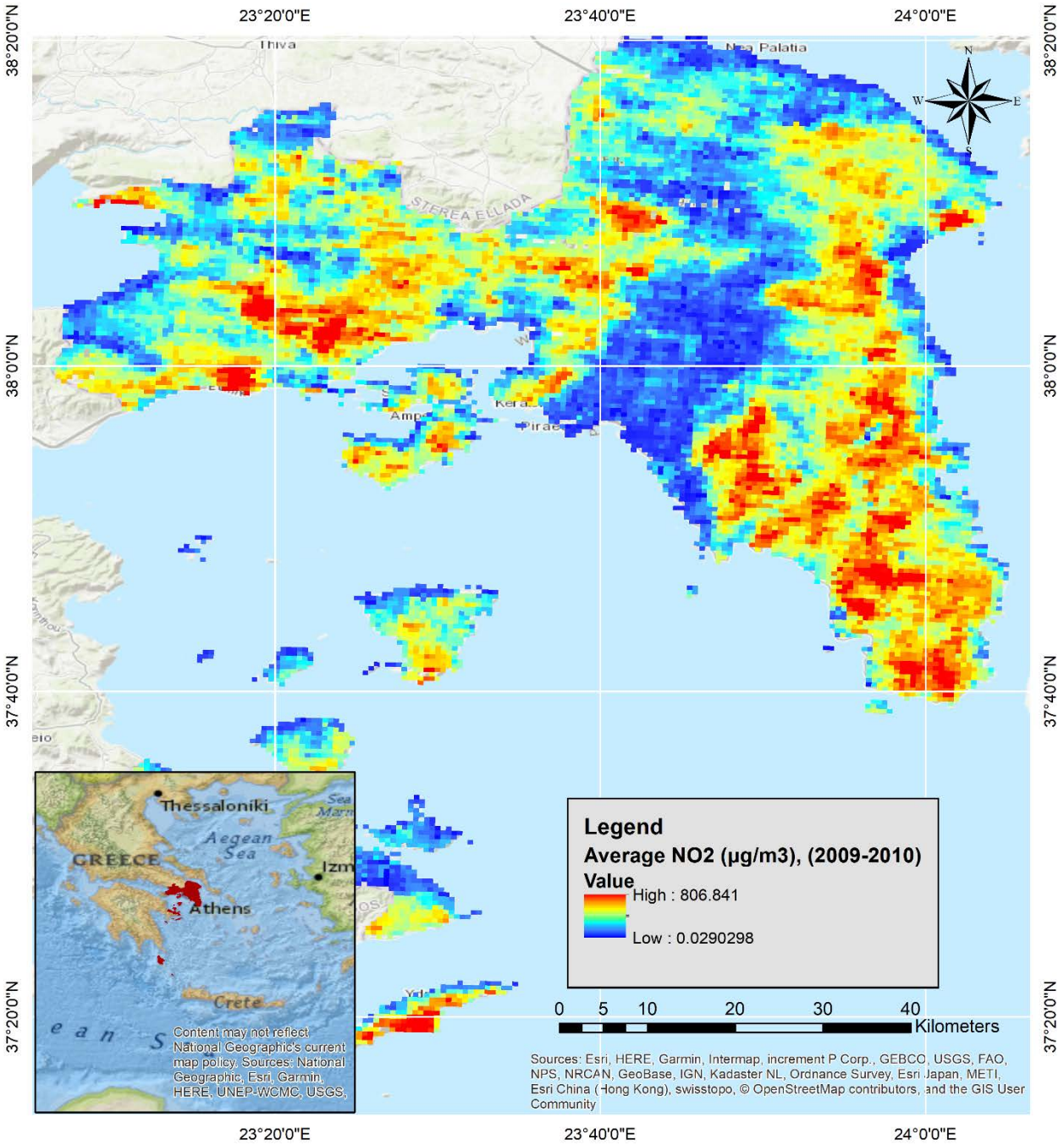

Map 4:9 Average NO_2 (µg/m^3) concentrations in 2009-2010

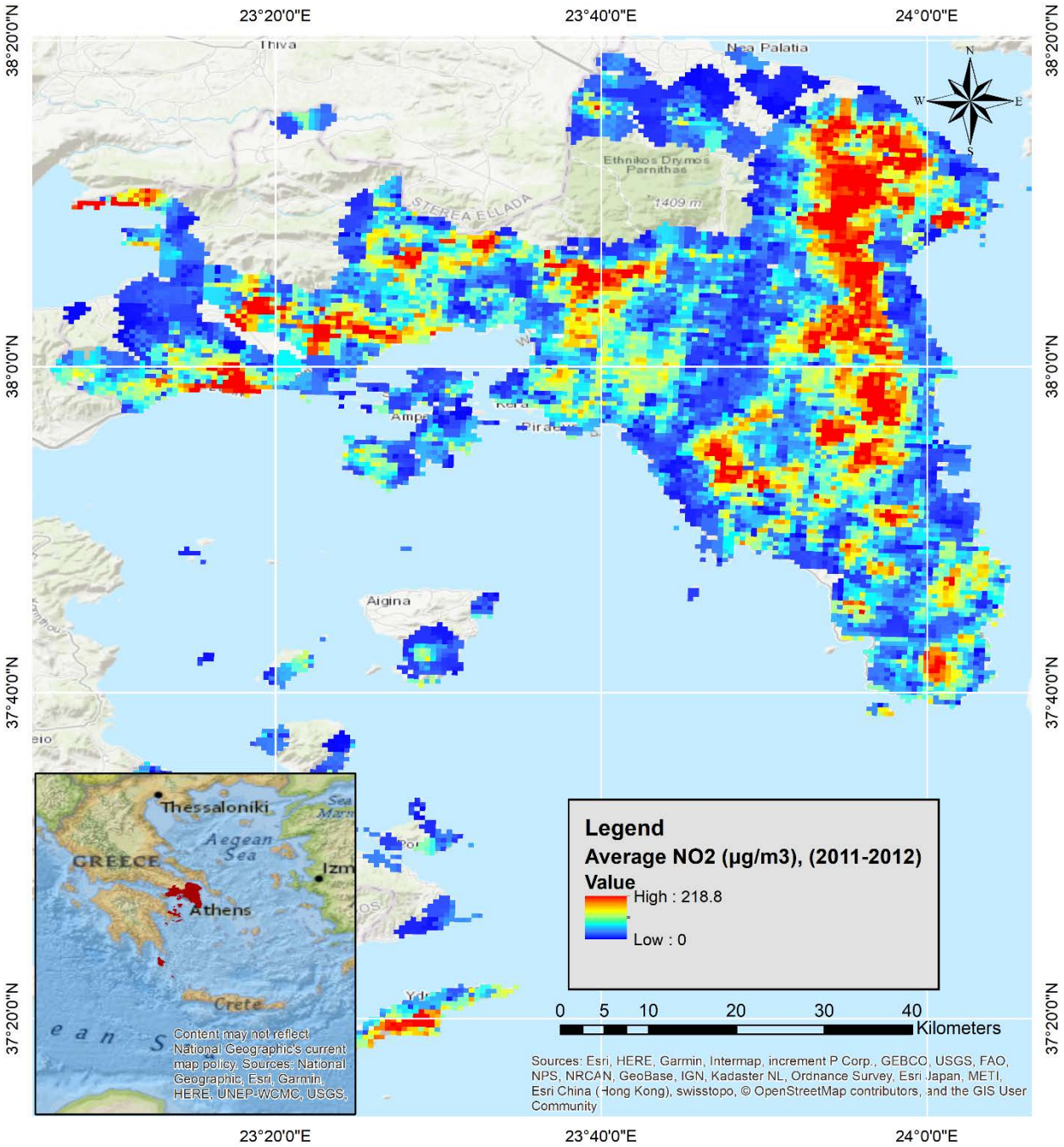

Map 4:10 Average NO_2 (µg/m^3) concentrations in 2011-2012

Between 2007 and 2010, concentrations appear to increase substantially in industrialized areas of the south section and small areas of the north section of West Attica. The highest increase between the periods is observed in almost all the south section and most of the north section of East Attica, Salamina island and most of Aegina Island also exhibit increases in concentrations. On the other hand, most of the north section of West Attica and all Central Attica exhibit decreasing concentrations, similar to extended coastal areas in the north section of East Attica and the north part of Aegina Island. The urban area of Megara, in the south section of West Attica, presents relatively stable concentrations.

During 2009-2012, almost all the previously observed changes in all of Attica appear to reverse, with areas previously presenting decreases now exhibiting increases and the opposite for areas previously presenting increases in concentrations of NO_2. The magnitude of max increase between the two periods is 68.8% of the magnitude of max decrease between 2007-2010, while the magnitude of max decrease in 2009-2012 is 95.2% of the magnitude of max increase in NO_2 concentrations between 2007 and 2010.

Generally, between 2007 and 2012, most of Attica does not exhibit a dominant trend, with small areas of either increasing or decreasing concentrations surrounded by extended areas of relatively stable concentrations. The highest concentration increases are observed mainly in the north section of East Attica and in industrialized areas in the south section of West Attica, which are substantially smaller in size to the corresponding high concentration industrialized areas of West Attica’s south section during the 2007-2008 period. The highest concentration decreases are observed in the north section of West Attica and a large coastal region in the southern boundary of East Attica. Athens's urban area, which takes up most of the south section of Central Attica, exhibits no dominant trend, with extended areas of relatively stable concentrations surrounding very small and isolated between them areas of mildly increasing or decreasing concentrations.

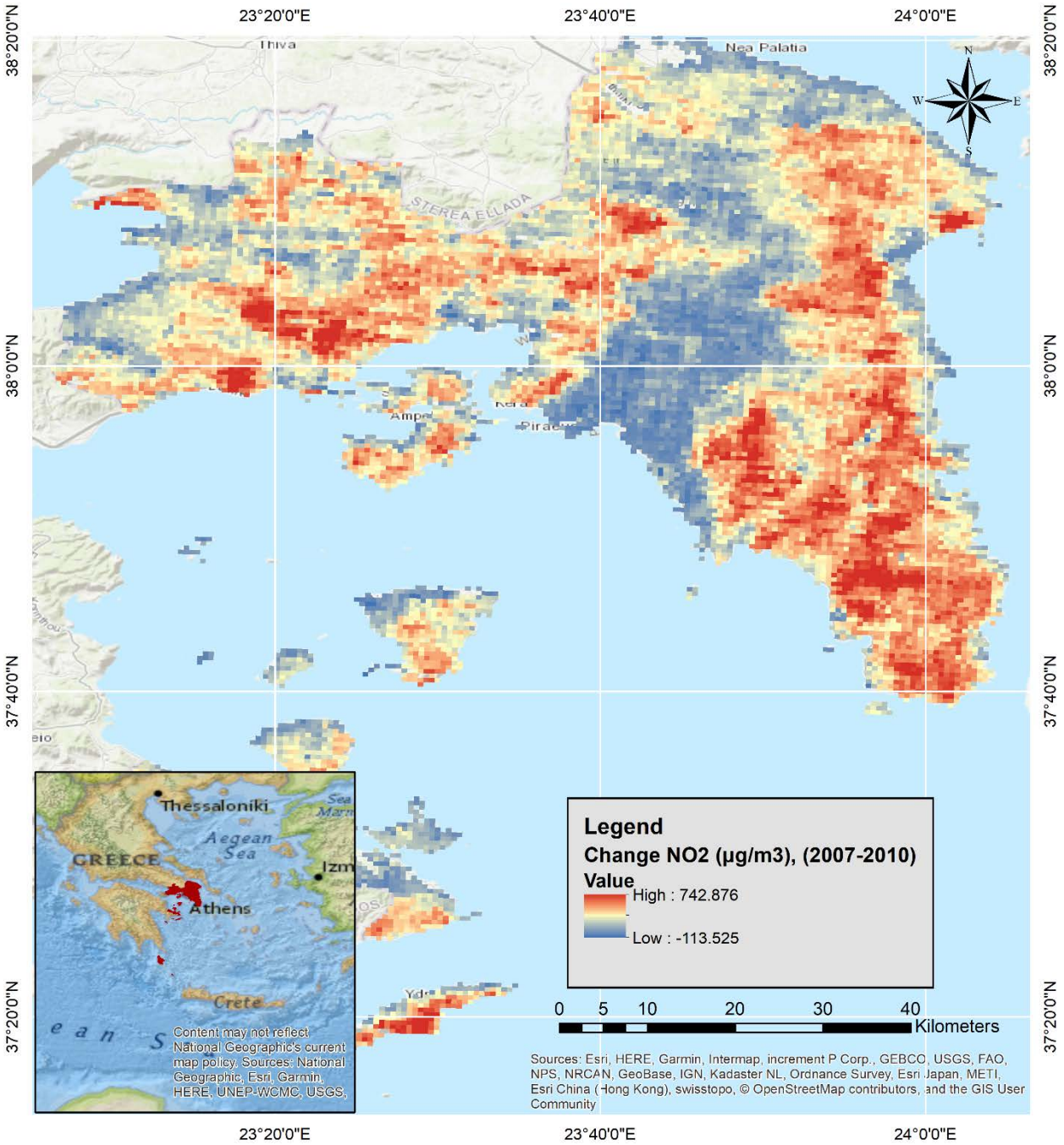

Map 4:11 Change in NO_2 ($\mu g/m^3$) concentrations in 2007-2010

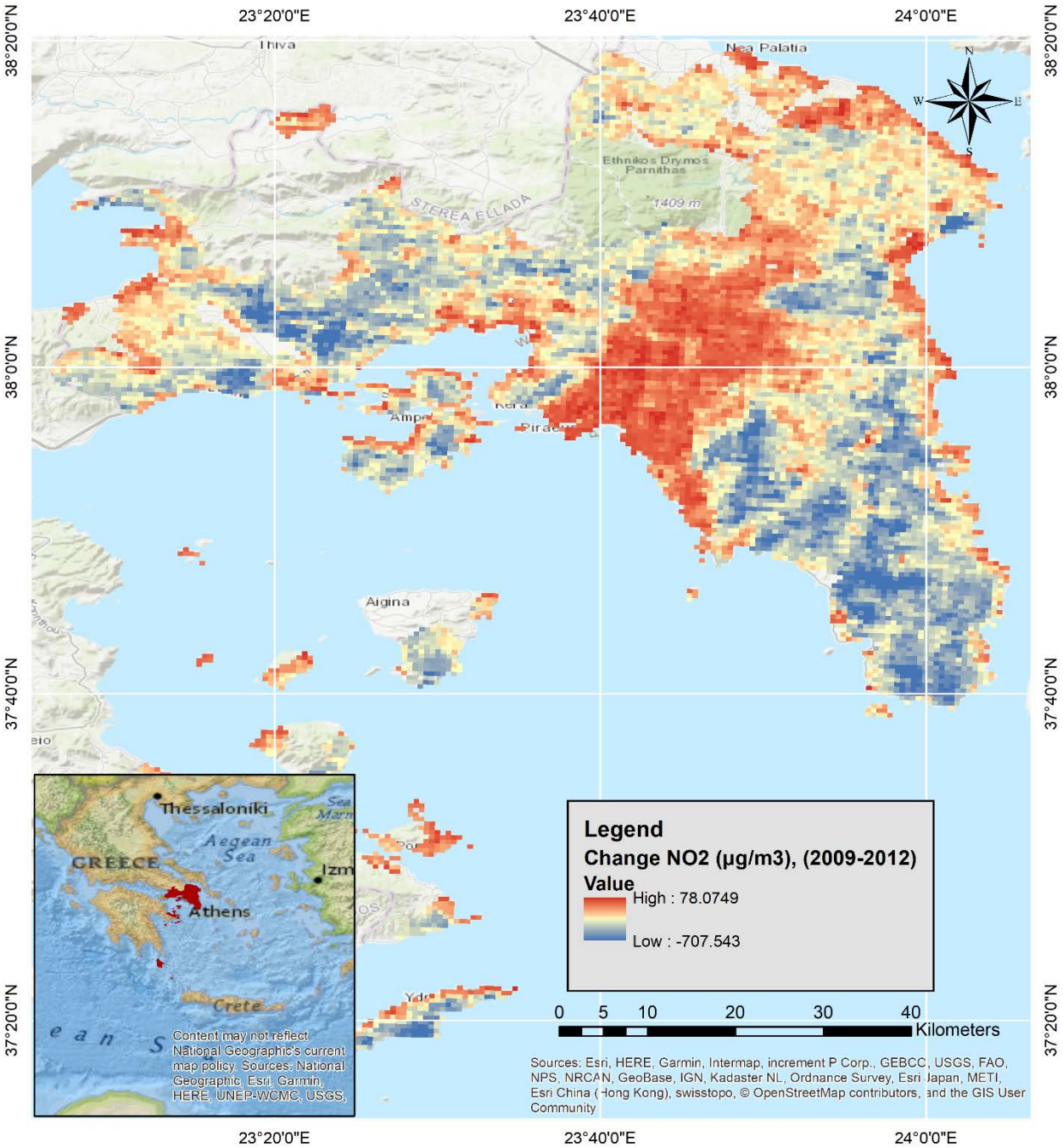

Map 4:12 Change in NO_2 ($\mu g/m^3$) concentrations in 2009-2012

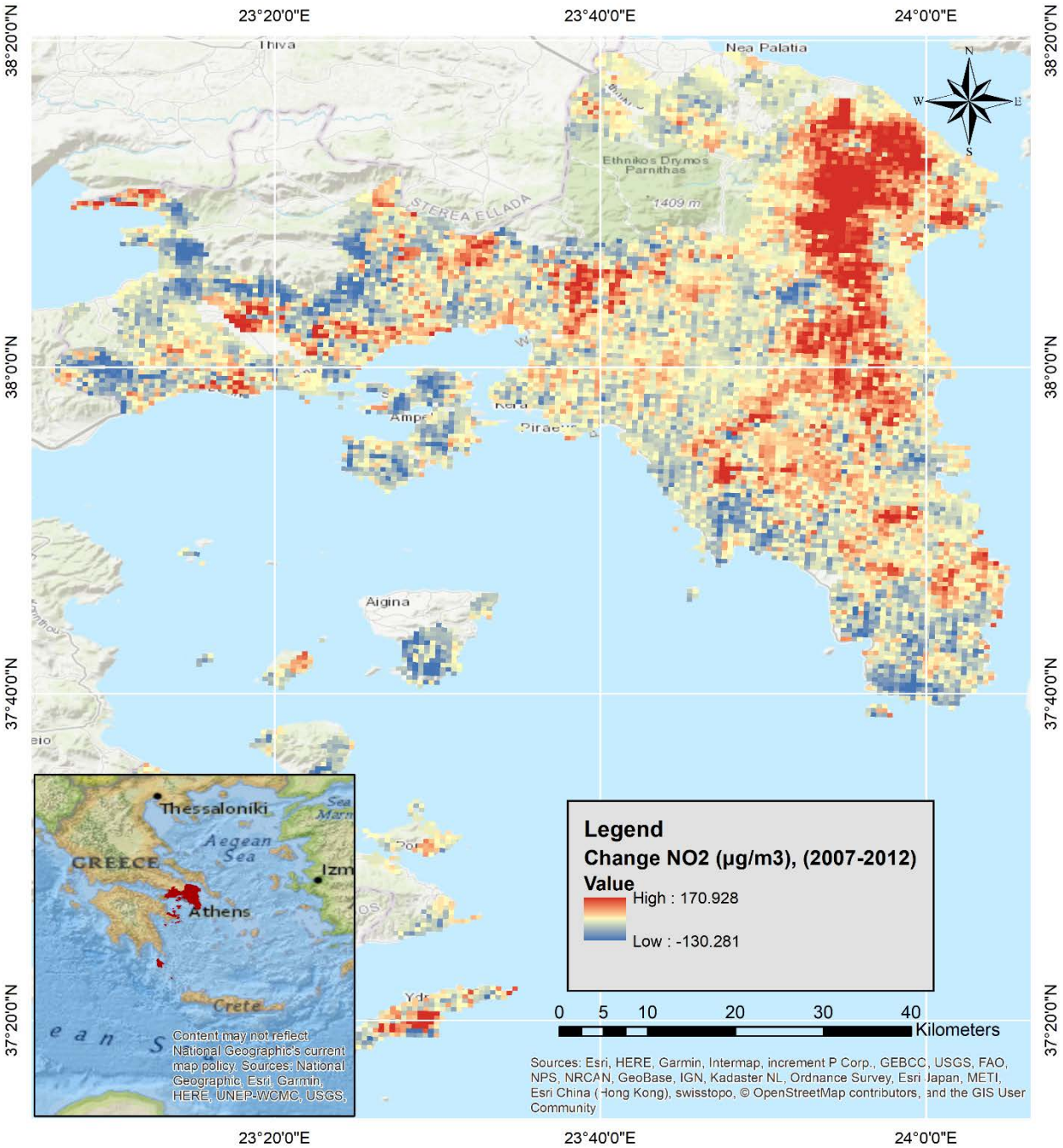

Map 4:13 Change in NO_2 ($\mu g/m^3$) concentrations in 2007-2012

Max SO_2 concentrations remain relatively stable between 2007 and 2012, with 2011-2012 concentrations being just 4% less than the corresponding max concentrations of 2007-2008. Similar to other pollutants, a spike is observed during 2009-2010, with max concentrations being 79% higher than 2007-2008. The south section of Central Attica and coastal areas of East Attica maintain low concentrations throughout all three periods, while large areas in the north sections of West and Central Attica and a small area in the south section of East Attica maintain high concentrations.

During 2007-2008, most of the north section and industrialized areas in the south section of West Attica exhibit a mixture of stable and high concentration areas, while the rest of West Attica presents low concentrations. The north section of Central Attica exhibits two distinct areas, one having the highest concentrations while the other having the lowest ones for the period. Almost all the south section of Central Attica exhibits low concentrations, which are closer to average compared to other areas. East Attica exhibits mostly low concentrations, however multiple small areas and a large one in the south boundary present average and high concentrations. Finally, both Salamina and Aegina islands present no dominant trend, with areas of both decreasing and increasing concentrations.

During 2009-2010, the highest concentrations for the period are observed in the southern sections of West and East Attica. Large areas in the north sections of all Attica also exhibit lower but still high concentrations, similar to most of Salamina and Aegina islands. The remaining areas of the northern sections, a large area in the westmost boundary of West Attica's south section, and most of the south section of Central Attica exhibit low concentrations, with the latter exhibiting the lowest for the period.

During 2011-2012, most of Attica exhibits low concentrations. Very large areas in the north sections of West and Central Attica exhibit the highest concentrations for the period, while the Megara urban area in the south section of West Attica exhibits high concentrations of smaller magnitude, the lowest concentrations for the period are observed in a large area in the westmost boundary of West Attica. Finally, multiple areas in the south section of East Attica present average concentrations for the period.

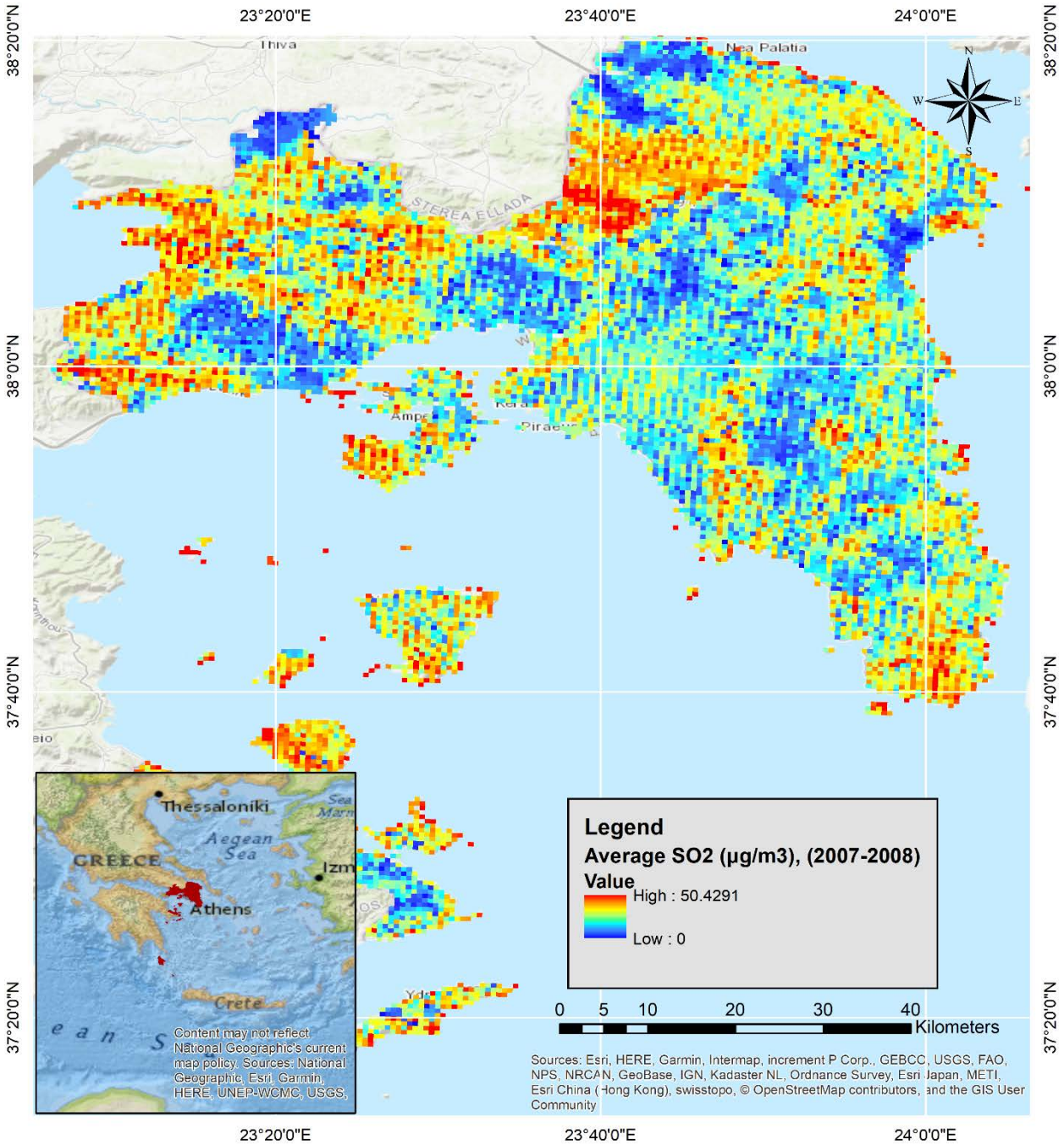

Map 4:14 Average SO_2 (µg/m^3) concentrations in 2007-2008

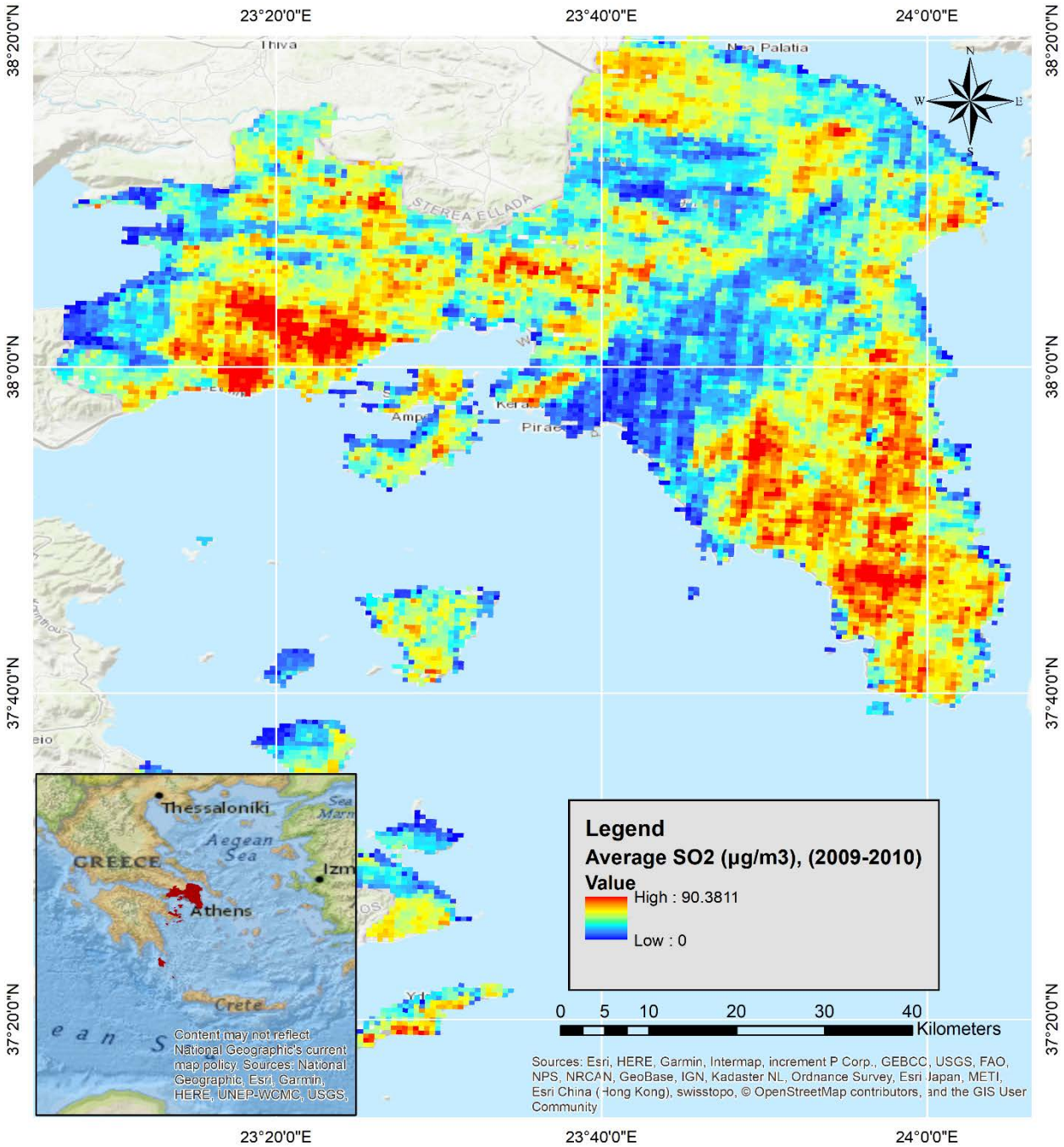

Map 4:15 Average SO_2 (µg/m^3) concentrations in 2009-2010

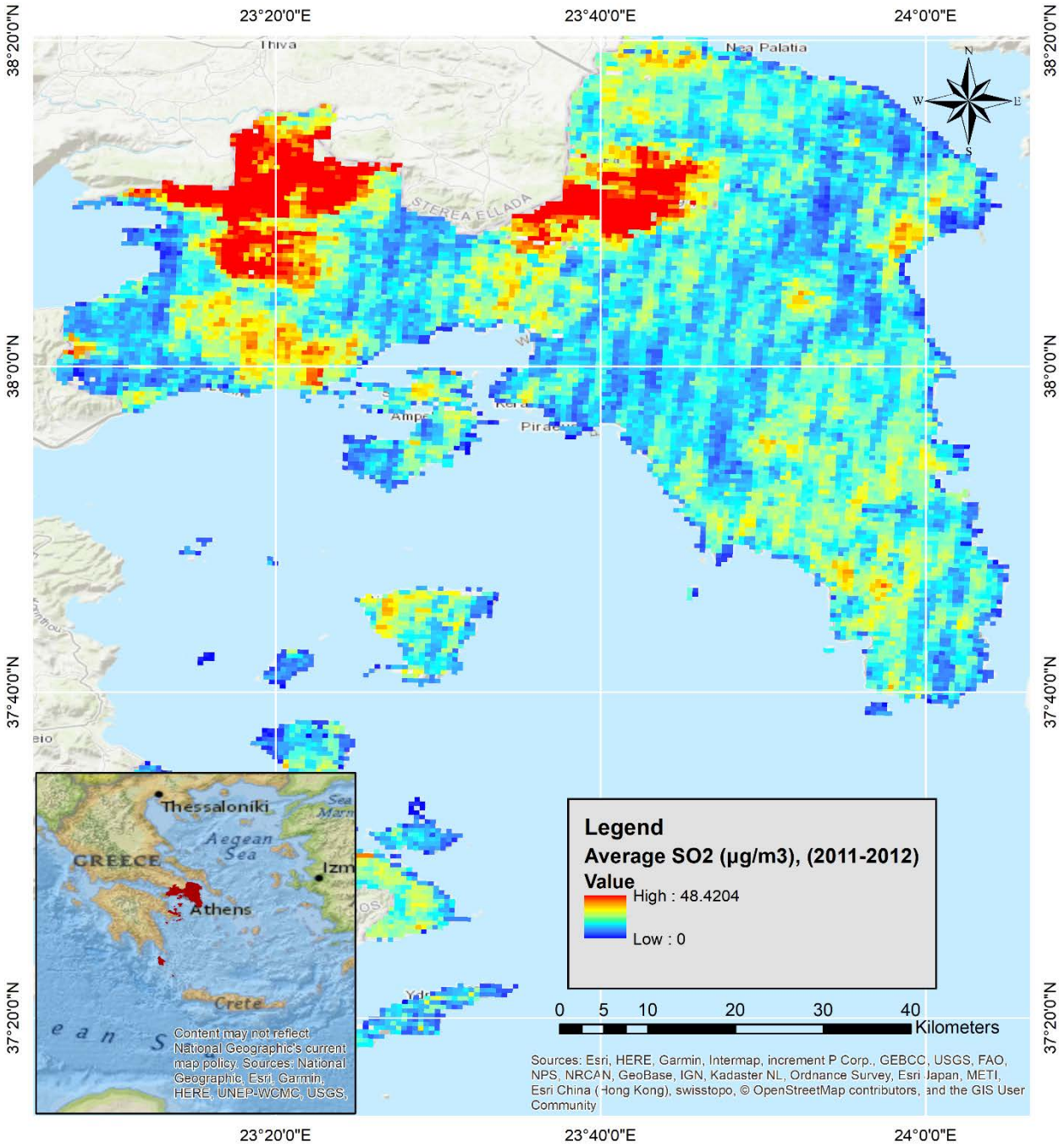

Map 4:16 Average SO_2 (µg/m^3) concentrations in 2011-2012

Between 2007 and 2010, the highest concentration increases of SO_2 are observed in most of the south section of West Attica and almost all the south section of East Attica. Large areas in the north sections of Attica also exhibit increases of SO_2 concentrations, with smaller magnitudes. The highest concentration decrease between the periods is observed in a very large area in the westmost boundary of West Attica, extending in both the north and the south section. Extended areas in the north section of West Attica, almost all the south section and a large area in the north section of Central Attica, small areas in the north section, and limited coastal areas of East Attica also exhibit decreases of lower magnitude. Both Salamina and Aegina islands show no dominant trends between the periods, with the first island presenting slightly more areas of increasing concentrations than the second.

Between 2009-2012, concentration changes are almost reversed. The highest concentration increases between the periods are observed in very large areas in the north sections of West and Central Attica. Almost all the south section of Central Attica, small areas in the north section of East Attica, and a large area in the westmost boundary of the south section of West Attica also exhibit increases, but of lower magnitude. The highest concentration decreases between the periods are observed in almost all the south sections of West and East Attica, while small areas in the north sections of Attica also exhibit lower magnitude decreases. Finally, both Salamina and Aegina islands continue to exhibit no dominant trend.

Generally, between 2007-2012, the highest concentration increases are observed in industrialized areas of the south section of West Attica and almost all the north section of East Attica. Large areas in the north section of West Attica and the south section of East Attica also exhibit increases with smaller magnitude. Almost all Central Attica exhibits decreasing concentrations with large areas of stable concentrations in the south section. The highest decreases are observed in the Megara urban area of West Attica and small areas in the boundary between the south and the north sections of Central Attica. Small areas in the south section of East Attica and the north section of West Attica also exhibit lower magnitude decreases. Aegina island exhibits mainly decreases in SO_2 concentrations, however Salamina island does not exhibit a dominant trend.

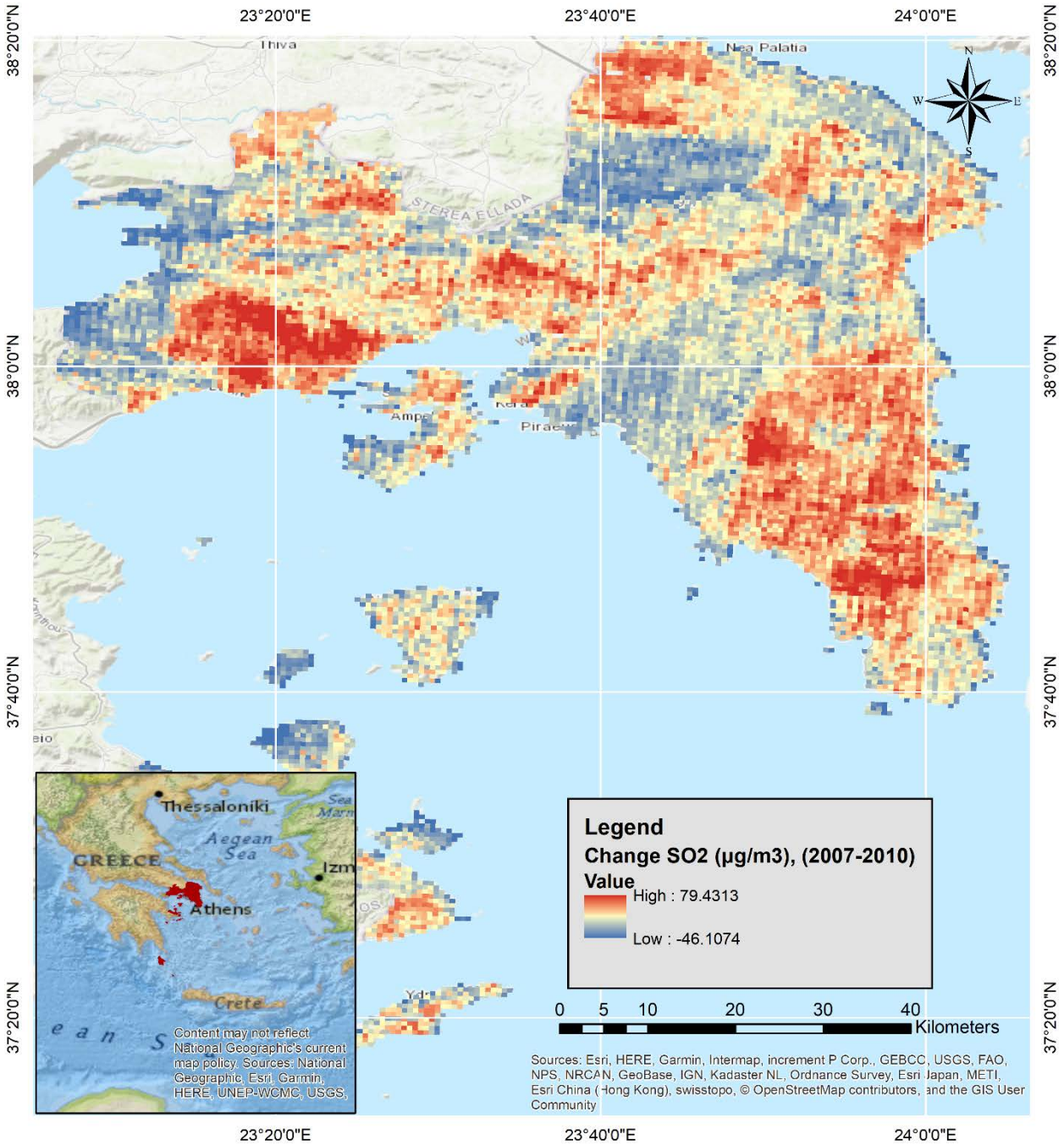

Map 4:17 Change in SO_2 (µg/m^3) concentrations in 2007-2010

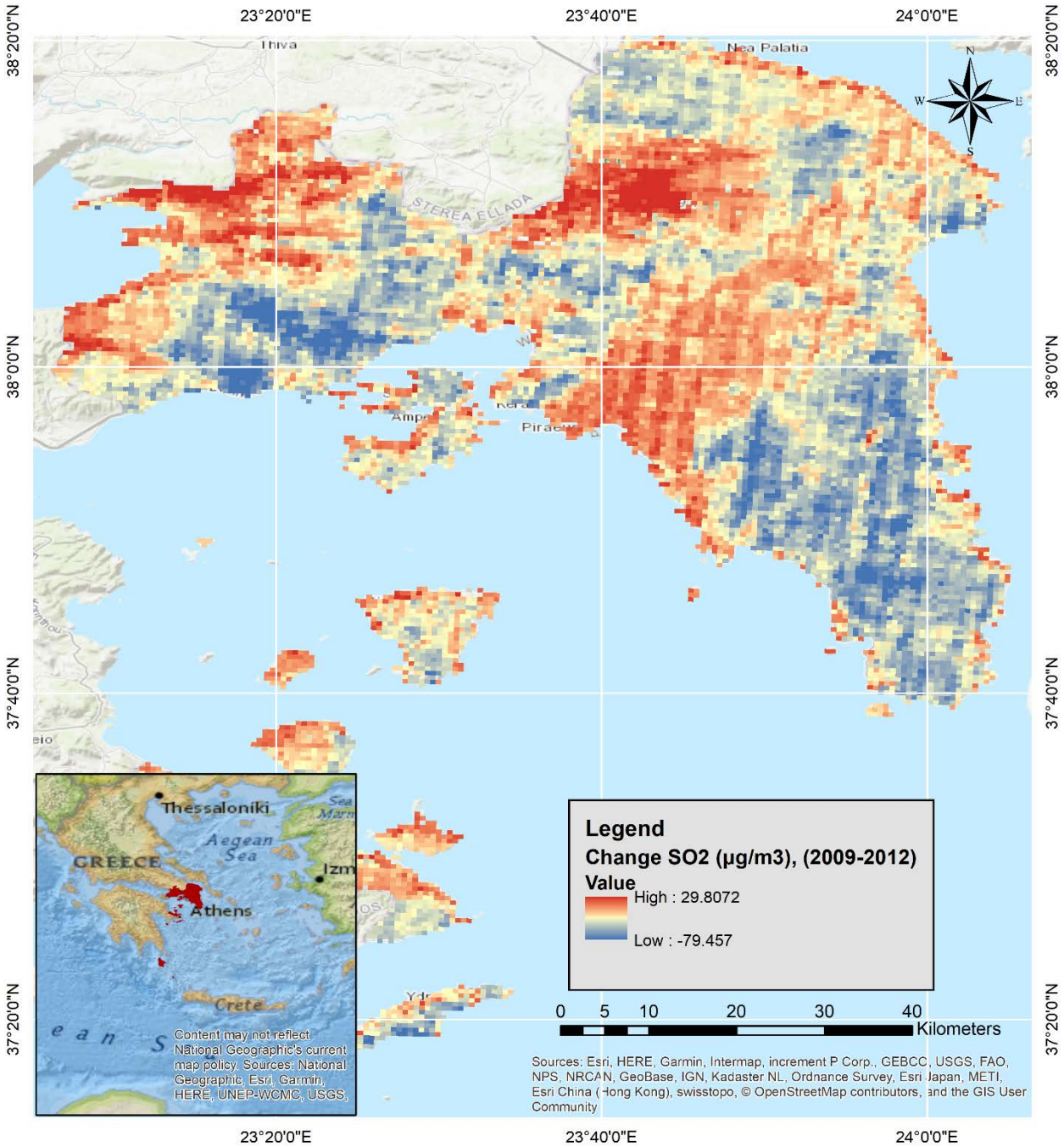

Map 4:18 Change in SO_2 ($\mu g/m^3$) concentrations in 2009-2012

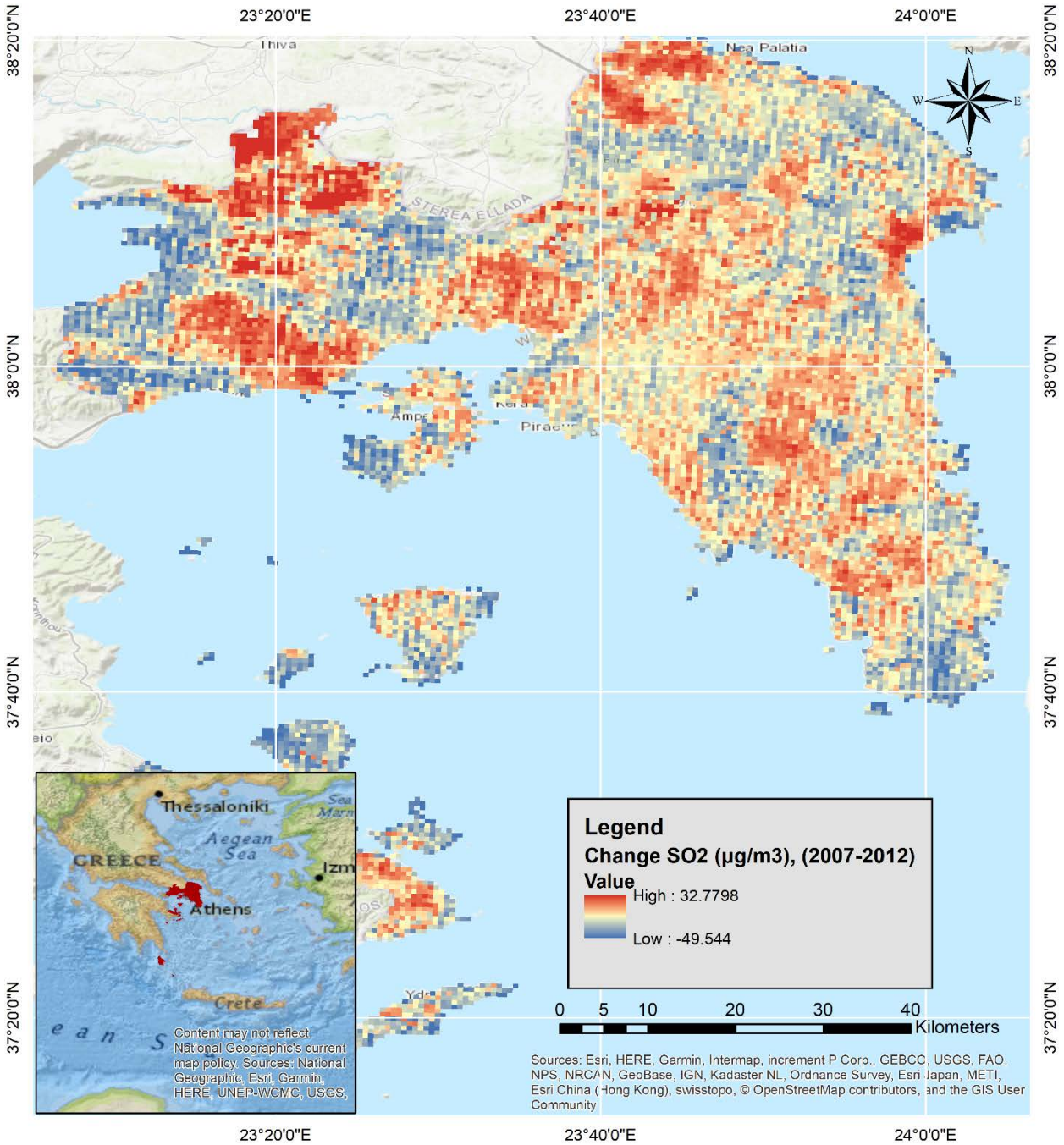

Map 4:19 Change in SO_2 (µg/m^3) concentrations in 2007-2012

Max PM_{10} concentrations, unlike other pollutants, fluctuate much less between periods. The general trend is positive, with 2011-2012 concentrations being 31.2% higher than corresponding concentrations in 2007-2008, while 2009-2010 concentrations are 28,2% lower. No area maintains high or low concentrations constantly through 2007-2012.

During 2007-2008, high concentrations are observed mainly in the south sections of Attica, with industrialized areas and Megara urban area in West Attica, almost all the south section of Central Attica, and small areas in the south section of East Attica. The highest concentrations for the period are observed in small areas between the north and south sections of West and Central Attica, while the remaining high concentrations areas in the south sections have relatively lower but still high concentrations. The south section of East Attica only shows very small areas of high concentrations, surrounded by extended areas of average for the period concentrations. All north sections of Attica exhibit low concentrations during the period, similar to the rest of the south sections of West and Central Attica, and multiple areas of various sizes in the southern sections of East Attica. Most of the Salamina and Aegina islands also present low concentrations.

During 2009-2010, high concentrations are observed mainly in Central Attica, with the highest concentrations for the period observed in the north section. Other areas with high concentrations are observed in small areas of the north section of West Attica and coastal areas of East Attica. Almost all East Attica and the south section of West Attica exhibit low concentrations, similar to Salamina and Aegina islands.

During 2011-2012, high concentrations are observed in industrialized areas of West Attica's south section, almost all the north section and large areas of the south section of East Attica, and a small area in the north section of West Attica. Megara urban area and most of the north section of West Attica, almost all Central Attica, coastal areas, and other small areas of East Attica exhibit low concentrations during the period similar to Aegina and Salamina islands.

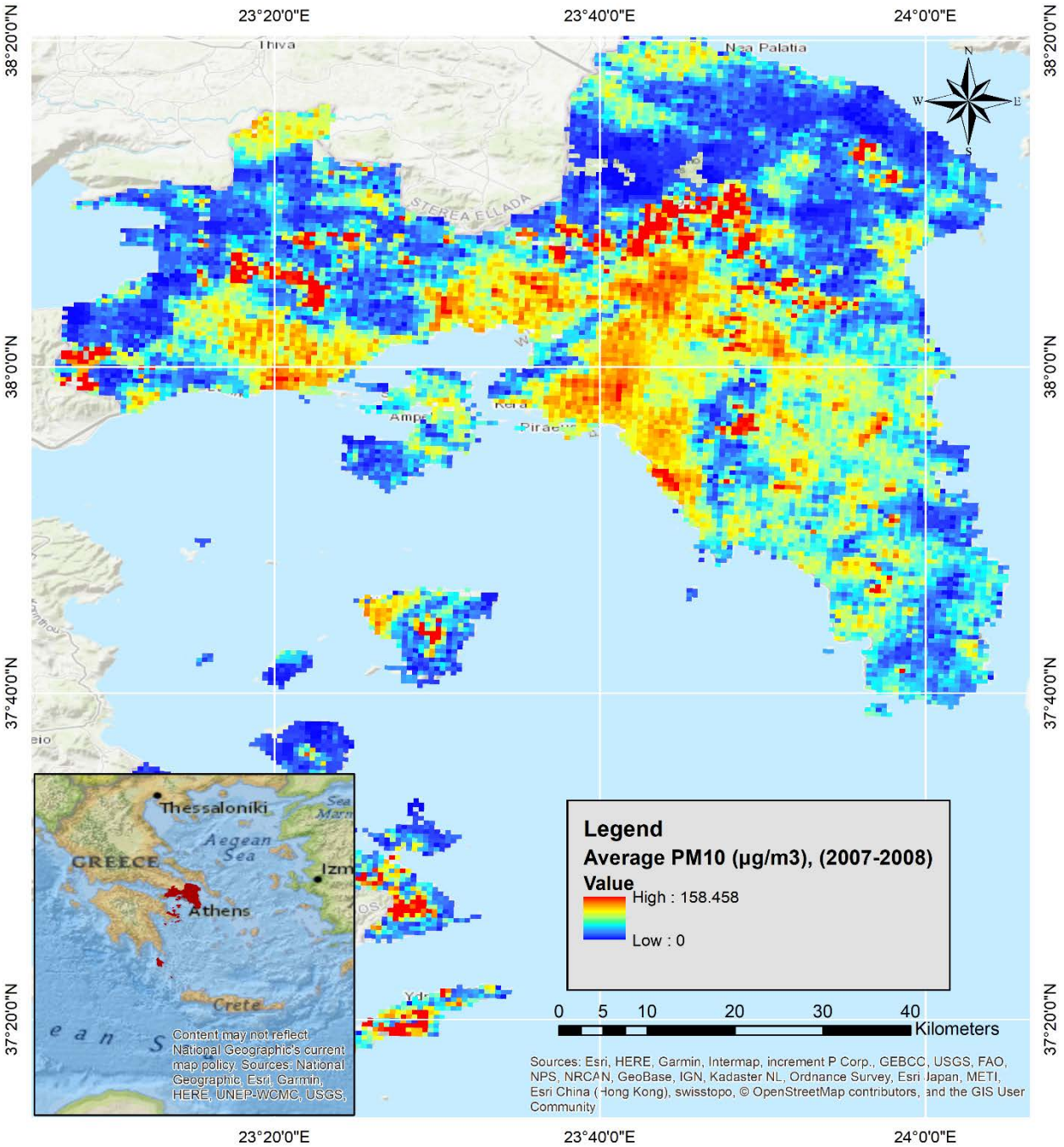

Map 4:20 Average PM_{10} ($\mu g/m^3$) concentrations in 2007-2008

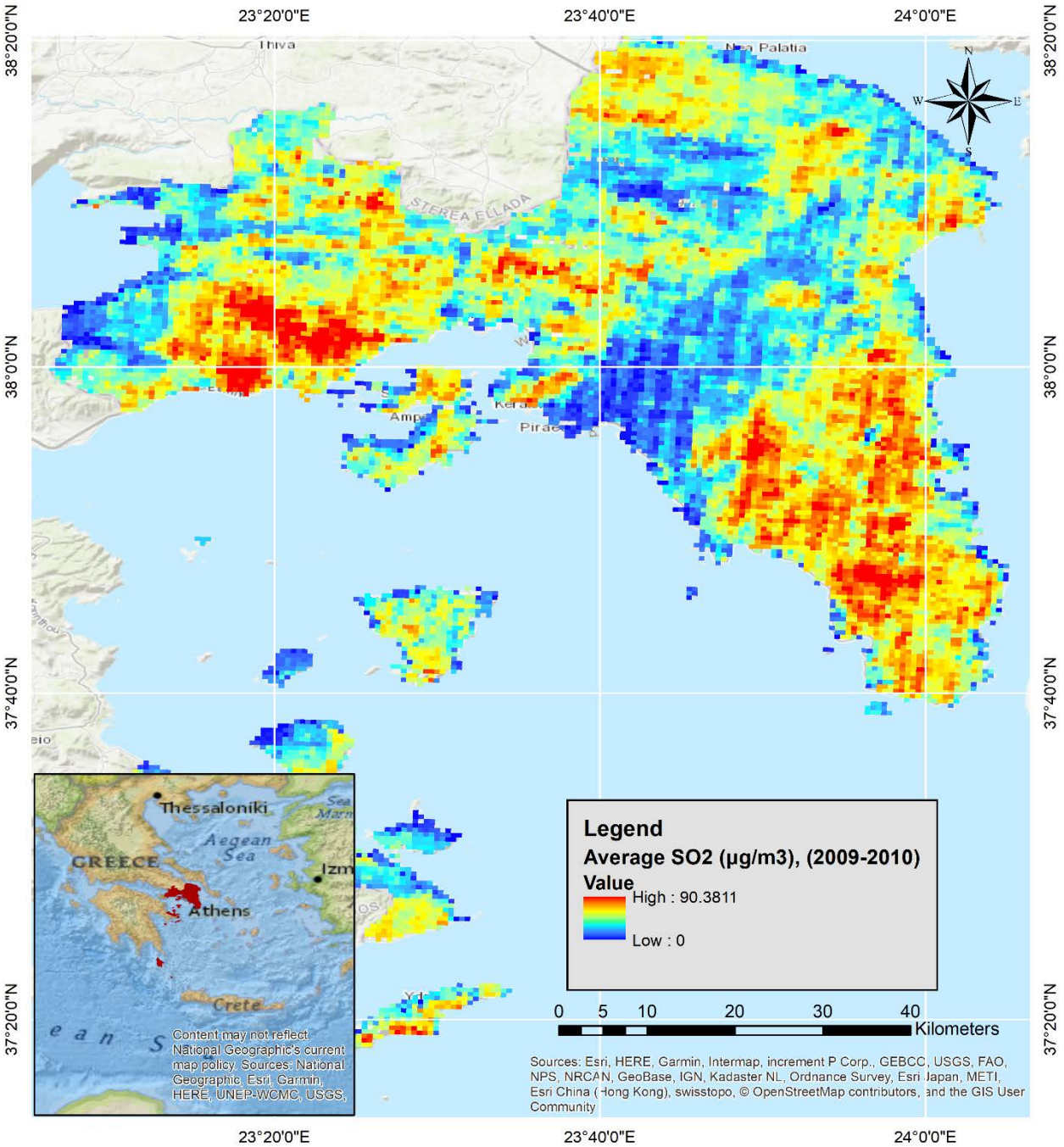

Map 4:21 Average PM_{10} (µg/m^3) concentrations in 2009-2010

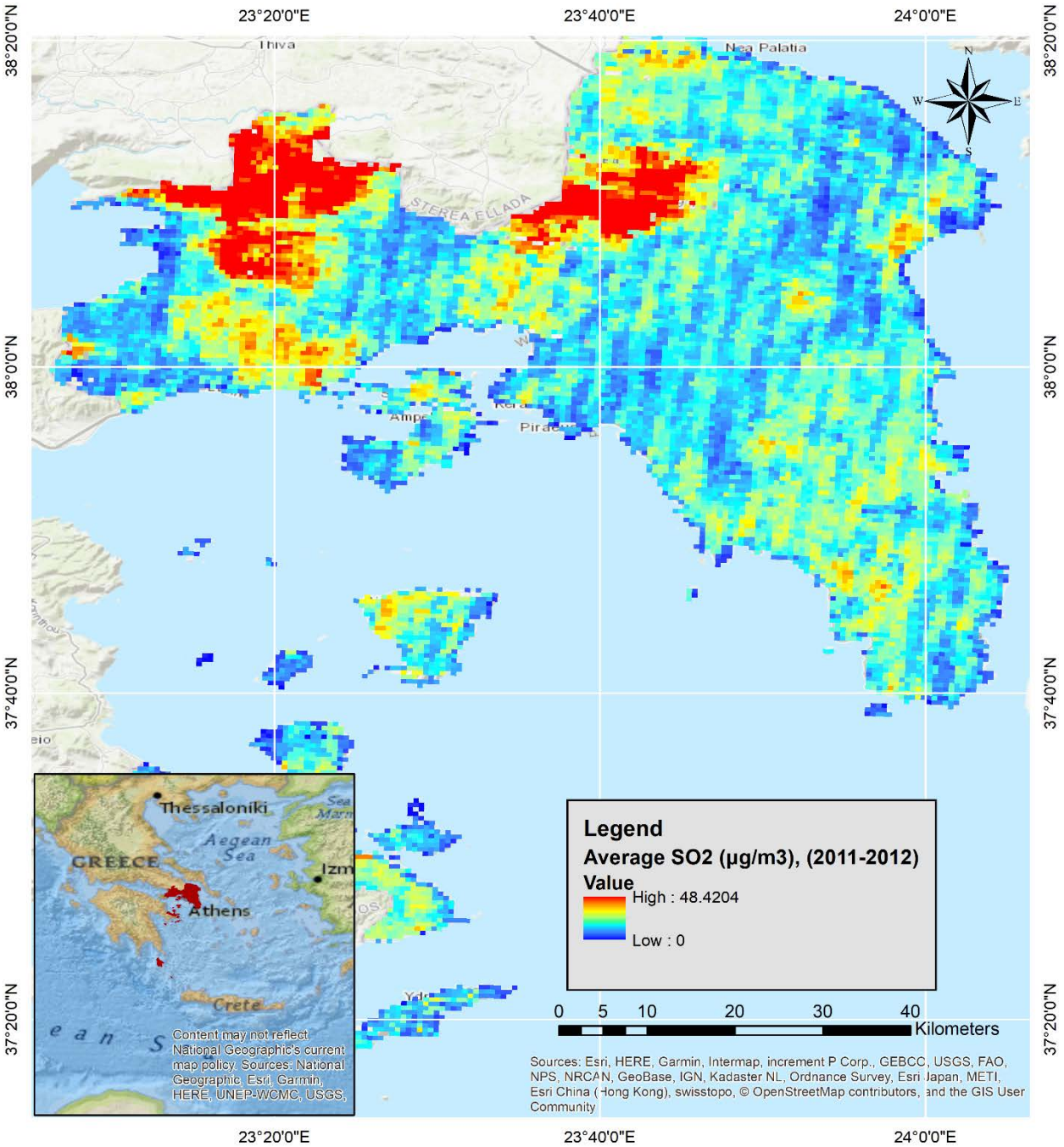

Map 4:22 Average PM_{10} ($\mu g/m^3$) concentrations in 2011-2012

Between 2007 and 2010, the highest increases and decreases in concentrations are observed in the north sections of West and Central Attica. Increases of PM_{10} concentrations are mainly observed in the north sections of West and Central Attica, a large area in the boundary of Central and East Attica, and coastal areas of East Attica. On the other hand, the south sections of West and Central Attica, and most of East Attica exhibit low concentrations with multiple small areas of stable concentrations. Both Salamina and Aegina islands exhibit no dominant trends, with small areas exhibiting either decreases, increases, or stable concentrations.

Between 2009 and 2012, changes almost reverse, with most areas previously exhibiting decreases now presenting increases and the opposite for areas previously exhibiting increases. Megara urban area is the only area that maintains a decreasing trend both during 2007-2010 and during 2009-2012. Salamina island again exhibits no dominant trend, however Aegina Island now exhibits mainly a small decreasing trend during 2009-2012.

Generally, between 2007 and 2012, changes in concentrations are almost identical to those between 2009-2012. The highest increases of concentrations are observed in industrialized areas of the south section of West Attica, most of the north section, and large areas of the south section of East Attica. Most of the north section of West Attica, almost all Central Attica, multiple small areas in the south section of East Attica, and most of Aegina Island present decreases of concentrations. Salamina island generally presents no dominant trend, with small exhibiting increases, decreases, or stable concentrations.

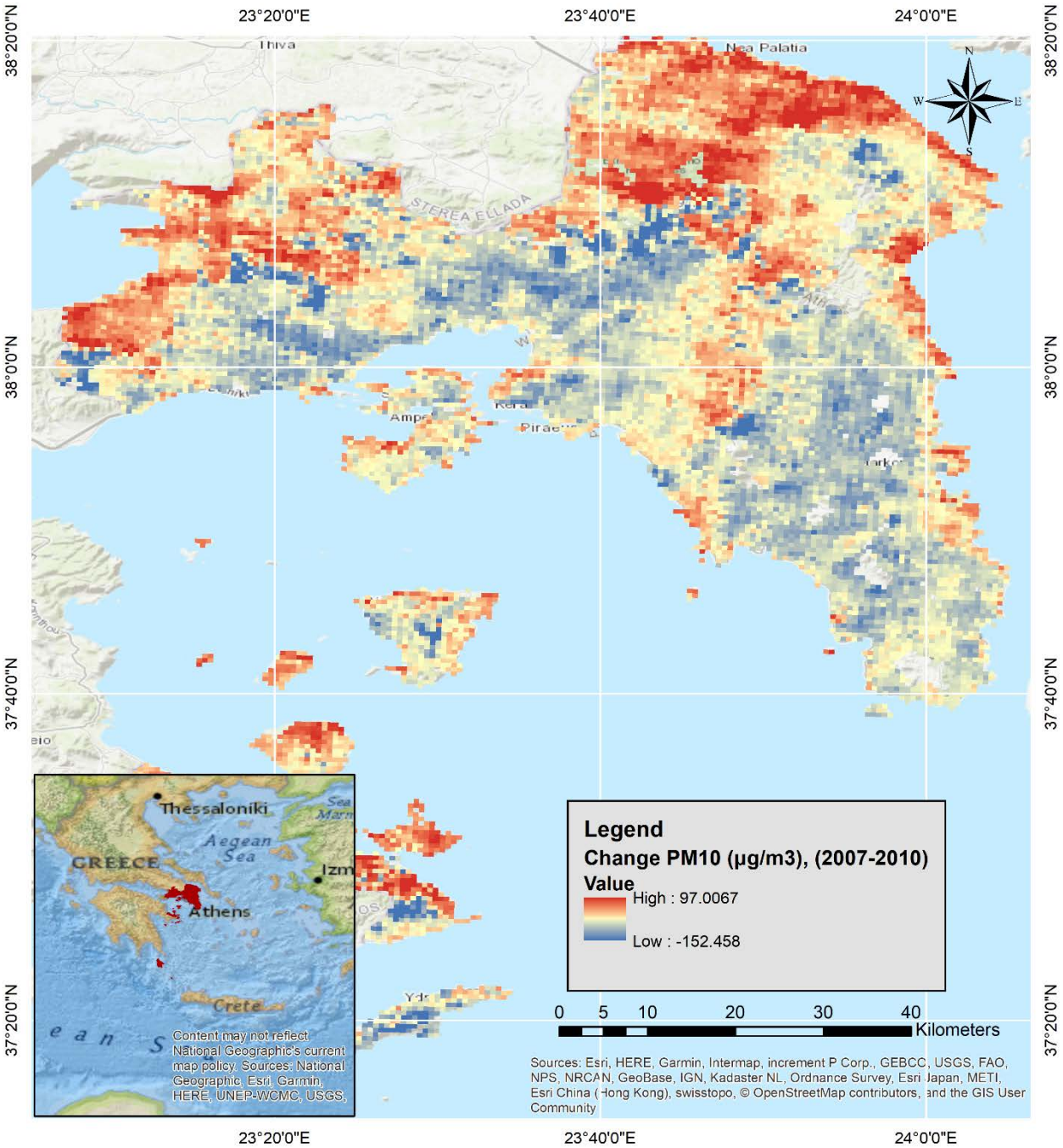

Map 4:23 Change in PM_{10} ($\mu g/m^3$) concentrations in 2007-2010

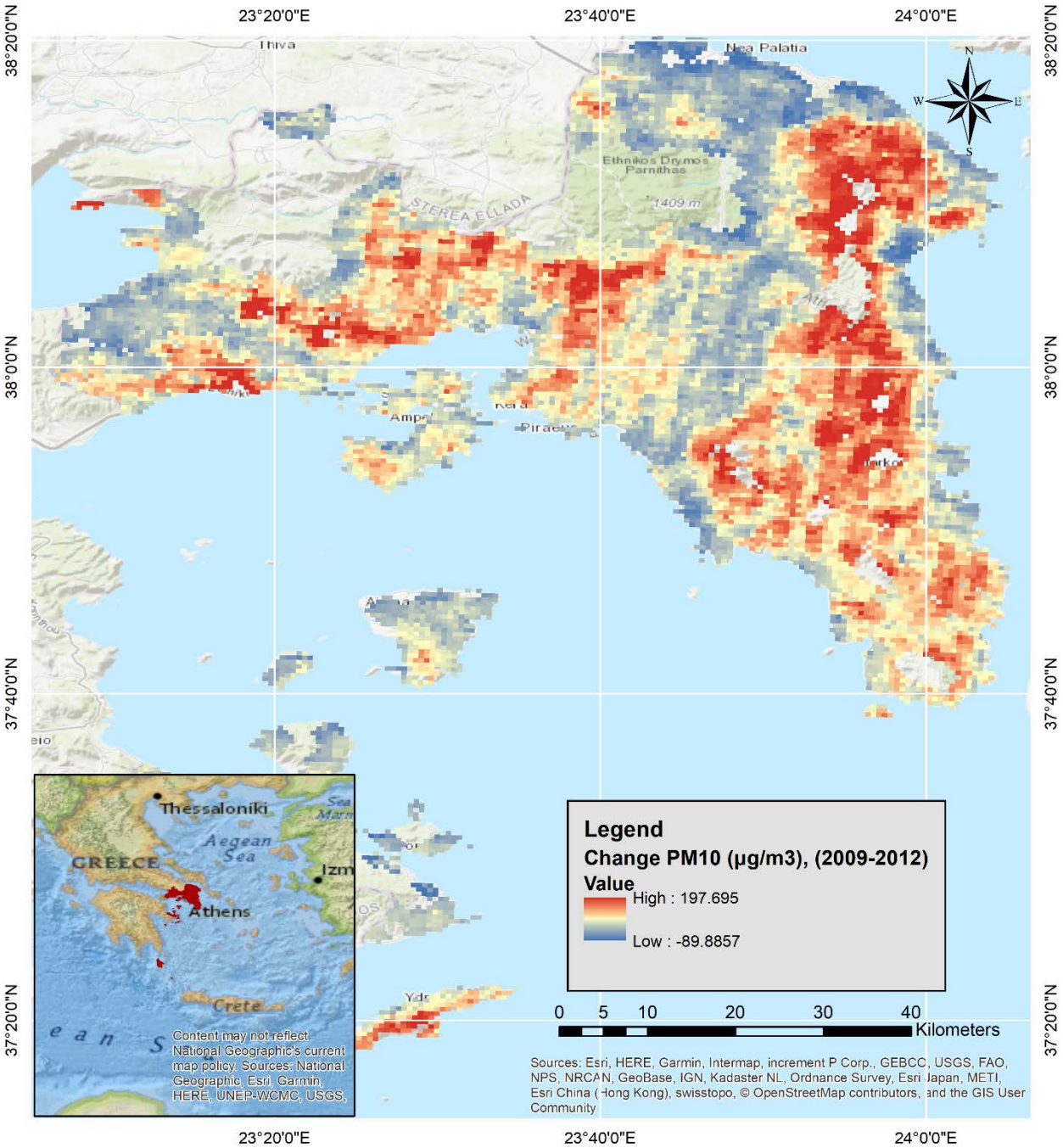

Map 4:24 Change in PM_{10} ($\mu g/m^3$) concentrations in 2009-2012

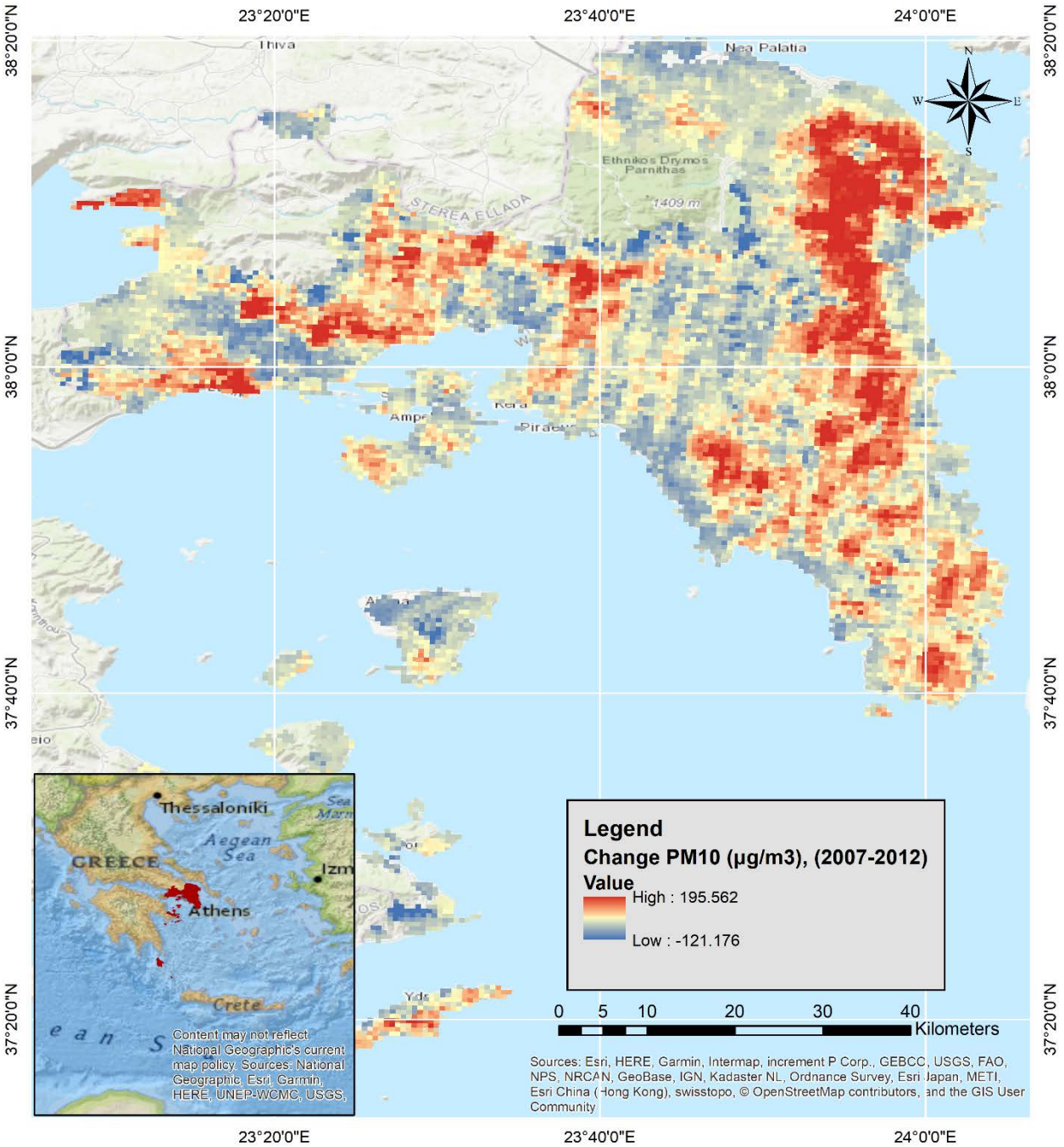

Map 4:25 Change in PM_{10} ($\mu g/m^3$) concentrations in 2007-2012

4.4. Association between Heating Systems and pollutants' ratios

Between 2007 and 2010, the dominant trend in petrol consumption of urban areas in Attica is decrease. Multiple areas of various sizes around Attica present this trend, such as very large areas in the center of Athens and its northern and southern suburbs and smaller areas in the western suburbs and urban areas of East Attica. Only small areas exhibit increases in petrol consumption, mainly located in the west suburbs of Athens and East Attica, where they are surrounded by extended areas of no significant change.

Between 2009 and 2012, the dominant trend remains the same, with almost all of Athens and its suburbs exhibiting decreases in petrol consumption. Only small areas exhibit increases in consumption, however between these two periods they are located mainly in coastal areas of the southern suburbs of Athens and East Attica while being almost absent in the west suburbs of Athens. Again, areas of increases in consumption are surrounded by areas of no significant change.

Generally, almost all of Attica exhibits a decrease in petrol consumption throughout 2007-2012 with very few areas, located mainly in the coastal boundaries of East Attica and the southern suburbs of Athens, exhibiting increases in petrol consumption. Locations with no significant change are also few and isolated, located mostly in East Attica. A relatively extended area with no observable change between 2007 and 2012 is also located in the center of Athens, surrounded by areas of decreasing consumption.

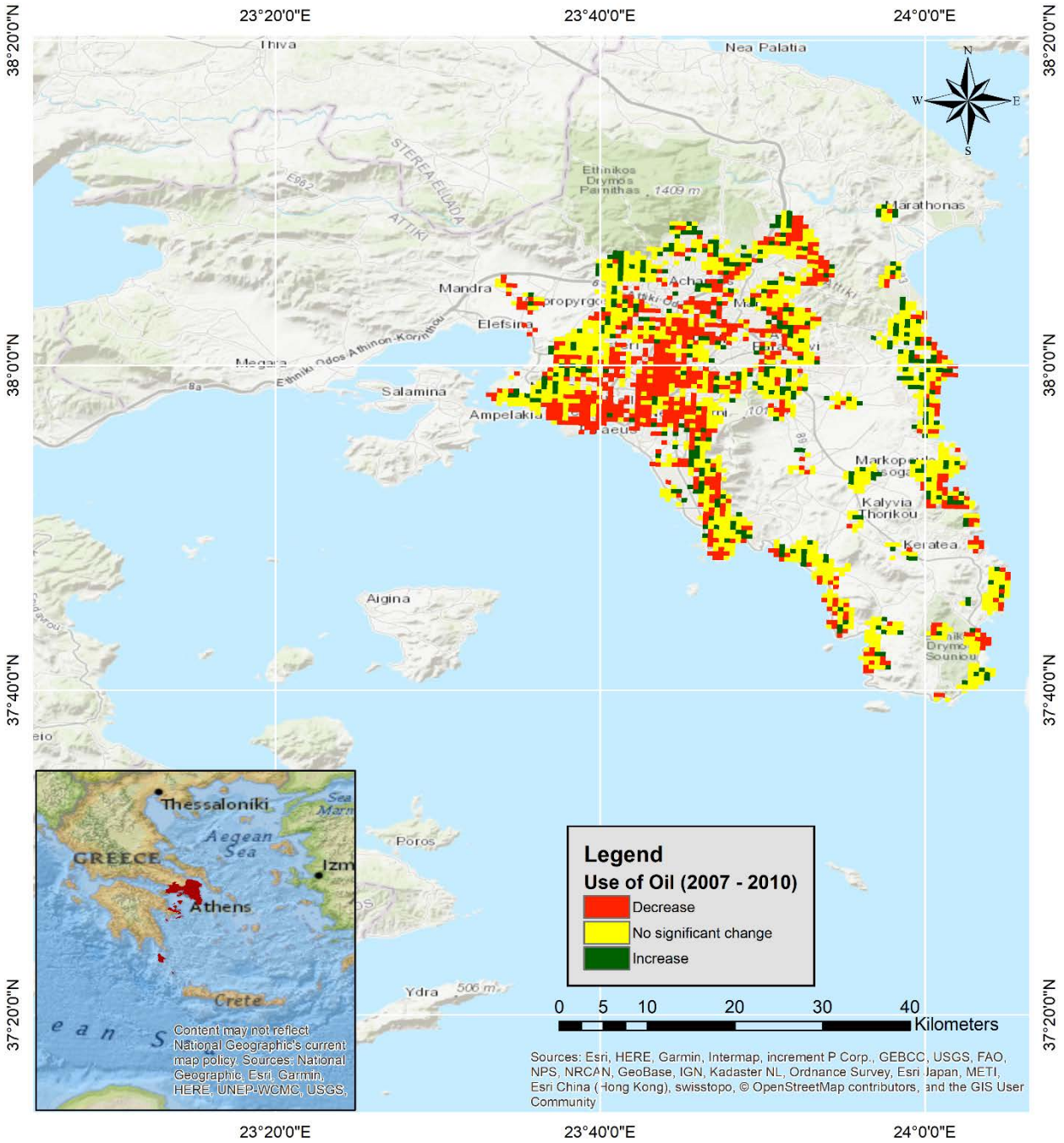

Map 4:26 Change in the use of oil between 2007-2008 and 2009-2010

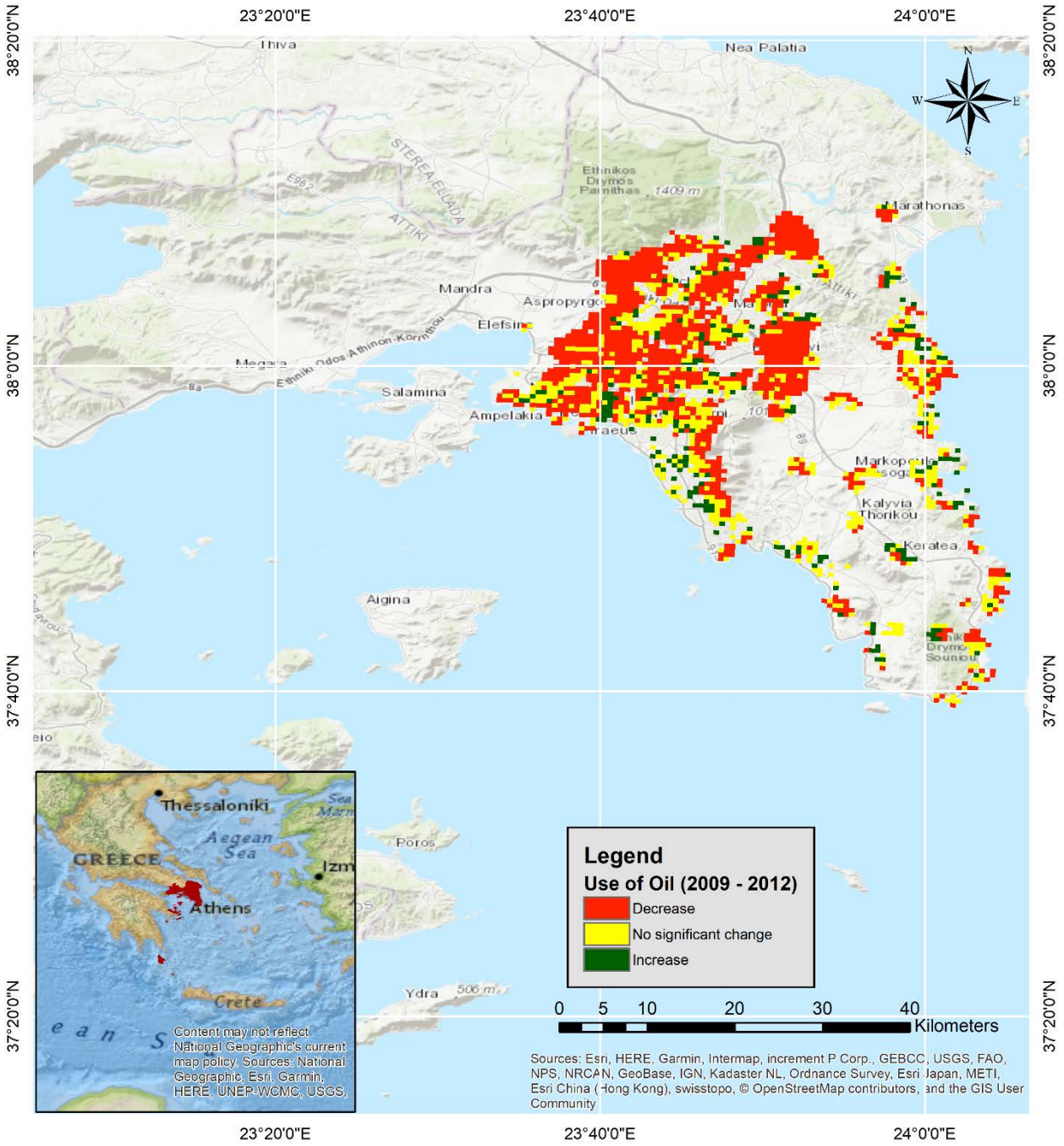

Map 4:27 Change in the use of oil between 2009-2010 and 2011-2012

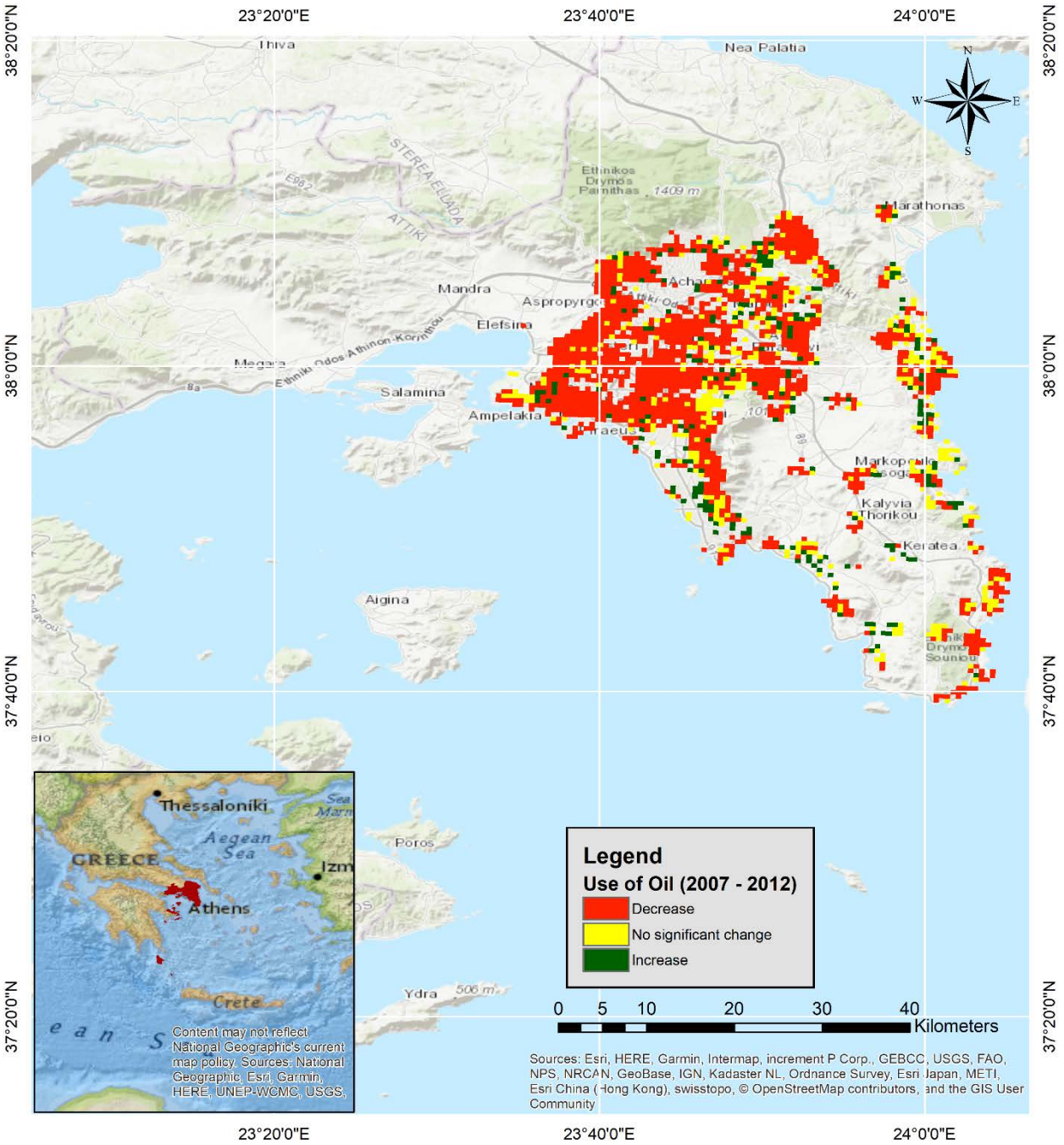

Map 4:28 Change in the use of oil between 2007-2008 and 2011-2012

Between 2007 and 2010, the dominant trend in gas consumption in urban areas of Attica is increase. Most of Attica presents an increase in gas consumption, while only a few, small and isolated areas exhibit decrease in consumption. Extended areas with no significant change are observed in the coastal boundary of East Attica and around the areas of decreasing consumption.

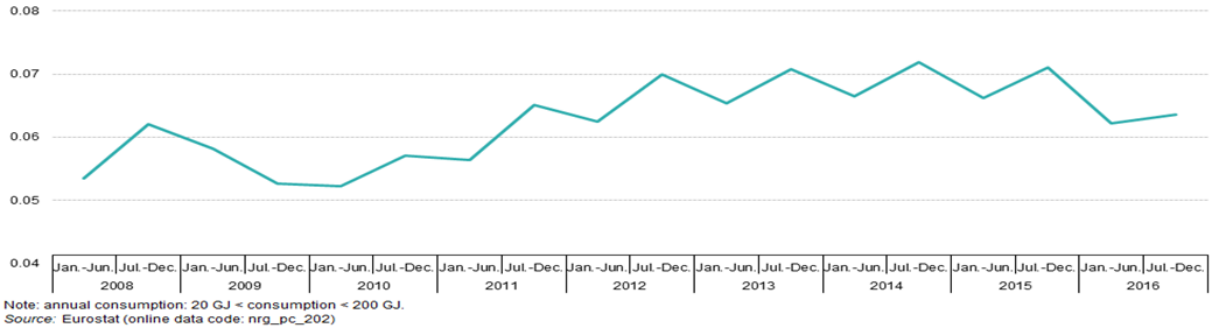

Note: annual consumption: 20 GJ < consumption < 200 GJ.
Source: Eurostat (online data code: nrg_pc_202)

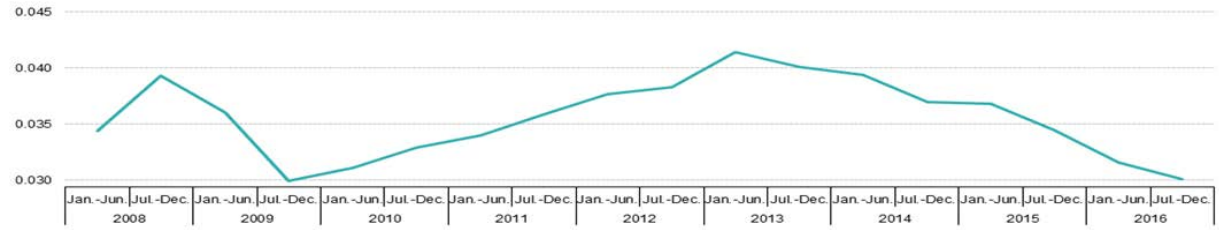

Note: annual consumption: 10 000 GJ < consumption < 100 000 GJ. Excluding VAT.
Source: Eurostat (online data code: nrg_pc_203)

Between 2009 and 2012, the previously observed trend is reversed, with most of Attica now exhibiting decreases in gas consumption. Only small areas, located in the central and north sections of Athens, present an increase in consumption. Extended coastal areas in East Attica again exhibit no significant change in gas consumption.

Generally, between 2007 and 2012, most of Attica exhibits no significant change in gas consumption. Multiple areas of various sizes in Athens and surrounding urban areas exhibit an increase in gas consumption, while areas with decreases are small and mainly located in East Attica and the western urban areas of Athens. Coastal areas in East Attica maintain the neutral nature of no significant change throughout all three periods

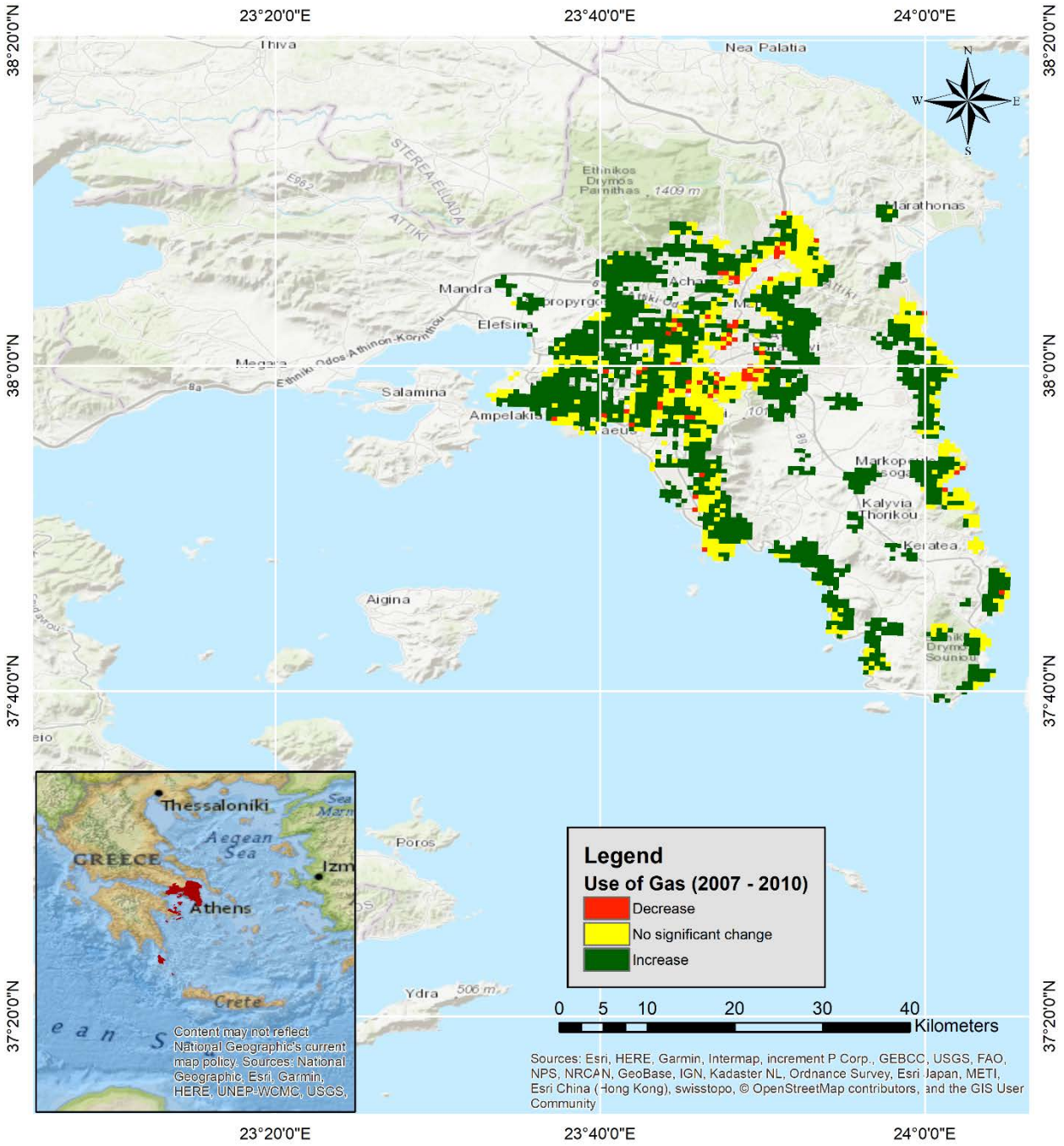

Map 4:29 Change in the use of Natural Gas between 2007-2008 and 2009-2010

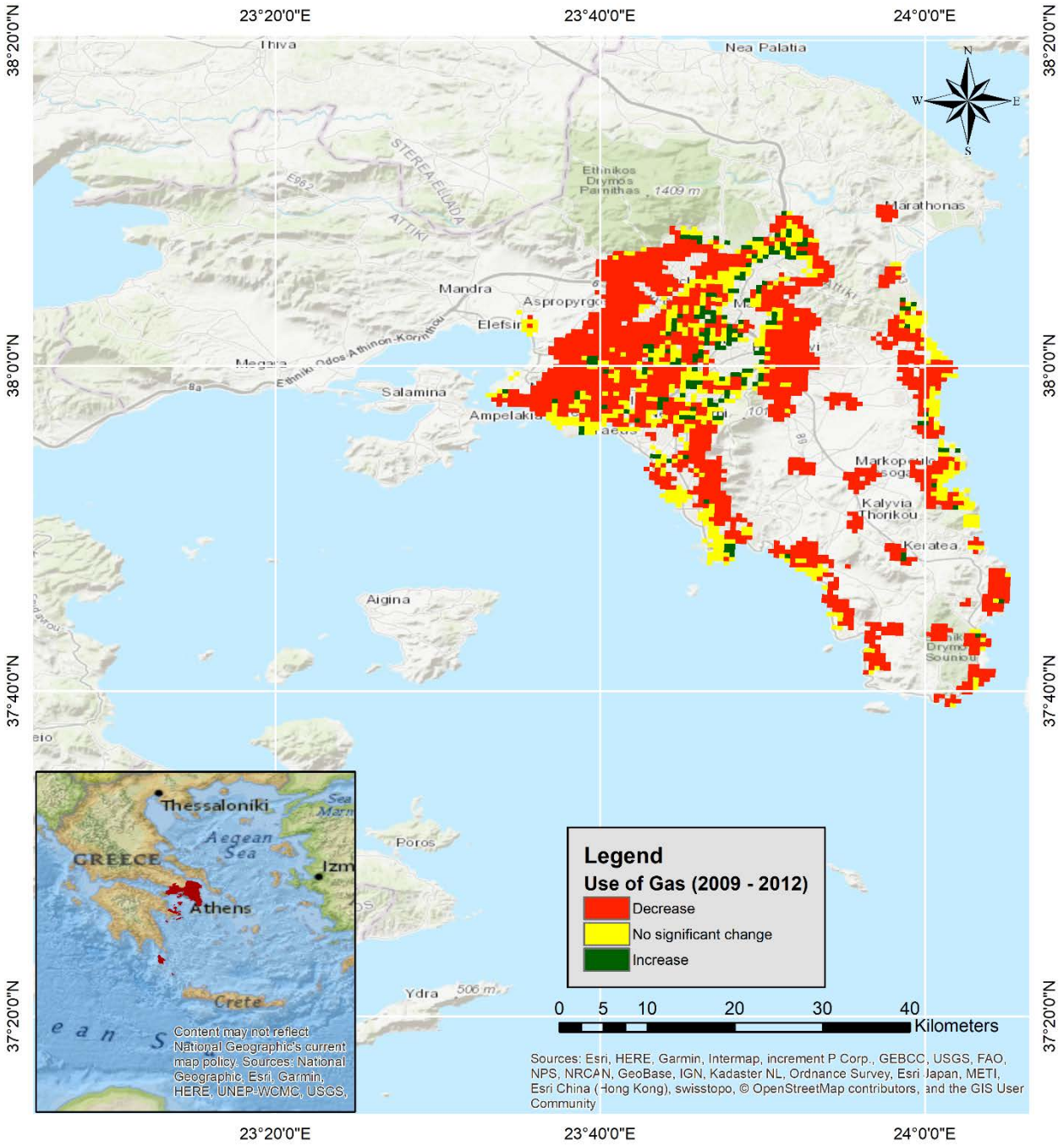

Map 4:30 Change in the use of Natural Gas between 2009-2010 and 2011-2012

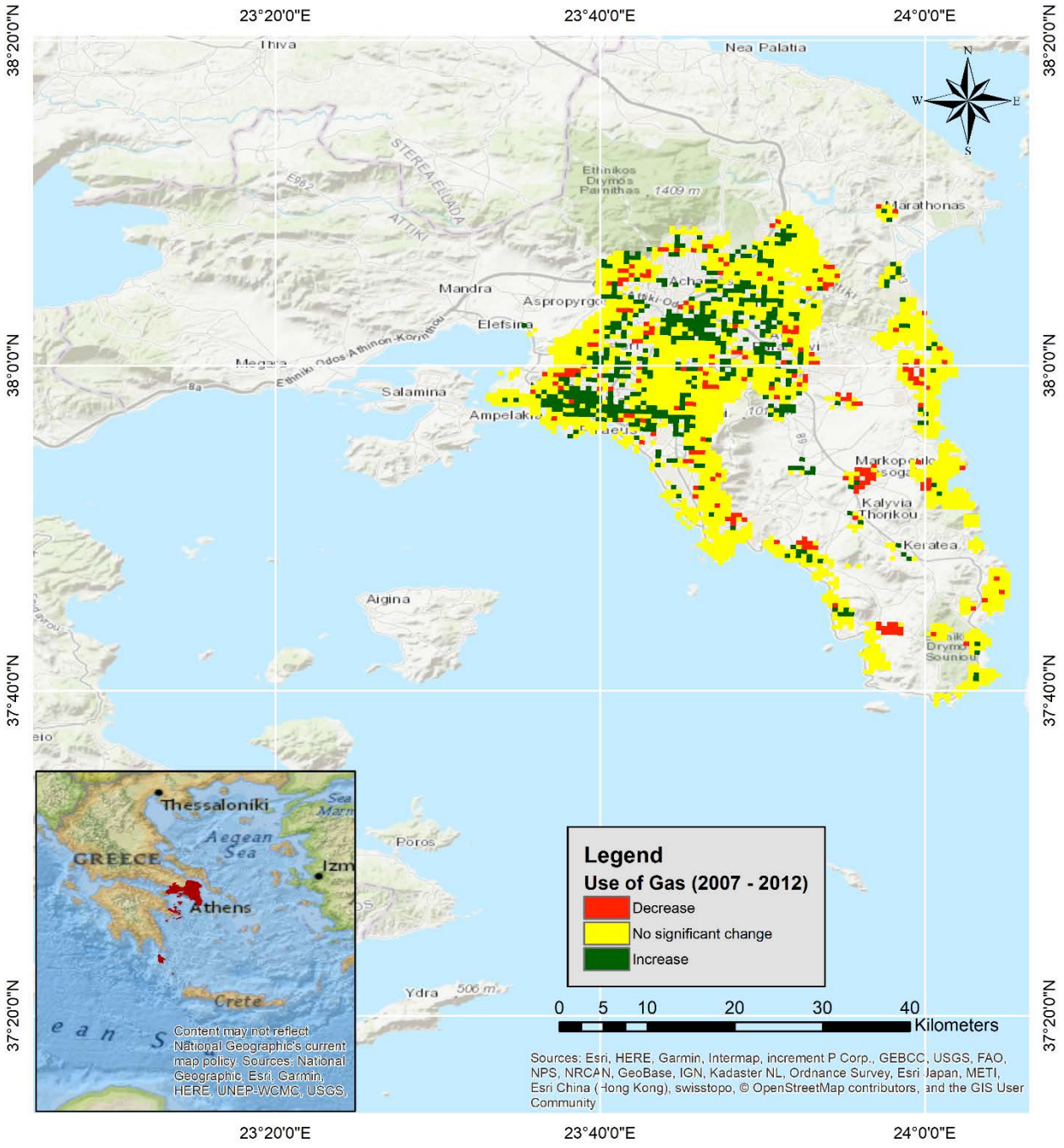

Map 4:31 Change in the use of Natural Gas between 2007-2008 and 2011-2012

Between 2007 and 2010, most of the urban areas in Attica present no significant change in firewood consumption. Small areas in Athens center present increases in firewood consumption, while small suburban areas around the center and urban areas in East Attica present decreases in consumption. The total extent, however, of areas presenting a significant change, either increase or decrease, is substantially smaller than the extent of areas with no significant change.

Between 2009 and 2012, the dominant trend in firewood consumption is an increase, observed in multiple large and small areas of Athens and small areas in East Attica. The extent of areas presenting an increase in consumption is comparable to the extent of areas with no significant change. The southern coastal urban areas, on the other hand, present a combination of small areas with a decrease in firewood consumption, and areas with no significant change. Finally, in the eastern coastal areas, there is a mixture of both areas with increasing or decreasing consumption of firewood and areas with no significant change.

Generally, between 2007 and 2012, the center and western urban sections of Athens present multiple areas of various sizes with increases in firewood consumption, while the rest of the urban sections in Attica present areas of similarly variable size where firewood consumption is decreased. Large urban areas of Attica exhibit no significant change through the study periods, with the largest one located in the central section of Athens. Finally, the southern coastal areas exhibit a dominant trend of decrease in consumption.

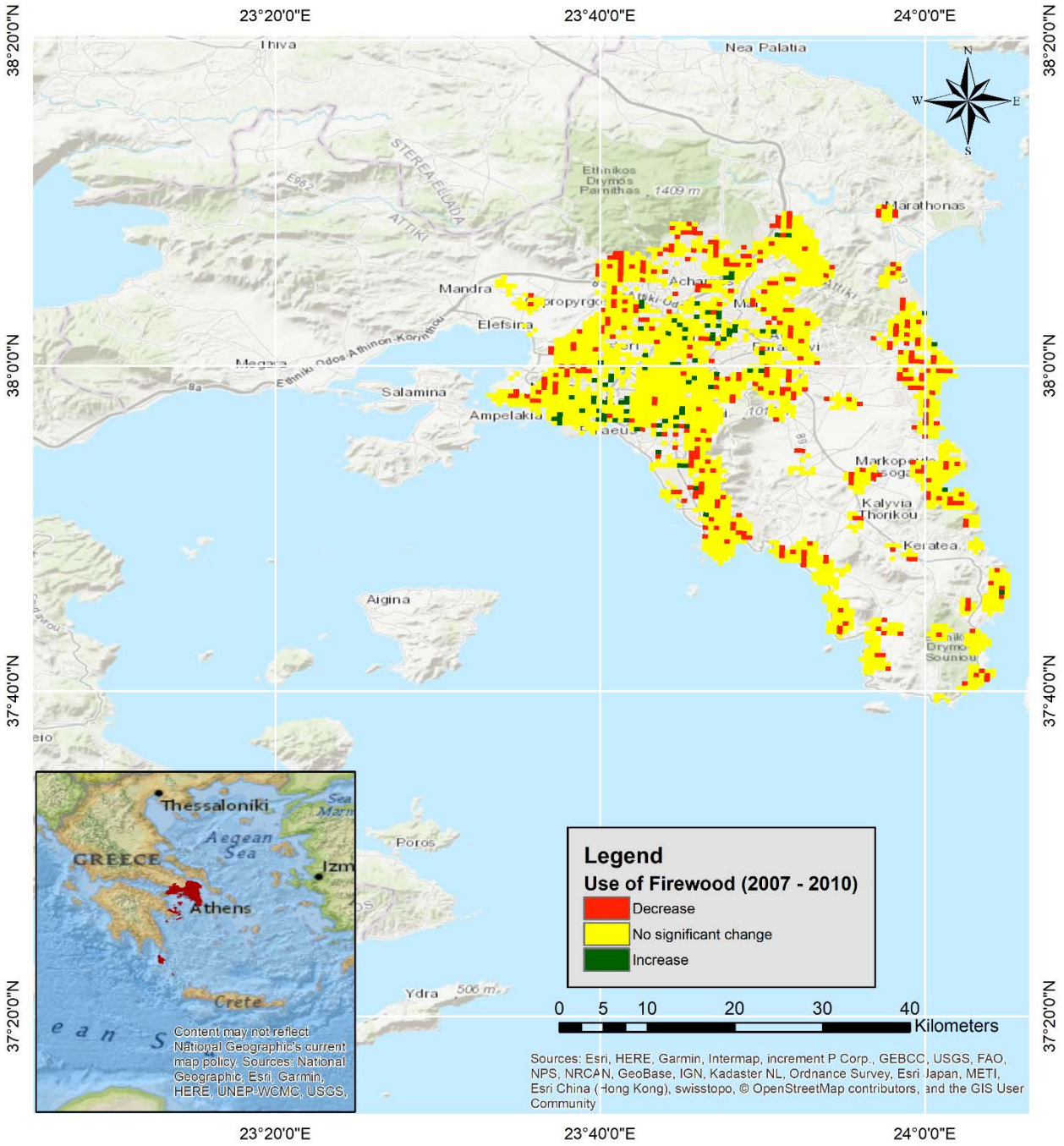

Map 4:32 Change in the use of wood (including pellet) between 2007-2008 and 2009-2010

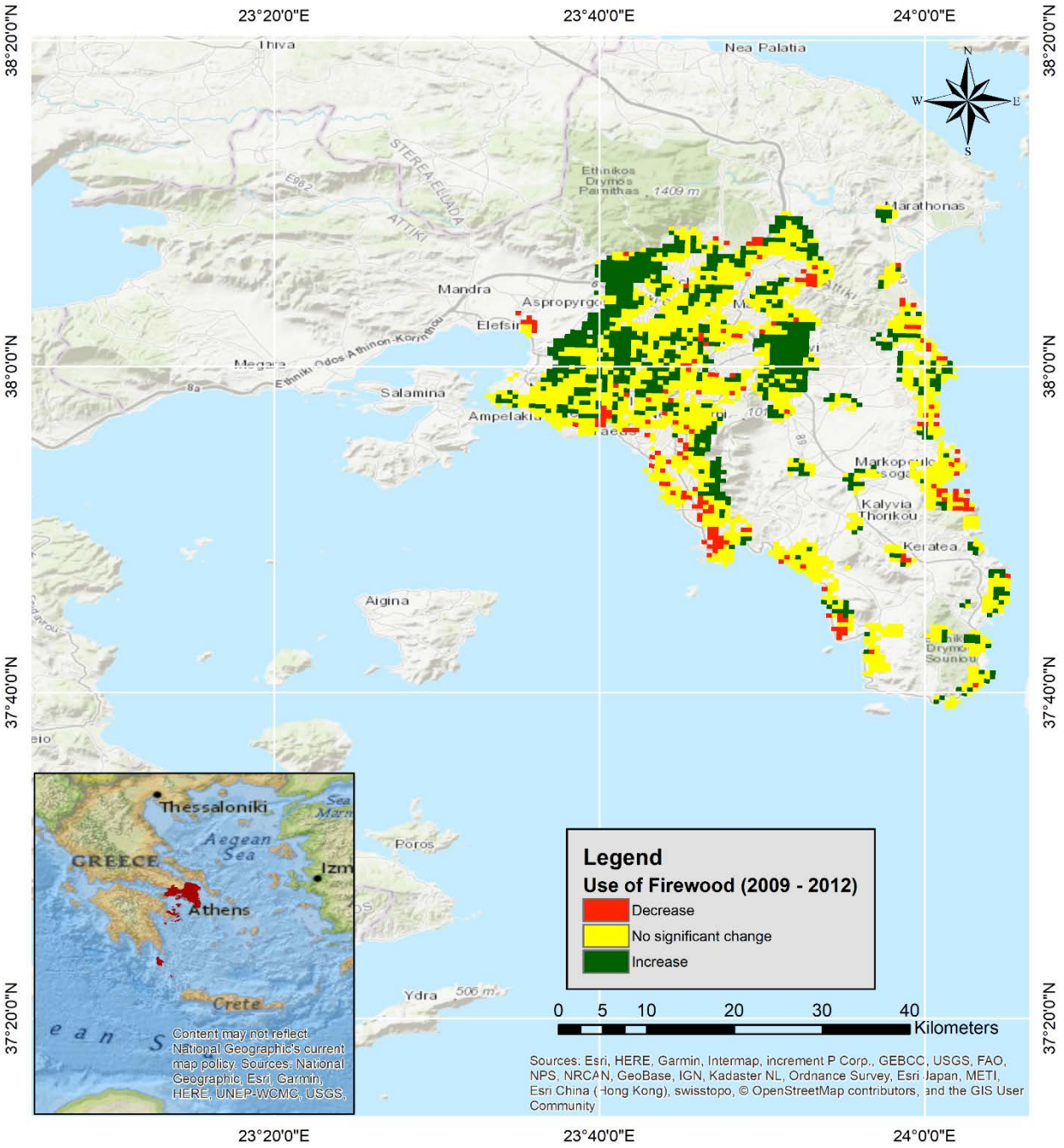

Map 4:33 Change in the use of wood (including pellet) between 2009-2010, and 2011-2012

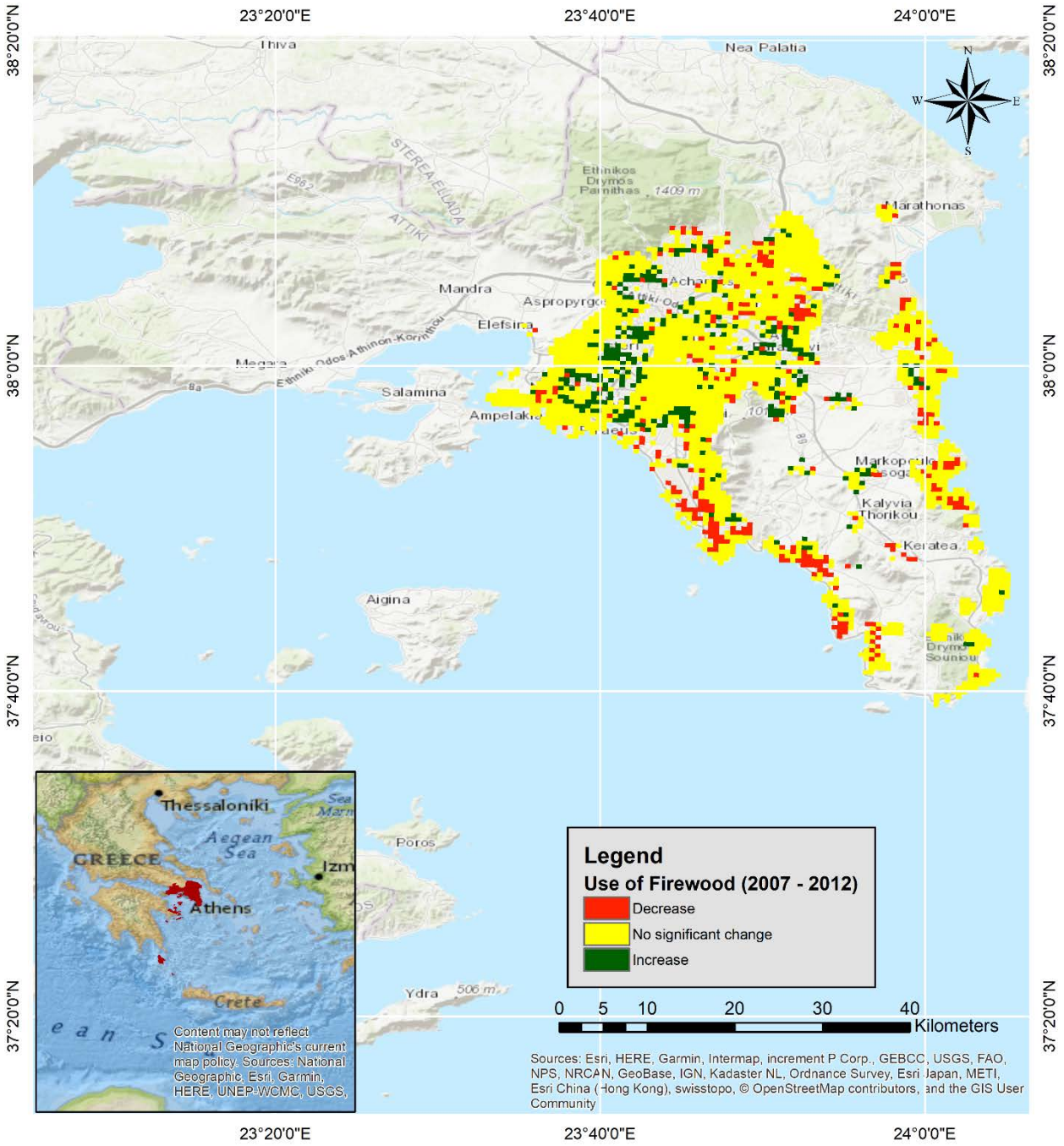

Map 4:34 Change in the use of wood (including pellet) between 2007-2008 and 2011-2012

5. Discussion - Conclusion

The aim of the current study was to investigate the impact the economic crisis, which started after 2008, had in air quality over the Great Athens Area. For this purpose, three distinct periods were examined, pre-crisis (2007-2008), crisis-onset (2009-2010), and during-crisis (2011-2012). Utilizing MODIS satellite data, air pollutant concentrations, and their changes were mapped over the Great Athens Area and associated with changes in fuel types used in residential heating systems.

Initially, the pollutant concentrations in virtual stations were calculated using regression analysis. Following the methodology from Ung, et al. (2001), multiple samples of varying sizes were tested for statistical significance, with the finally selected regressions being those that presented the highest p-value and smallest standard error. Although statistically significant results were produced with larger samples for most pollutants, the correlation (R squared) was much lower in most, reaching as low as 20%.

With the use of virtual stations, a second regression was performed, as described by the methodology described in Narashid & Mohd's (2010) research, in order to calculate the final formulas that would be utilized in the calculation of the pollutants' concentrations in the GAA.

The resulting concentration maps show that the Great Athens Area is divided into eight areas of interest, specifically:

1. The industrialized areas of West Attica
2. The urban area of Megara in West Attica
3. The northern section of West Attica
4. The main urban area of Athens and its adjacent suburbs
5. The north section of Central Attica
6. East Attica's south section excluding the coastal areas
7. East Attica's north section excluding the coastal areas
8. The coastal areas of East Attica

These areas present relatively homogenous pollutant concentrations for all pollutants and periods examined, while the rest of the Great Athens Area exhibits very heterogeneous mixtures of concentrations and concentration changes.

Between 2007-2010 and 2009-2012, most air pollutants exhibit a reversal in concentration changes in all areas of interest, except for PM_{10} that exhibits a constant concentration change

pattern throughout 2007-2012, with increases isolated in the northern section of West Attica and the north section of Central Attica.

5.1. Virtual stations identification

The thesis utilizes a methodology for virtual station identification. This is required as the number of available AQMS in the GAA area is small and statistically significant results utilizing data from these stations would be very hard to create.

As noted by Sifakis in (Sifakis & Deschamps, 1992), for an analysis of this type to have an accuracy of around 20%, at least 4 stations should be present per 2.5 km^2. For the GAA, with a total area of 3,808.10 km^2, this would mean that at least 6,093 AQMS should be present and correctly located for 20% accuracy using satellite data and actual pollutant measurements. Such a number of AQMS would constitute both a prohibitive cost to acquire and maintain, as well as an impractically large number of stations to monitor and analyze. The actual number of AQMS in the GAA is 16. Of these, not all record all pollutants required and not all measurements are correct due to mechanical or communication faults. It would be very difficult to get valid results for the entire GAA area only utilizing these stations, which strengthens the need for utilizing virtual stations in my study.

Although a proven method for densifying the pollutant measuring stations network, virtual stations estimation assumes that locations that share similar characteristics are also similar in nature. Although two locations may share very similar characteristics, their nature may differ in ways that are not visible nor measured, resulting in false positive selections. To minimize this risk, I utilized all available data to create the ID vector of each virtual station, increasing the possible factors utilized and decreasing the potential of false positive identifications. However, the regression validation shows that erroneous identifications are present in the results, but not to a degree that would substantially affect the study. As discussed in section 5.5, inclusion of more criteria in the virtual station identification could help mitigate this problem and further increase the accuracy of similar studies.

Furthermore, the multidimensional vector that is utilized in the identification of these virtual stations is based on the available data for the examined area. In my thesis, these include the visual bands 1,3, and 4 from MODIS, which are similar in nature to the visible light bands utilized in other studies employing this method, MODIS products that were available to me at the time of the study, and CORINE land cover dataset. All these datasets have inherent faults in them that increase the ambiguity of the ID vector and increase the likelihood of false positives as well.

5.2. Pollutant estimation regression and validation

Based on the regression results attached in the results section of this document and in Appendix A (1st and 2nd OLS regression results accordingly), the standard errors of the estimates are relatively low, which means that the accuracy of the regressions should be high enough to allow for accurate observations on the air pollutant concentrations and further analysis in air pollutant changes, ratios, and association with other aspects of the study.

The initial regressions in my thesis utilize a very small population of AQMS to derive their results. This can lead to biased results or overfitting, which need to be taken into consideration. The use of large validation sets, compared to the training sets, helps in identifying, quantifying, and, if possible, offsetting these limitations. Additionally, the virtual-stations methodology employed was specifically designed to compensate for the fact that AQMS, in general, are few and sparsely located in any given area. The results from my initial regression indicate that some degree of overfitting may be present. However, due to the small size of the initial AQMS available this problem cannot be avoided.

The validations of the regressions were performed using the AQMS which were not selected in the training sets. Again, stations with missing or erroneous data were excluded to ensure the validation is as accurate as possible. A possible source of errors, in both the training and validation sets, is the presence of industrialized zones near some of the AQMS, however the initial concentration comparisons between the various AQMS showed no indication such an effect existed in the data.

For PM_{10} validations only 3 AQMS could be utilized in each set. Although the general rule of 70% training set (6 stations) to 30% validation set (3 stations) is satisfied, the validation is more vulnerable to outlier effects compared to other pollutants' validations.

In my validation results, some of the AQMS that are utilized for the validation of the regression results are affected by the areas that they are located in. Those AQMS located near industrial areas tend to show underestimation of the results, while the single AQMS located in a forest area on the Northeast section of GAA (when data is available, and it is used for validation) tends to show large overestimations of pollutants.

For the second regression, which utilizes virtual stations in combination with AQMS, the accuracy of the estimates is directly related to the quality of the virtual stations' selection. The more factors that are utilized in the selection process, the better the selection is. The accuracy of

the regressions is derived from the accuracy of the 1st set of regression, as virtual stations' pollutant concentration estimates are produced from them.

5.3. Average air pollutant mapping

The maps produced using the regression formulae from the second regression represent the estimated pollution levels observed for each period using satellite data from the MODIS system. They are an intermediate step utilized for comparing differences in air pollutant concentrations between the 3 distinct time periods examined in this study. Areas in the GAA are clearly defined in almost all the maps, with the central urban area of Athens, the more rural areas in the east, and the industrial area of Elefsina in the West, which signifies the different pollutant profiles for each area, based on the different uses and surface covers.

Except for CO for 2009-2010 period, the produced maps can be effectively utilized in the next step for comparison between time periods. The aforementioned map, due to the very low accuracy of the results, with the large overestimation of pollutant concentration, cannot yield usable results. However, because the analysis main concern is focused on comparing the first and last time periods, this does not greatly affect the final results of the study.

Concentration difference maps present the next step in the analysis with the difference in pollutant concentrations between the different periods examined between each period and the one after it and between the stat and the end of the analysis, which is also the most significant comparison. Except for maps comparing CO pollutant for 2009-2010 period with other periods, all maps can be successfully used to determine changes, specifically increases, or decreases, in pollutant concentrations between periods. The comparison between these changes observed in the pollutant maps between the periods are then utilized to estimate the relationship between heating systems and the observed air quality.

5.4. Relation between Heating Systems and Air Quality

The thesis is written with the assumption that it is impossible to directly relate concentrations of pollutants in the atmosphere between the periods examined with the amount of fuel utilized per type of fuel for the same periods. For most fuel types, there is no official data on the amount of fuel produced/imported or the amount of fuel consumed by households.

To allow comparison between periods, I utilize emission tables for the various fuels and estimate the ratio between the emissions. These ratios are then compared between the periods to estimate changes (positive or negative) in fuel consumptions. It is assumed that the fundamental

chemical composition of the fuel remains relatively unchanged between the periods and small changes that are present between different batches of the fuel in question do not remarkably alter its emission profile. Throughout the initial research for the thesis, no evidence of substantial chemical changes was identified for any of the fuels in this thesis.

5.5. Limitations

The analysis utilizes MODIS satellite images, which have a lower resolution compared to other instruments but have daily coverage of the study area. This allows us to overcome cloud cover limitations; The reduced resolution, however, also means that smaller fluctuations are not visible during the analysis. At the same time, the small number of AQMS in the study area means that the regression analysis applied to produce the virtual stations utilized in the next steps has a larger standard error and the available number of initial observations from which the regression analysis sample is drawn is limited.

Due to their large sizes, urban areas present sufficient sizes for the analysis and small outliers are easier to identify in the final products. Based on the regression results attached in the results section of this document and in Appendix A (1st and 2nd OLS regression results accordingly), the standard errors of the estimates are relatively low, which means that the accuracy of the regressions should be high enough to allow for accurate observations on the air pollutant concentrations and further analysis in air pollutant changes, ratios, and association with other aspects of the study.

The initial regressions in my thesis utilize a very small population of AQMS to derive their results. This can lead to biased results or overfitting, which need to be taken into consideration, however because the purpose of the regressions is not to estimate future values but describe the observed state, its effect is not as severe. This is most possibly the reason for the regression results being almost perfect, but the lack of other data sources prevented me, at the time of the study, from finding and utilizing measures for correcting this problem. The use of large validation sets, compared to the training sets, helps in identifying, quantifying, and, if possible, offsetting these limitations. Additionally, the virtual-stations methodology employed was specifically designed to compensate for the fact that AQMS, in general, are few and sparsely located in any given area.

The validations of the regressions were performed using the AQMS which were not selected in the training sets. Again, stations with missing or erroneous data were excluded to ensure the validation is as accurate as possible. A possible source of errors, in both the training and validation sets, is the presence of industrialized zones near some of the AQMS, however the initial

concentration comparisons between the various AQMS showed no indication such an effect existed in the data.

For PM_{10} validations only 3 AQMS could be utilized in each set. Although the general rule of 70% training set (6 stations) to 30% validation set (3 stations) is satisfied, the validation is more vulnerable to outlier effects compared to other pollutants' validations.

Because my analysis utilizes comparison between the time periods and the accuracy of each pollutant appears to be similar between them, the impact of over/under-estimations is reduced in my study. The comparison does not directly examine the estimated concentrations but their difference between periods. As such, utilizing the ratios allows for accurate results as long as accuracies for the same pollutant are comparable between periods.

For the second regression, which utilizes virtual stations in combination with AQMS, the accuracy of the estimates is directly related to the quality of the virtual stations' selection. The more factors that are utilized in the selection process, the better the selection is. The accuracy of the regressions is derived from the accuracy of the 1st set of regression, as virtual stations' pollutant concentration estimates are produced from them.

5.6. Expansion and possible improvements

One possible improvement in the analysis of air pollutant concentrations over a study area such as the Great Athens Area could be the inclusion of satellite data from multiple instruments and the verification of the results between these instruments. Utilization of additional AQMS, even temporary ones, can have a significant impact in the regression analysis results, as the increase in the number of observations could considerably reduce the error potential of the analysis, decrease overfitting risk, and increase the accuracy of the final formulas in the computation of virtual stations' air pollutant concentration.

Expansion of the analysis in additional regions and inclusion of larger time periods could provide insights into trends that are not visible in a smaller area or trends that develop more slowly and have smaller fluctuations over the years. Finally, the air pollutant concentrations can be associated with other socioeconomic, healthcare, and environmental aspects of the study area.

In conclusion, the analysis performed shows a clear association of air pollutant changes and changes in the fuels utilized in household heating systems. This visibly demonstrates that the economic crisis had a substantial impact on the environment of the Great Athens Area in addition

to socioeconomic aspects affected by it, with heating fuel consumption decreasing through the economic crisis.

5.7. Conclusion

The change in air pollutant ratios indicates that the consumption of heating petrol was reduced during the economic crisis with the reduction increasing and expanding to the suburbs of Athens and other urban areas in East Attica between 2009-2012. Natural GAS use appears to increase between 2007-2010 but again decreases during 2009-2012, following the continuous increase in N.G. prices from 2010 onwards. Finally, wood consumption appears to increase in most of Attica between 2009-2012, but only a few areas demonstrate a significant increase in firewood consumption throughout all three periods examined. On the other hand, no significant firewood consumption changes appear to occur during the onset of the economic crisis.

References

(IPCC), I. P. (2007). Climate Change 2007: The Physical Science Basis. Summary for Policymakers. Paris: IPCC.

A., L., Remer, D. T., & Kaufman, Y. J. (n.d.). *ALGORITHM FOR REMOTE SENSING OF TROPOSPHERIC AEROSOL FROM MODIS: Collection 5*. Retrieved from NASA: https://modis-images.gsfc.nasa.gov/_docs/MOD04-MYD04_ATBD_C005.pdf

Al-Saadi, J., Pierce, R. B., Kittaka , C., Neil , D., Chu, D. A., Remen, L., . . . Fishman, J. (2005). Improving mational air quality forecasts with satellite aerosol observations. *American Meteorological Society*, 1249-1262. doi:doi: 10.1175/BANS-86-9-1249

Barnes, W. L., Pagano, T. S., & Salomonson, V. (1998). Prelaunch characteristics of the moderate resolution imaging spectroradiometer (MODIS) on EOS-AMI.

Barregard, L., Sallsten, G., Gustafson, P., Andersson, L., Johanson, L., Basu, S., & Stigendal, L. (2006). Experimental exposure to woodsmoke particles in healthy humans: Effects on markers of inflammation, coagulation, and lipid peroxidation. *Inhalation Toxicol, 18*(11), 845-853.

Basly, L., & Wald, L. (2000). Remote sensing and air quality in urban areas. In Proceedings of the 2nd international workshop on telegeoprocessing. Sophia Antipolis, France: TeleGeo'2000.

Boardman, B. (2010). *Fixing Fuel Poverty: Challenges and Solutions.* London: Earthscan.

Burrough, P., & McDonnell, R. (1998). *Principles of Geographical Information Systems.* Oxford University Press.

Cairns, M., Hao, W. M., Alvardo, E., & Haggerty, P. (1999). *Carbon Emissions from Spring 1998 Fires in Tropical Mexico.* NTIS: Springfield, VA: U.S. Environmental Protection Agency.

Canadell, J. G., Le Quere, C., Raupach, M. R., Field, C. B., Buitenhuis, E. T., Ciais, P., . . . Marland, G. (2010). Contributions to accelerating atmospheric CO2 growth from economic activity, carbon intensity, and efficiency of natural sinks. *Proceedings of the National Academy of Sciences (PNAS) of the United States of America*, *104*, pp. 18866-18870.

Chang, A. M., & Lam, L. W. (1997). Evaluation of a health care assistant pilot programme. *Journal of Nursing Management, 5*(4), 229-236.

Chitade, A., & Katiyar, S. K. (2004). AIR POLLUTION PREDICTION MODEL USING GIS. *Annual Review Workshop, Asian Regional Research Programme on Environmental Technology Phase II (ARRPET II)*.

Chu, D., Kaufman, Y., Zibordi, G., Chern, J., Mao, J., Li, C., & Holben, B. (2003). Global Monitoring of Air Pollution over Land from the Earth Observing System-Terra Moderate Resolution Imaging Spectroradiometer (MODIS). *Journal of Geophysical Research, 108*(D21), 46-61. doi:10.1029/2002JD003179

Combrink, J., Diab, R., Sokolic, F., & Brunke, E. (1994). Relationship between Surface, Free Tropospheric and Total Column Ozone in Two Contrasting Areas in South Africa. *Atmospheric Environment, 29*, 685-691.

Cook, J. D. (2009, March 6). *John D. Cook consulting*. Retrieved from Example of efficiency for mean vs. median: https://www.johndcook.com/blog/2009/03/06/student-t-distribution-mean-median/

Delfino, R. J., Sioutas, C., & Malik, S. (2005). Potential role of ultrafine particles in associations between airborne particle mass and cardiovascular health. *Environmental Health Perspectives, 113*(8), 934-946.

Demirov, E., & Pinardi, N. (2002). Simulation of the Mediterranean Sea circulation from 1979 to 1993: Part I. The interannual variability. *Journal of Marine Systems*(33), 23-50.

Ec.europa.eu. (2017, May 29). *Industrial production (volume) index overview - Statistics Explained.* . Retrieved May 29, 2017, from http://ec.europa.eu/eurostat/statistics-explained/index.php/Industrial_production_(volume)_index_overview

EEA. (2016). *Air quality in Europe — 2016 report.* Copenhagen: EEA office for official publication.

Engel-Cox, J. A., Holloman, C. H., Coutant, B. W., & Hoff, R. M. (2004). Qualitative and quantitative evaluation of MODIS satellite sensor data for regional and urban scale air quality. *Atmospheric Environment, 38*(16), 2495–2509.

Engel-Cox, J., DeFelice, T., & Falke, S. (2001). *Transboundary Movement of Airborne Pollutants: A Methodology for Integrating Spaceborne Images and Ground Based Data.* GRID Sioux Falls Center: Sioux Falls, SD: United Nations Environment Programme.

Finzi, G., & Lechi, G. (1991). LANDSAT Images of Urban Air Pollution in Stable Meteorological Conditions. *Il Nuovo Cimento C, 14C*(5), 433-443.

Fishman, J. (2000). Observing Tropospheric Ozone from Space. *Progress in Environmental Science , 2*(12), 275-290.

Fishman, J., Vukovich, F., Cahoon, D., & Shipham, M. (1987). The Characterization of an Air Pollution Episode Using Satellite Total Ozone Measurements. *Journal of Applied Meteorology and Climatology, 56*(4), 1638-1654.

Florou, K. K., M, P. N., & Pandis, S. (2013). Wintertime Air Pollution and the Greek Financial Crisis. *15.* Vienna, Austria: EGU General Assembly 2013. Retrieved from http://adsabs.harvard.edu/abs/2013EGUGA..15.7091F

Hellenic Statistical Authority . (2014). *Cars and motorcycles circulating in Greece.* Retrieved from http://www.statistics.gr/portal/page/portal/ESYE/BUCKET/A1106/Other/A1106_SME18_TS_MM_00_1985_00_2014_01_F_BI_0.xls

Hellenic Statistical Authority. (2012). *Energy Consumptiom Survey in Households.* Retrieved from http://www.statistics.gr/portal/page/portal/ESYE/BUCKET/A0805/PressReleases/A0805_SFA40_DT_5Y_00_2012_01_F_GR.pdf

Hellenic Statistical Authority. (2013). *Consumption of petroleum products by region and county.* Retrieved from http://www.statistics.gr/portal/page/portal/ESYE/BUCKET/A0901/Other/A0901_SDE15_TS_AN_00_2000_00_2013_01_F_GR.xls

Hidy, G. M., Brook, J. R., Chow, J. C., Green, M., Husar, R. B., Lee, C., . . . Watson, J. G. (2009). Remote Sensing of Particulate Pollution from Space: Have We Reached the Promised Land? *Journal of the Air & Waste Management Association, 59*(10), 1130-1139. doi:10.3155/1047-3289.59.10.1130

Hodan, W. M., & Barnard, W. R. (2004). Evaluating the Contribution of PM2.5 Precursor Gases and Re-entrained Road Emissions to Mobile Source PM2.5 Particulate Matter Emissions. Florida: 13th International Emission Inventory Conference "Working for Clean Air in Clearwater.

Hsu, N. C., Jeong, M. J., Bettenhausen, C., Sayer, A. M., Hansell, R., Seftor, C. S., . . . Tsay, S. C. (2013). Enhanced Deep Blue aerosol retrieval algorithm: The second generation. *Journal of Geophysical Research: Atmospheres, 118*(15), 1-20.

Husar, R., Prospero, J., & Stowe, L. L. (1997). Characterization of Tropospheric Aerosols over the Oceans with the NOAA Advanced Very High Resolution Radiometer Optical Thickness Operational Product. *Journal of Geophysical Research, 102*(16), 889-916.

Hutchinson, K. D. (2003). Applications of MODIS Satellite Data and Products for Monitoring Air Quality in the State of Texas. *Atmospheric Environment, 37*, 2403-2412.

Kakaras, E., Karellas, S., Vourliotis, P., Giannakopoulos, D., Grammelis, P., Pallis, P., & Karabinis, E. (2013). *Emission indices by type of fuel and heating technology.* Athens: Ministry of Reconstruction of Production, Environment and Energy.

Kallos, G., Kassomenos, P., & Pielke, R. A. (1993). Synoptic and mesoscale weather conditions during air pollution episodes in Athens, Greece. *Boundary Layer Meteorology, 62*, 163-184.

Kanakidou, M., Mihalopoulos , N., Kindap T, I. K., Vrekousis , M., Gerasopoulos, E., Dermitzaki, E., . . . Moubasher, H. (2011). Magacities as hot spots of air pollution in the East Mediterranean. *Atmospheric Environment, 45*, 1223-1235. doi:10.1016/j.atmosenv.2010.11.048

Kassomenos, P. A., & Katsoulis, B. D. (2006). Mesoscale and macroscale aspects of the morning urban Heat island around Athens, Greece. *Meteorology and Atmospheric Physics, 94*, 209-2018. doi:10.1007/s00703-006-0191-x

Kaufman, Y. J., & Sendra, C. (1998). Algorithm for Automatic Atmospheric Corrections to Visible and Near-IR Satellite Imagery. *Journal of Geophysical Reasearch, 8*, 1357-1381.

Kaufman, Y. J., Fraser, R. S., & Ferrare, R. A. (1990). Satellite Measurements of Large-Scale Air Pollution: Methods. *Journal of Geophysical Research, 95*, 9895-9909.

Kjallstrand, J., & Petersson, G. (2001). Phenolic antioxidants in wood smoke. *Science of Total Environment, 277*(1-3), 69-75.

Kriegler, F., Malila, W., Nalepka, R. F., & Richardson, W. (1969). Preprocessing transformations and their effects on multispectral recognition. (pp. 97-131). Michigan: Proceedings of the Sixth International Symposium on Remote Sensing of Environment.

Lawrence, M. G., Butler, T. M., Steinkamp, J., Gurjar, B. R., & Lelieveld, J. (2007). Regional pollution potentials of megacities and other major population centers. *Atmospheric Chemistry and Physics, 7*, 3969-3987. doi:10.5194/acp-7-3969-2007

Levy, R., Mattoo, S., Munchak, L., Kleidman, R., Patadia, F., & Gupta, P. (2014). *MODIS atmosphere team webinar series #2: Overview of collection 6 dark-target aerosol product.* NASA. Retrieved from http://aerocenter.gsfc.nasa.gov/ext/registration/

Liu, Y., Sarnat, J. A., Kilaru, V., Jacob, D. J., & Koutrakis, P. (2005). Estimating ground-level PM2.5 in the eastern United States using satellite remote sensing. *Environmental Science & Technology, 39*(9), 3269-3278.

Liu, Y., Sarnat, J. A., Kilaru, V., Jacob, D. J., & Koutrakis, P. (2005). Estimating ground-level PM2.5 in the eastern United States using satellite remote sensing. *Environmental Science and Technology, 39*(9), 3269-3278. doi:10.1021/es049352m

Livada, I., Santamouris, M., Niachou, K., Papanikolaou, N., & Mihalakakou, G. (2002). Determination of places in the great Athens area where the heat island effect is observed. *Theoretical and Applied Climatology, 71*, 219-230.

Markakis, K. I., Unal, A., Melas, D., Yenigun, O., & Incecik, S. (2009). A computational approach for the compilation of a high spatially and temporally resolved emission inventory for the Istanbul Greater Area. Instanbul: 7th International Conference on Air Quality Science and Application.

Melas, D., Ziomas, I. C., & Zerefos, C. (1995). Boundary layer dynamics in an urban coastal environment under sea breeze conditions. *Atmospheric Environment, 29*, 3605-3617.

Melas, D., Ziomas, I., Klemm, O., & Zerefos, C. (1998). Anatomy of sea breeze circulation in Greater Athens under weak large-scale ambient winds. *Atmospheric Environment, 32*, 2223-2237.

Ministry of Reconstruction of Production, Y. (2017). *EE Mapping of Air pollution.* Retrieved April 30, 2017, from http://www.ypeka.gr/Default.aspx?tabid=491&language=el-GR

Morgan, T. E., Davis , D. A., Iwata , N., Tannewe , J. A., Snyder, D., Ning, Z., . . . Finch, C. (2011). Glutamatergic neurons in rodent models respond to nanoscale particulate urban air pollutants in vivo and in vitro. *Environmental Health Perspectives, 119*(7), 1003-1009.

Mozumder, M. S., Zhu, J., & Perinpanayagam, H. (2012). Enhanced Human Mesenchymal Cell Responses. *Jurnal of Biomedical Materials Research, 100A*(10), 2695-2710. doi:10.1002/jbm.a.34199

Muller, J., Doll, C., & Elvidge, C. (2000). *Nighttime 36-band MODIS data for mapping global urban population, GDP and CO2 emissions.* Retrieved from https://modis.gsfc.nasa.gov/: https://modis.gsfc.nasa.gov/sci_team/meetings/199905/presentations/Muller_Night-Time.pdf

Narashid , H. R., & Mord, W. M. (2006). Micro-scale air quality monitoring using remote sensing and GIS technology. *Build Environmental Journal, 3*(2), 33-41.

Narashid, R. H., & Mohd, W. M. (2010). Air quality monitoring using remote sensing and GIS technologies. *Science and Social Research (CSSR), 2010 International Conference on* (pp. 1186-1191). IEEE.

NASA. (2010). *Aerosols: Tiny Particles, Big Impact*. Retrieved from https://earthobservatory.nasa.gov/Features/Aerosols

Observation, Y. C. (2010). *Obtaining and Processing MODIS Data. The Center for Earth Observation.* New Haven, Connecticut: Yale University. Retrieved from http://www.yale.edu/ceo

Panas, E. (2012). *Research of Fuel Poverty in Greece November 2012.* Athens: Department of Statistics (University of Economics and Business).

Pantavou, K., Theoharatos, G., Mavrakis, A., & Santamouris , M. (2011). Evaluating thermal comfort conditions and health responses during an extremely hot summer in Athens. *Building and Environment, 46*, 339-344.

Penttinen, P., Timonen, K. L., Tiittanen, P., Mirme, A., Ruuskanen, J., & Pekkanen, J. (2001). Ultrafine particles in urban air and respiratory health among adult asthmatics. *European Respiratory Journal , 17*(3), 428-435.

Prospero, J. (1999). Long-Term Measurements of the Transport of African Mineral Dust to the Southeastern United States: Implications for Regional Air Quality. *Journal of Geophysical Research , 104*(15), 917-927.

Ramanathan, V., Crutzen, P., Kiehl, J., & Rosenfeld, D. (2001). Aerosols, Climate, and the Hydrological Cycle. *Science, 294*(5549), 2119-2124.

Retalis, A., Cartalis, C., & Athanassiou, E. (1999). Assessment of the Distribution of Aerosols in the Area of Athens with the Use of Landsat Thematic Mapper Data. *International Journal of Remote Sensing, 20*(5), 939-945. doi:10.1080/014311699213000

Rouse, J. W., Haas, R. H., Schell, J. A., & Deering, D. W. (1973). Monitoring vegetation systems in the Great Plains with ERTS. *Third ERTS Symposium. 1,* pp. 309-317. Washington DC: NASA SP-351 I.

Saathesh, S. K. (2002). Radiative forcing by aerosols over Bay of Bengal region. *Geophysical Research Letters, 29*(22), 1-4. doi:10.1029/2002GL015334

Saffari A., D. N., Samara, C., Voutsa, D., Kouras, A., Manoli, E., Karagkiozidou, O., . . . C., S. (2013). Increased Biomass Burning Due to the Economic Crisis in Greece and Its Adverse Impact on Wintertime Air Quality in Thessaloniki. *Environment Science Technology, 47*(23), 13313-13320. doi:10.1021/es403847h

Samuels, M. L., Witmer, J. A., & Schaffner, A. A. (2012). Mean versus median. In M. L. Samuels, J. A. Witmer, & A. A. Schaffner, *Statistics for the life sciences* (pp. 56-57). London: Pearson education.

Santamouris, M. (2007). Heat Island Research in Europe, The state of the art. *Advances Building Energy Research (Review Paper), 1*(1), 123-150. doi:10.1080/17512549.2007.9687272

Santamouris, M., Paravantis, J. A., Founda, D., Kolokosta, D., Michalakakou, P., Papadopoulos, A. M., . . . Matthiessen, A. (2013). Financial crisis and energy consumption: A household survey in Greece. *Energy and Buildings, 65*, 477-487. doi:10.1016/j.enbuild.2013.06.024

Santamouris, M., Pavlou, K., Synnefa, A., Niachou, K., & Kolokotsa, D. (2007). Recent progress on passive cooling techniques. Advanced technological developments to improve survivability levels in low-income households. *Energy and Buildings, 39*(7), 859-866. doi:10.1016/j.enbuild.2007.02.008

Sardianou, E. (2008). Estimating space heating determinants: an analysis of Greekhouseholds. *Energy and Buildings, 40*(6), 1084-1093.

Sifakis, N., & Deschamps, P. Y. (1992). Mapping of Air Pollution Using SPOT Satellite Data. *Photogrammetric Engineering & Remote Sensing , 58*(10), 1433-1437.

Sifakis, N., & Soulakellis, N. (2000). Satellite Image Processing for Haze and Aerosol Mapping (SIPHA): Code Description and Presentation of Results. Honolulu: In Proceedings of the IGARSS; IEEE.

Sifakis, N., Soulakellis, N., & Paronis, D. (1998). Quantitative Mapping of Air Pollution Density Using Earth Observations: A New Processing Method and Application to an Urban Area. *International Journal of Remote Sensing, 19*(17), 3289-3300. doi:10.1080/014311698213975

Solomon, S., Qin, D., Manning, M., Chen, Z., Marquis, M., Averyt, K. B., . . . L., H. (2007). *Climate Change 2007: The Physical Science Basis, Contribution of Working Group I to*

the Fourth Assessment Report of the Intergovernmental Panel on Climate Change (IPCC). 996: Cambridge University Press.

Spichtinger, N., Wenigm, M., James, P., Wagner, T., Platt, U., & Stohl, A. (2001). Satellite Detection of a Continental-Scale Plume of Nitrogen Oxides from Boreal Forest Fires. *Geophysical Research Letters, 28*(24), 4579-4582.

Stathopoulou, E., Michalakakos, G., Santamouris, M., & Bargiorgas, H. (2008). Impact of temperature on tropospheric ozone concentration levelsin urban environments. *Journal of Earth System Science, 117*(5), 227-236. Retrieved from http://www.ias.ac.in/article/fulltext/jess/117/03/0227-0236

Sunwoo, Y., Kotamarthi, V., & Carmichael, G. (1992). The Regional Distribution of Tropospheric Ozone in East Asia from Satellite-Based Measurements. *Journal of Atmospheric Chemistry, 14*(1-4), 285-295.

Ung, A., Wald, L., Ranchin, T., Weber, C., Hirsch, J., Perron, G., & Kleinpeter, J. (2001). Satellite data for the air pollution mapping over a city–The use of virtual stations. *EARSeL Symposium 2001 "Observing our environment from space: new solutions for a new millenium"* (pp. 147-151). Balkema.

Valavanidis, A., Vlachogianni, T., Loridas, S., & Fiotakis, C. (2015). *Atmospheric Pollution in Urban Areas of Greece and Economic Crisis. Trends in air quality and atmospheric pollution data, research and adverse health effects.* Athens: Department of Chemistry, National Kapodistrian University of Athens. Retrieved from www.chem.uoa.gr

Vijayaraghavan, K., Snell, H., & Seigneur, C. (2008). Practical Aspects of Using Satellite Data in Air Quality Modeling. *Environmental Science & Technology, 42*(11), 8187-8192.

Vrekoussis, M., Richter, A., Hilboll, J., Burrows, P., Gerasopoulos, E., Lelieveld, J., . . . Mihalopoulos, N. (2013). Economic crisis detected from space: Air quality observations over Athens/Greece. *Geophysical Research Letters, 40*(2), 458-463.

Wald, L., & Baleynaud, J. M. (1999). Observing air quality over the city of Nantes by means of LANDSAT thermal infrared data. *International Journal of Remote Sensing, 20*(5), 947-959.

Wallace, J. M., & Hobbs, P. V. (2006). *Atmospheric Science* (2nd ed.). Washington: Elsevier.

Wang, J., & Christopher, S. (2003). Comparison between Satellite-Derived Aerosol Optical Thickness and PM2.5 Mass: Implications for Air Quality Studies. *Geophysical Research Letters, 30*(21), 2095. doi:10.1029/ 2003GL018174

Weber, C., Hirsch, J., Perron, G., Kleinpeter, J., Ranchin, T., Ung, A., & Wald, L. (2001). Urban morphology, remote sensing and pollutants distribution: An application to the city of Strasbourg, France. Seoul: 12th World Clean Air & Environment Congress.

Wijeratne, I. (2003). Mapping of dispersion of urban air pollution using remote sensing techniques and ground station data. ITC.

Appendix A: Second OLS regression (Raster calculator)

CO 2007-2008

Summary of OLS Results - Model Variables

Variable	Coefficient [a]	StdError	t-Statistic	Probability [b]	Robust_SE	Robust_t	Robust_Pr [b]	VIF [c]
Intercept	6.160641	0.025488	241.708415	0.000000*	0.035702	172.556814	0.000000*	--------
BAND 2 MEDIAN	-0.310349	0.001373	-226.101148	0.000000*	0.001523	-203.772936	0.000000*	12.566476
BAND 5 MEDIAN	0.206809	0.001843	112.193829	0.000000*	0.001040	198.769112	0.000000*	7.072405
BAND 6 MEDIAN	1.609020	0.008690	185.148130	0.000000*	0.011481	140.151001	0.000000*	23.218813
BAND 7 MEDIAN	-3.824572	0.016745	-228.398436	0.000000*	0.026040	-146.870525	0.000000*	8.901734

OLS Diagnostics

Input Features:	FirstOLScomplete	Dependent Variable:	CO_0708
Number of Observations:	930	Akaike's Information Criterion (AICc) [d]:	-1790.750650
Multiple R-Squared [d]:	0.988914	Adjusted R-Squared [d]:	0.988866
Joint F-Statistic [e]:	20628.271211	Prob(>F), (4,925) degrees of freedom:	0.000000*
Joint Wald Statistic [e]:	95704.759140	Prob(>chi-squared), (4) degrees of freedom:	0.000000*
Koenker (BP) Statistic [f]:	3.871183	Prob(>chi-squared), (4) degrees of freedom:	0.423720
Jarque-Bera Statistic [g]:	1707170.667732	Prob(>chi-squared), (2) degrees of freedom:	0.000000*

CO 2009-2010

Summary of OLS Results - Model Variables

Variable	Coefficient [a]	StdError	t-Statistic	Probability [b]	Robust_SE	Robust_t	Robust_Pr [b]	VIF [c]
Intercept	-5.298908	0.041293	-128.323620	0.000000*	0.037997	-139.455446	0.000000*	--------
BAND 2 MEDIAN	-0.358801	0.001520	-236.098267	0.000000*	0.000395	-908.248401	0.000000*	5.232505
BAND 5 MEDIAN	0.040634	0.001971	20.613637	0.000000*	0.001065	38.164834	0.000000*	3.346145
BAND 6 MEDIAN	4.317036	0.008433	511.940136	0.000000*	0.002578	1674.702029	0.000000*	12.577807
BAND 7 MEDIAN	-7.940963	0.016524	-480.582794	0.000000*	0.011844	-670.466785	0.000000*	6.236926

OLS Diagnostics

Input Features:	FirstOLScomplete	Dependent Variable:	CO_0910
Number of Observations:	1108	Akaike's Information Criterion (AICc) [d]:	-1345.964880
Multiple R-Squared [d]:	0.996902	Adjusted R-Squared [d]:	0.996891
Joint F-Statistic [e]:	88732.066108	Prob(>F), (4,1103) degrees of freedom:	0.000000*
Joint Wald Statistic [e]:	7697860.976579	Prob(>chi-squared), (4) degrees of freedom:	0.000000*
Koenker (BP) Statistic [f]:	3.341519	Prob(>chi-squared), (4) degrees of freedom:	0.502381
Jarque-Bera Statistic [g]:	5233691.867231	Prob(>chi-squared), (2) degrees of freedom:	0.000000*

CO 2011-2012

Summary of OLS Results - Model Variables

Variable	Coefficient [a]	StdError	t-Statistic	Probability [b]	Robust_SE	Robust_t	Robust_Pr [b]	VIF [c]
Intercept	0.852259	0.014458	58.947008	0.000000*	0.005444	156.537330	0.000000*	--------
BAND 2 MEDIAN	-0.243949	0.000756	-322.853650	0.000000*	0.000624	-391.045893	0.000000*	9.966770
BAND 5 MEDIAN	0.199969	0.000938	213.227371	0.000000*	0.000565	353.781762	0.000000*	4.670922
BAND 6 MEDIAN	1.146139	0.004119	278.249953	0.000000*	0.003936	291.183129	0.000000*	17.284751
BAND 7 MEDIAN	-1.733110	0.007779	-222.794440	0.000000*	0.005550	-312.261870	0.000000*	7.557318

OLS Diagnostics

Input Features:	FirstOLScomplete	Dependent Variable:	CO_1112
Number of Observations:	1007	Akaike's Information Criterion (AICc) [d]:	-3253.954155
Multiple R-Squared [d]:	0.991795	Adjusted R-Squared [d]:	0.991763
Joint F-Statistic [e]:	30281.069142	Prob(>F), (4,1002) degrees of freedom:	0.000000*
Joint Wald Statistic [e]:	856439.335048	Prob(>chi-squared), (4) degrees of freedom:	0.000000*
	6.013712	Prob(>chi-squared), (4) degrees of freedom:	0.198127
Jarque-Bera Statistic [g]:	2750036.750038	Prob(>chi-squared), (2) degrees of freedom:	0.000000*

NO_2 2007-2008

Summary of OLS Results - Model Variables

Variable	Coefficient [a]	StdError	t-Statistic	Probability [b]	Robust_SE	Robust_t	Robust_Pr [b]	VIF [c]
Intercept	47.133873	0.567506	83.054453	0.000000*	0.701840	67.157609	0.000000*	--------
BAND 2 MEDIAN	-11.136043	0.033030	-337.149947	0.000000*	0.040835	-272.709264	0.000000*	13.690279
BAND 5 MEDIAN	17.529102	0.048417	362.046816	0.000000*	0.023857	734.756452	0.000000*	8.898559
BAND 6 MEDIAN	12.079973	0.187960	64.268767	0.000000*	0.176557	68.419761	0.000000*	21.123676
BAND 7 MEDIAN	-6.230845	0.347422	-17.934522	0.000000*	0.252345	-24.691771	0.000000*	8.011578

OLS Diagnostics

Input Features:	FirstOLScomplete	Dependent Variable:	NO2_0708
Number of Observations:	1039	Akaike's Information Criterion (AICc) [d]:	4645.204782
Multiple R-Squared [d]:	0.993428	Adjusted R-Squared [d]:	0.993403
Joint F-Statistic [e]:	39076.334672	Prob(>F), (4,1034) degrees of freedom:	0.000000*
Joint Wald Statistic [e]:	856878.966544	Prob(>chi-squared), (4) degrees of freedom:	0.000000*
Koenker (BP) Statistic [f]:	1.430669	Prob(>chi-squared), (4) degrees of freedom:	0.838847
Jarque-Bera Statistic [g]:	2644421.583106	Prob(>chi-squared), (2) degrees of freedom:	0.000000*

NO_2 2009-2010

Summary of OLS Results - Model Variables

Variable	Coefficient [a]	StdError	t-Statistic	Probability [b]	Robust_SE	Robust_t	Robust_Pr [b]	VIF [c]
Intercept	53.836978	0.817531	65.853132	0.000000*	1.010279	53.289207	0.000000*	--------
BAND 2 MEDIAN	3.591726	0.046683	76.938613	0.000000*	0.041139	87.307973	0.000000*	12.373371
BAND 5 MEDIAN	-3.511324	0.050456	-69.592184	0.000000*	0.019940	-176.093873	0.000000*	4.847111
BAND 6 MEDIAN	-29.212109	0.300988	-97.053963	0.000000*	0.115810	-252.241129	0.000000*	38.847518
BAND 7 MEDIAN	64.961279	0.609139	106.644469	0.000000*	0.202562	320.698148	0.000000*	20.031149

OLS Diagnostics

Input Features:	FirstOLScomplete	Dependent Variable:	NO2_0910
Number of Observations:	872	Akaike's Information Criterion (AICc) [d]:	4133.195782
Multiple R-Squared [d]:	0.948038	Adjusted R-Squared [d]:	0.947798
Joint F-Statistic [e]:	3954.573516	Prob(>F), (4,867) degrees of freedom:	0.000000*
Joint Wald Statistic [e]:	166898.054929	Prob(>chi-squared), (4) degrees of freedom:	0.000000*
Koenker (BP) Statistic [f]:	4.751039	Prob(>chi-squared), (4) degrees of freedom:	0.313809
Jarque-Bera Statistic [g]:	6709354.868513	Prob(>chi-squared), (2) degrees of freedom:	0.000000*

NO_2 2011-2012

Summary of OLS Results - Model Variables

Variable	Coefficient [a]	StdError	t-Statistic	Probability [b]	Robust_SE	Robust_t	Robust_Pr [b]	VIF [c]
Intercept	78.426079	0.931435	84.199188	0.000000*	0.374427	209.456061	0.000000*	--------
BAND 2 MEDIAN	-13.675611	0.054659	-250.198807	0.000000*	0.057421	-238.162901	0.000000*	12.632120
BAND 5 MEDIAN	5.306486	0.054397	97.550853	0.000000*	0.031569	168.093083	0.000000*	4.051588
BAND 6 MEDIAN	74.513699	0.291554	255.573954	0.000000*	0.341661	218.092794	0.000000*	22.187173
BAND 7 MEDIAN	-100.940784	0.504599	-200.041755	0.000000*	0.423923	-238.111077	0.000000*	7.857881

OLS Diagnostics

Input Features:	FirstOLScomplete	Dependent Variable:	NO2_1112
Number of Observations:	807	Akaike's Information Criterion (AICc) [d]:	3887.006745
Multiple R-Squared [d]:	0.989287	Adjusted R-Squared [d]:	0.989233
Joint F-Statistic [e]:	18514.764337	Prob(>F), (4,802) degrees of freedom:	0.000000*
Joint Wald Statistic [e]:	248369.132724	Prob(>chi-squared), (4) degrees of freedom:	0.000000*
Koenker (BP) Statistic [f]:	3.644606	Prob(>chi-squared), (4) degrees of freedom:	0.456234
Jarque-Bera Statistic [g]:	1974194.502590	Prob(>chi-squared), (2) degrees of freedom:	0.000000*

SO_2 2007-2008

Summary of OLS Results - Model Variables

Variable	Coefficient [a]	StdError	t-Statistic	Probability [b]	Robust_SE	Robust_t	Robust_Pr [b]	VIF [c]
Intercept	38.648330	0.336422	114.880455	0.000000*	0.212727	181.680300	0.000000*	--------
BAND 2 MEDIAN	1.494282	0.020454	73.055340	0.000000*	0.028883	51.734993	0.000000*	16.755611
BAND 5 MEDIAN	2.173242	0.023897	90.941126	0.000000*	0.016275	133.529056	0.000000*	6.904330
BAND 6 MEDIAN	-27.259440	0.190041	-143.439919	0.000000*	0.297802	-91.535467	0.000000*	58.710777
BAND 7 MEDIAN	45.710658	0.349265	130.876898	0.000000*	0.493809	92.567461	0.000000*	26.060730

OLS Diagnostics

Input Features:	FirstOLScomplete	Dependent Variable:	SO2_0708
Number of Observations:	758	Akaike's Information Criterion (AICc) [d]:	2301.877238
Multiple R-Squared [d]:	0.972057	Adjusted R-Squared [d]:	0.971908
Joint F-Statistic [e]:	6548.640038	Prob(>F), (4,753) degrees of freedom:	0.000000*
Joint Wald Statistic [e]:	55597.747127	Prob(>chi-squared), (4) degrees of freedom:	0.000000*
Koenker (BP) Statistic [f]:	8.319693	Prob(>chi-squared), (4) degrees of freedom:	0.080545
Jarque-Bera Statistic [g]:	822075.444150	Prob(>chi-squared), (2) degrees of freedom:	0.000000*

SO_2 2009-2010

Summary of OLS Results - Model Variables

Variable	Coefficient [a]	StdError	t-Statistic	Probability [b]	Robust_SE	Robust_t	Robust_Pr [b]	VIF [c]
Intercept	-29.207665	0.168331	-173.513667	0.000000*	0.196662	-148.516744	0.000000*	--------
BAND 2 MEDIAN	-0.263247	0.006114	-43.053645	0.000000*	0.003294	-79.908834	0.000000*	5.125139
BAND 5 MEDIAN	-0.635737	0.007984	-79.629655	0.000000*	0.004504	-141.139759	0.000000*	3.405652
BAND 6 MEDIAN	16.538871	0.033196	498.217208	0.000000*	0.016482	1003.426600	0.000000*	12.500588
BAND 7 MEDIAN	-37.922041	0.066515	-570.125312	0.000000*	0.059156	-641.050544	0.000000*	6.303216

OLS Diagnostics

Input Features:	FirstOLScomplete	Dependent Variable:	SO2_0910
Number of Observations:	1177	Akaike's Information Criterion (AICc) [d]:	1947.140683
Multiple R-Squared [d]:	0.997342	Adjusted R-Squared [d]:	0.997332
Joint F-Statistic [e]:	109921.464779	Prob(>F), (4,1172) degrees of freedom:	0.000000*
Joint Wald Statistic [e]:	1411334.156231	Prob(>chi-squared), (4) degrees of freedom:	0.000000*
Koenker (BP) Statistic [f]:	6.113345	Prob(>chi-squared), (4) degrees of freedom:	0.190842
Jarque-Bera Statistic [g]:	2681569.427759	Prob(>chi-squared), (2) degrees of freedom:	0.000000*

SO_2 2011-2012

Summary of OLS Results - Model Variables

Variable	Coefficient [a]	StdError	t-Statistic	Probability [b]	Robust_SE	Robust_t	Robust_Pr [b]	VIF [c]
Intercept	-7.136211	0.053721	-132.837439	0.000000*	0.097867	-72.917218	0.000000*	--------
BAND 2 MEDIAN	0.714232	0.000900	793.590683	0.000000*	0.000649	1100.497683	0.000000*	1.605350
BAND 5 MEDIAN	-1.134528	0.003038	-373.441033	0.000000*	0.001360	-834.194583	0.000000*	3.491382
BAND 6 MEDIAN	1.138016	0.011678	97.445527	0.000000*	0.006533	174.201644	0.000000*	11.962760
BAND 7 MEDIAN	-2.957344	0.027209	-108.691555	0.000000*	0.015725	-188.066236	0.000000*	7.967997

OLS Diagnostics

Input Features:	FirstOLScomplete	Dependent Variable:	SO2_1112
Number of Observations:	1166	Akaike's Information Criterion (AICc) [d]:	-349.749001
Multiple R-Squared [d]:	0.998420	Adjusted R-Squared [d]:	0.998414
Joint F-Statistic [e]:	183373.332877	Prob(>F), (4,1161) degrees of freedom:	0.000000*
Joint Wald Statistic [e]:	34344483.424754	Prob(>chi-squared), (4) degrees of freedom:	0.000000*
Koenker (BP) Statistic [f]:	8.444326	Prob(>chi-squared), (4) degrees of freedom:	0.076593
Jarque-Bera Statistic [g]:	7392921.333121	Prob(>chi-squared), (2) degrees of freedom:	0.000000*

PM_{10} 2007-2008

Summary of OLS Results - Model Variables

Variable	Coefficient [a]	StdError	t-Statistic	Probability [b]	Robust_SE	Robust_t	Robust_Pr [b]	VIF [c]
Intercept	-35.134234	0.408766	-85.951875	0.000000*	0.749592	-46.871147	0.000000*	--------
BAND 2 MEDIAN	9.461163	0.024298	389.376994	0.000000*	0.031646	298.965075	0.000000*	16.118147
BAND 5 MEDIAN	-4.691377	0.023285	-201.477727	0.000000*	0.003929	-1193.958587	0.000000*	4.170752
BAND 6 MEDIAN	-67.932053	0.185987	-365.251682	0.000000*	0.297250	-228.534735	0.000000*	39.824856
BAND 7 MEDIAN	142.129767	0.369181	384.986766	0.000000*	0.740665	191.894761	0.000000*	17.536558

OLS Diagnostics

Input Features:	FirstOLScomplete	Dependent Variable:	PM10_0708
Number of Observations:	951	Akaike's Information Criterion (AICc) [d]:	3384.498412
Multiple R-Squared [d]:	0.994698	Adjusted R-Squared [d]:	0.994676
Joint F-Statistic [e]:	44372.895164	Prob(>F), (4,946) degrees of freedom:	0.000000*
Joint Wald Statistic [e]:	2055399.875004	Prob(>chi-squared), (4) degrees of freedom:	0.000000*
Koenker (BP) Statistic [f]:	9.586530	Prob(>chi-squared), (4) degrees of freedom:	0.047999*
Jarque-Bera Statistic [g]:	14433249.837092	Prob(>chi-squared), (2) degrees of freedom:	0.000000*

PM_{10} 2009-2010

Summary of OLS Results - Model Variables

Variable	Coefficient [a]	StdError	t-Statistic	Probability [b]	Robust_SE	Robust_t	Robust_Pr [b]	VIF [c]
Intercept	15.028505	0.072213	208.114886	0.000000*	0.030239	496.989064	0.000000*	--------
BAND 2 MEDIAN	6.702548	0.003717	1803.273025	0.000000*	0.000896	7480.577048	0.000000*	10.730202
BAND 5 MEDIAN	-6.703279	0.004299	-1559.165603	0.000000*	0.000967	-6930.127634	0.000000*	4.955527
BAND 6 MEDIAN	-29.355439	0.019985	-1468.855453	0.000000*	0.011324	-2592.331329	0.000000*	23.802608
BAND 7 MEDIAN	55.140650	0.038142	1445.649323	0.000000*	0.018765	2938.512967	0.000000*	10.722876

OLS Diagnostics

Input Features:	FirstOLScomplete	Dependent Variable:	PM10_0910
Number of Observations:	1043	Akaike's Information Criterion (AICc) [d]:	-1.481949
Multiple R-Squared [d]:	0.999771	Adjusted R-Squared [d]:	0.999770
Joint F-Statistic [e]:	1131664.734919	Prob(>F), (4,1038) degrees of freedom:	0.000000*
Joint Wald Statistic [e]:	1413996343.188991	Prob(>chi-squared), (4) degrees of freedom:	0.000000*
Koenker (BP) Statistic [f]:	0.695868	Prob(>chi-squared), (4) degrees of freedom:	0.951838
Jarque-Bera Statistic [g]:	29693499.234285	Prob(>chi-squared), (2) degrees of freedom:	0.000000*

PM_{10} 2011-2012

Summary of OLS Results - Model Variables

Variable	Coefficient [a]	StdError	t-Statistic	Probability [b]	Robust_SE	Robust_t	Robust_Pr [b]	VIF [c]
Intercept	27.168691	0.357496	75.997096	0.000000*	0.160772	168.989115	0.000000*	--------
BAND 2 MEDIAN	-9.198371	0.017528	-524.784698	0.000000*	0.005313	-1731.198415	0.000000*	8.816075
BAND 5 MEDIAN	1.149739	0.019954	57.619470	0.000000*	0.016040	71.678719	0.000000*	3.767142
BAND 6 MEDIAN	67.943343	0.103726	655.027262	0.000000*	0.102868	660.490012	0.000000*	17.636572
BAND 7 MEDIAN	-97.427604	0.193545	-503.384606	0.000000*	0.189007	-515.471220	0.000000*	7.434594

OLS Diagnostics

Input Features:	FirstOLScomplete	Dependent Variable:	PM10_1112
Number of Observations:	1026	Akaike's Information Criterion (AICc) [d]:	3282.183468
Multiple R-Squared [d]:	0.997879	Adjusted R-Squared [d]:	0.997870
Joint F-Statistic [e]:	120063.542706	Prob(>F), (4,1021) degrees of freedom:	0.000000*
Joint Wald Statistic [e]:	51046428.630493	Prob(>chi-squared), (4) degrees of freedom:	0.000000*
Koenker (BP) Statistic [f]:	1.743949	Prob(>chi-squared), (4) degrees of freedom:	0.782720
Jarque-Bera Statistic [g]:	34588799.954131	Prob(>chi-squared), (2) degrees of freedom:	0.000000*

Appendix C: Descriptive segmentation of Attica (GAA)

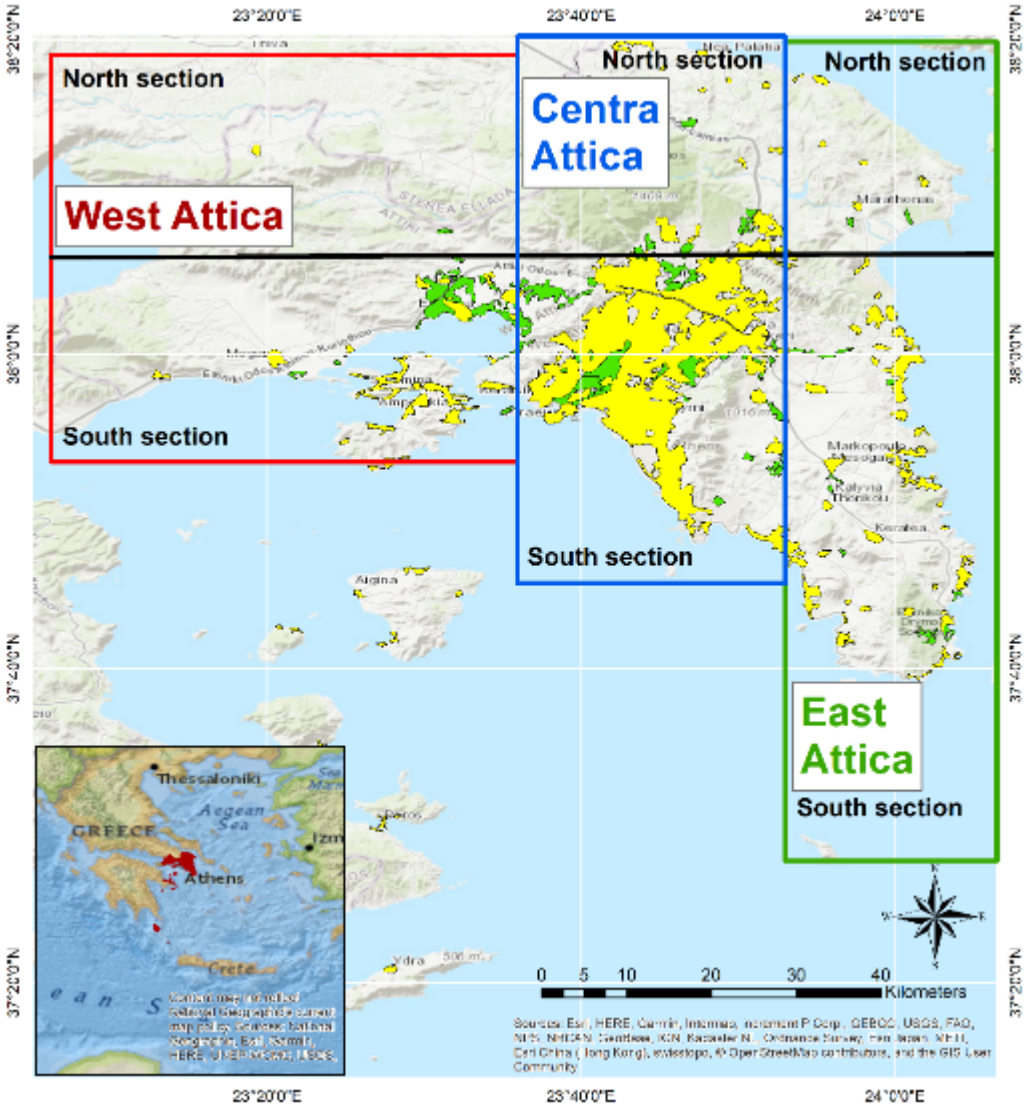

Appendix D: Land Cover map of GAA according to CORINE 2000

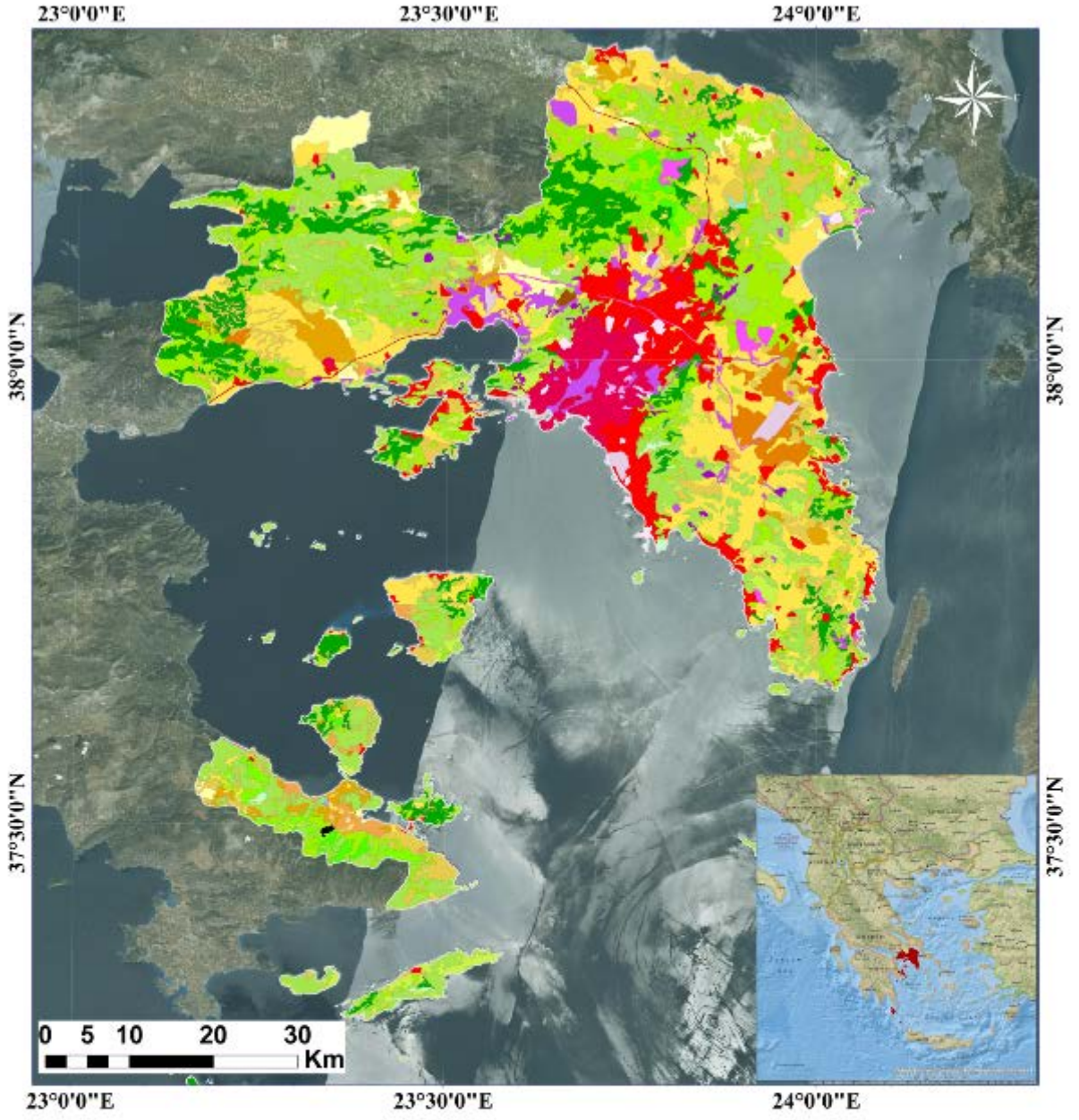

Legend

- GAA
- Continuous Urban Fabric
- Discontinuous Urban Fabric
- Industrial or Commercial Units
- Road and Rail Networks and Associated lands
- Port Areas
- Airports
- Mineral Extraction sites
- Dump sites
- Construction sites
- Green Urban areas
- Sport and Leisure facilities
- Non-irrigated Arable land
- Vineyards
- Fruit trees and berry plantations
- Olive groves
- Pastures
- Annual crops associated with permanent crops
- Complex cultivation patterns
- Land principally occupied by agriculture, with significant areas of natural vegetation
- Broad-leaved forest
- Coniferous forest
- Mixed forest
- Natural grasslands
- Sclerophyllous vegetation
- Transitional woodland-shrub
- Beaches, dunes, sands
- Bare rocks
- Sparsely vegetated areas
- Burnt areas
- Inland marshes
- Salt marshes
- Salines
- Water bodies

Series from Lund University

Department of Physical Geography and Ecosystem Science

Master Thesis in Geographical Information Science

1. *Anthony Lawther:* The application of GIS-based binary logistic regression for slope failure susceptibility mapping in the Western Grampian Mountains, Scotland (2008).

2. *Rickard Hansen:* Daily mobility in Grenoble Metropolitan Region, France. Applied GIS methods in time geographical research (2008).

3. *Emil Bayramov:* Environmental monitoring of bio-restoration activities using GIS and Remote Sensing (2009).

4. *Rafael Villarreal Pacheco:* Applications of Geographic Information Systems as an analytical and visualization tool for mass real estate valuation: a case study of Fontibon District, Bogota, Columbia (2009).

5. *Siri Oestreich Waage:* a case study of route solving for oversized transport: The use of GIS functionalities in transport of transformers, as part of maintaining a reliable power infrastructure (2010).

6. *Edgar Pimiento:* Shallow landslide susceptibility – Modelling and validation (2010).

7. *Martina Schäfer:* Near real-time mapping of floodwater mosquito breeding sites using aerial photographs (2010).

8. *August Pieter van Waarden-Nagel:* Land use evaluation to assess the outcome of the programme of rehabilitation measures for the river Rhine in the Netherlands (2010).

9. *Samira Muhammad:* Development and implementation of air quality data mart for Ontario, Canada: A case study of air quality in Ontario using OLAP tool. (2010).

10. *Fredros Oketch Okumu*: Using remotely sensed data to explore spatial and temporal relationships between photosynthetic productivity of vegetation and malaria transmission intensities in selected parts of Africa (2011).

11. *Svajunas Plunge:* Advanced decision support methods for solving diffuse water pollution problems (2011).

12. *Jonathan Higgins:* Monitoring urban growth in greater Lagos: A case study using GIS to monitor the urban growth of Lagos 1990 - 2008 and produce future growth prospects for the city (2011).

13. *Mårten Karlberg:* Mobile Map Client API: Design and Implementation for Android (2011).

14. *Jeanette McBride:* Mapping Chicago area urban tree canopy using color infrared imagery (2011).

15. *Andrew Farina:* Exploring the relationship between land surface temperature and vegetation abundance for urban heat island mitigation in Seville, Spain (2011).

16. *David Kanyari*: Nairobi City Journey Planner: An online and a Mobile Application (2011).

17. *Laura V. Drews:* Multi-criteria GIS analysis for siting of small wind power plants - A case study from Berlin (2012).

18. *Qaisar Nadeem:* Best living neighborhood in the city - A GIS based multi criteria evaluation of ArRiyadh City (2012).

19. *Ahmed Mohamed El Saeid Mustafa:* Development of a photo voltaic building rooftop integration analysis tool for GIS for Dokki District, Cairo, Egypt (2012).

20. *Daniel Patrick Taylor*: Eastern Oyster Aquaculture: Estuarine Remediation via Site Suitability and Spatially Explicit Carrying Capacity Modeling in Virginia's Chesapeake Bay (2013).

21. *Angeleta Oveta Wilson:* A Participatory GIS approach to *unearthing* Manchester's Cultural Heritage '*gold mine'* (2013).

22. *Ola Svensson:* Visibility and Tholos Tombs in the Messenian Landscape: A Comparative Case Study of the Pylian Hinterlands and the Soulima Valley (2013).

23. *Monika Ogden:* Land use impact on water quality in two river systems in South Africa (2013).

24. *Stefan Rova:* A GIS based approach assessing phosphorus load impact on Lake Flaten in Salem, Sweden (2013).

25. *Yann Buhot:* Analysis of the history of landscape changes over a period of 200 years. How can we predict past landscape pattern scenario and the impact on habitat diversity? (2013).

26. *Christina Fotiou:* Evaluating habitat suitability and spectral heterogeneity models to predict weed species presence (2014).

27. *Inese Linuza:* Accuracy Assessment in Glacier Change Analysis (2014).

28. *Agnieszka Griffin:* Domestic energy consumption and social living standards: a GIS analysis within the Greater London Authority area (2014).

29. *Brynja Guðmundsdóttir:* Detection of potential arable land with remote sensing and GIS - A Case Study for Kjósarhreppur (2014).

30. *Oleksandr Nekrasov:* Processing of MODIS Vegetation Indices for analysis of agricultural droughts in the southern Ukraine between the years 2000-2012 (2014).

31. *Sarah Tressel:* Recommendations for a polar Earth science portal in the context of Arctic Spatial Data Infrastructure (2014).

32. *Caroline Gevaert:* Combining Hyperspectral UAV and Multispectral Formosat-2 Imagery for Precision Agriculture Applications (2014).

33. *Salem Jamal-Uddeen:* Using GeoTools to implement the multi-criteria evaluation analysis - weighted linear combination model (2014).

34. *Samanah Seyedi-Shandiz:* Schematic representation of geographical railway network at the Swedish Transport Administration (2014).

35. *Kazi Masel Ullah:* Urban Land-use planning using Geographical Information System and analytical hierarchy process: case study Dhaka City (2014).

36. *Alexia Chang-Wailing Spitteler:* Development of a web application based on MCDA and GIS for the decision support of river and floodplain rehabilitation projects (2014).

37. *Alessandro De Martino:* Geographic accessibility analysis and evaluation of potential changes to the public transportation system in the City of Milan (2014).

38. *Alireza Mollasalehi:* GIS Based Modelling for Fuel Reduction Using Controlled Burn in Australia. Case Study: Logan City, QLD (2015).

39. *Negin A. Sanati:* Chronic Kidney Disease Mortality in Costa Rica; Geographical Distribution, Spatial Analysis and Non-traditional Risk Factors (2015).

40. *Karen McIntyre:* Benthic mapping of the Bluefields Bay fish sanctuary, Jamaica (2015).

41. *Kees van Duijvendijk:* Feasibility of a low-cost weather sensor network for agricultural purposes: A preliminary assessment (2015).

42. *Sebastian Andersson Hylander:* Evaluation of cultural ecosystem services using GIS (2015).

43. *Deborah Bowyer:* Measuring Urban Growth, Urban Form and Accessibility as Indicators of Urban Sprawl in Hamilton, New Zealand (2015).

44. *Stefan Arvidsson:* Relationship between tree species composition and phenology extracted from satellite data in Swedish forests (2015).

45. *Damián Giménez Cruz*: GIS-based optimal localisation of beekeeping in rural Kenya (2016).

46. *Alejandra Narváez Vallejo:* Can the introduction of the topographic indices in LPJ-GUESS improve the spatial representation of environmental variables? (2016).

47. *Anna Lundgren:* Development of a method for mapping the highest coastline in Sweden using breaklines extracted from high resolution digital elevation models (2016).

48. *Oluwatomi Esther Adejoro:* Does location also matter? A spatial analysis of social achievements of young South Australians (2016).

49. *Hristo Dobrev Tomov:* Automated temporal NDVI analysis over the Middle East for the period 1982 - 2010 (2016).

50. *Vincent Muller:* Impact of Security Context on Mobile Clinic Activities A GIS Multi Criteria Evaluation based on an MSF Humanitarian Mission in Cameroon (2016).

51. *Gezahagn Negash Seboka:* Spatial Assessment of NDVI as an Indicator of Desertification in Ethiopia using Remote Sensing and GIS (2016).

52. *Holly Buhler:* Evaluation of Interfacility Medical Transport Journey Times in Southeastern British Columbia. (2016).

53. *Lars Ole Grottenberg*: Assessing the ability to share spatial data between emergency management organisations in the High North (2016).

54. *Sean Grant:* The Right Tree in the Right Place: Using GIS to Maximize the Net Benefits from Urban Forests (2016).

55. *Irshad Jamal:* Multi-Criteria GIS Analysis for School Site Selection in Gorno-Badakhshan Autonomous Oblast, Tajikistan (2016).

56. *Fulgencio Sanmartín:* Wisdom-volkano: A novel tool based on open GIS and time-series visualization to analyse and share volcanic data (2016).

57. *Nezha Acil:* Remote sensing-based monitoring of snow cover dynamics and its influence on vegetation growth in the Middle Atlas Mountains (2016).

58. *Julia Hjalmarsson:* A Weighty Issue: Estimation of Fire Size with Geographically Weighted Logistic Regression (2016).

59. *Mathewos Tamiru Amato:* Using multi-criteria evaluation and GIS for chronic food and nutrition insecurity indicators analysis in Ethiopia (2016).

60. *Karim Alaa El Din Mohamed Soliman El Attar:* Bicycling Suitability in Downtown, Cairo, Egypt (2016).

61. *Gilbert Akol Echelai:* Asset Management: Integrating GIS as a Decision Support Tool in Meter Management in National Water and Sewerage Corporation (2016).

62. *Terje Slinning:* Analytic comparison of multibeam echo soundings (2016).

63. *Gréta Hlín Sveinsdóttir:* GIS-based MCDA for decision support: A framework for wind farm siting in Iceland (2017).

64. *Jonas Sjögren:* Consequences of a flood in Kristianstad, Sweden: A GIS-based analysis of impacts on important societal functions (2017).

65. *Nadine Raska:* 3D geologic subsurface modelling within the Mackenzie Plain, Northwest Territories, Canada (2017).

66. *Panagiotis Symeonidis*: Study of spatial and temporal variation of atmospheric optical parameters and their relation with PM 2.5 concentration over Europe using GIS technologies (2017).

67. *Michaela Bobeck:* A GIS-based Multi-Criteria Decision Analysis of Wind Farm Site Suitability in New South Wales, Australia, from a Sustainable Development Perspective (2017).

68. *Raghdaa Eissa*: Developing a GIS Model for the Assessment of Outdoor Recreational Facilities in New Cities Case Study: Tenth of Ramadan City, Egypt (2017).

69. *Zahra Khais Shahid*: Biofuel plantations and isoprene emissions in Svea and Götaland (2017).

70. *Mirza Amir Liaquat Baig*: Using geographical information systems in epidemiology: Mapping and analyzing occurrence of diarrhea in urban - residential area of Islamabad, Pakistan (2017).

71. *Joakim Jörwall*: Quantitative model of Present and Future well-being in the EU-28: A spatial Multi-Criteria Evaluation of socioeconomic and climatic comfort factors (2017).

72. *Elin Haettner*: Energy Poverty in the Dublin Region: Modelling Geographies of Risk (2017).

73. *Harry Eriksson*: Geochemistry of stream plants and its statistical relations to soil- and bedrock geology, slope directions and till geochemistry. A GIS-analysis of small catchments in northern Sweden (2017).

74. *Daniel Gardevärn:* PPGIS and Public meetings – An evaluation of public participation methods for urban planning (2017).

75. *Kim Friberg:* Sensitivity Analysis and Calibration of Multi Energy Balance Land Surface Model Parameters (2017).

76. *Viktor Svanerud:* Taking the bus to the park? A study of accessibility to green areas in Gothenburg through different modes of transport (2017).

77. *Lisa-Gaye Greene*: Deadly Designs: The Impact of Road Design on Road Crash Patterns along Jamaica's North Coast Highway (2017).

78. *Katarina Jemec Parker*: Spatial and temporal analysis of fecal indicator bacteria concentrations in beach water in San Diego, California (2017).

79. *Angela Kabiru*: An Exploratory Study of Middle Stone Age and Later Stone Age Site Locations in Kenya's Central Rift Valley Using Landscape Analysis: A GIS Approach (2017).

80. *Kristean Björkmann*: Subjective Well-Being and Environment: A GIS-Based Analysis (2018).

81. *Williams Erhunmonmen Ojo*: Measuring spatial accessibility to healthcare for people living with HIV-AIDS in southern Nigeria (2018).

82. *Daniel Assefa*: Developing Data Extraction and Dynamic Data Visualization (Styling) Modules for Web GIS Risk Assessment System (WGRAS). (2018).

83. *Adela Nistora*: Inundation scenarios in a changing climate: assessing potential impacts of sea-level rise on the coast of South-East England (2018).

84. *Marc Seliger*: Thirsty landscapes - Investigating growing irrigation water consumption and potential conservation measures within Utah's largest master-planned community: Daybreak (2018).

85. *Luka Jovičić*: Spatial Data Harmonisation in Regional Context in Accordance with INSPIRE Implementing Rules (2018).

86. *Christina Kourdounouli*: Analysis of Urban Ecosystem Condition Indicators for the Large Urban Zones and City Cores in EU (2018).

87. *Jeremy Azzopardi*: Effect of distance measures and feature representations on distance-based accessibility measures (2018).

88. *Patrick Kabatha*: An open source web GIS tool for analysis and visualization of elephant GPS telemetry data, alongside environmental and anthropogenic variables (2018).

89. *Richard Alphonce Giliba*: Effects of Climate Change on Potential Geographical Distribution of Prunus africana (African cherry) in the Eastern Arc Mountain Forests of Tanzania (2018).

90. *Eiður Kristinn Eiðsson*: Transformation and linking of authoritative multi-scale geodata for the Semantic Web: A case study of Swedish national building data sets (2018).

91. *Niamh Harty*: HOP!: a PGIS and citizen science approach to monitoring the condition of upland paths (2018).

92. *José Estuardo Jara Alvear*: Solar photovoltaic potential to complement hydropower in Ecuador: A GIS-based framework of analysis (2018).

93. *Brendan O'Neill*: Multicriteria Site Suitability for Algal Biofuel Production Facilities (2018).

94. *Roman Spataru*: Spatial-temporal GIS analysis in public health – a case study of polio disease (2018).

95. *Alicja Miodońska*: Assessing evolution of ice caps in Suðurland, Iceland, in years 1986 - 2014, using multispectral satellite imagery (2019).

96. *Dennis Lindell Schettini*: A Spatial Analysis of Homicide Crime's Distribution and Association with Deprivation in Stockholm Between 2010-2017 (2019).

97. *Damiano Vesentini*: The Po Delta Biosphere Reserve: Management challenges and priorities deriving from anthropogenic pressure and sea level rise (2019).

98. *Emilie Arnesten*: Impacts of future sea level rise and high water on roads, railways and environmental objects: a GIS analysis of the potential effects of increasing sea levels and highest projected high water in Scania, Sweden (2019).

99. *Syed Muhammad Amir Raza*: Comparison of geospatial support in RDF stores: Evaluation for ICOS Carbon Portal metadata (2019).

100. *Hemin Tofiq*: Investigating the accuracy of Digital Elevation Models from UAV images in areas with low contrast: A sandy beach as a case study (2019).

101. *Evangelos Vafeiadis*: Exploring the distribution of accessibility by public transport using spatial analysis. A case study for retail concentrations and public hospitals in Athens (2019).

102. *Milan Sekulic*: Multi-Criteria GIS modelling for optimal alignment of roadway by-passes in the Tlokweng Planning Area, Botswana (2019).

103. *Ingrid Piirisaar*: A multi-criteria GIS analysis for siting of utility-scale photovoltaic solar plants in county Kilkenny, Ireland (2019).

104. *Nigel Fox*: Plant phenology and climate change: possible effect on the onset of various wild plant species' first flowering day in the UK (2019).

105. *Gunnar Hesch*: Linking conflict events and cropland development in Afghanistan, 2001 to 2011, using MODIS land cover data and Uppsala Conflict Data Programme (2019).

106. *Elijah Njoku*: Analysis of spatial-temporal pattern of Land Surface Temperature (LST) due to NDVI and elevation in Ilorin, Nigeria (2019).

107. *Katalin Bunyevácz*: Development of a GIS methodology to evaluate informal urban green areas for inclusion in a community governance program (2019).

108. *Paul dos Santos*: Automating synthetic trip data generation for an agent-based simulation of urban mobility (2019).

109. *Robert O' Dwyer*: Land cover changes in Southern Sweden from the mid-Holocene to present day: Insights for ecosystem service assessments (2019).

110. *Daniel Klingmyr*: Global scale patterns and trends in tropospheric NO2 concentrations (2019).

111. *Marwa Farouk Elkabbany*: Sea Level Rise Vulnerability Assessment for Abu Dhabi, United Arab Emirates (2019).

112. *Jip Jan van Zoonen*: Aspects of Error Quantification and Evaluation in Digital Elevation Models for Glacier Surfaces (2020).

113. *Georgios Efthymiou*: The use of bicycles in a mid-sized city – benefits and obstacles identified using a questionnaire and GIS (2020).

114. *Haruna Olayiwola Jimoh*: Assessment of Urban Sprawl in MOWE/IBAFO Axis of Ogun State using GIS Capabilities (2020).

115. *Nikolaos Barmpas Zachariadis*: Development of an iOS, Augmented Reality for disaster management (2020).

116. *Ida Storm*: ICOS Atmospheric Stations: Spatial Characterization of CO2 Footprint Areas and Evaluating the Uncertainties of Modelled CO2 Concentrations (2020).

117. *Alon Zuta*: Evaluation of water stress mapping methods in vineyards using airborne thermal imaging (2020).

118. *Marcus Eriksson*: Evaluating structural landscape development in the municipality Upplands-Bro, using landscape metrics indices (2020).

119. *Ane Rahbek Vierø*: Connectivity for Cyclists? A Network Analysis of Copenhagen's Bike Lanes (2020).

120. *Cecilia Baggini*: Changes in habitat suitability for three declining Anatidae species in saltmarshes on the Mersey estuary, North-West England (2020).

121. *Bakrad Balabanian*: Transportation and Its Effect on Student Performance (2020).

122. *Ali Al Farid*: Knowledge and Data Driven Approaches for Hydrocarbon Microseepage Characterizations: An Application of Satellite Remote Sensing (2020).

123. *Bartlomiej Kolodziejczyk*: Distribution Modelling of Gene Drive-Modified Mosquitoes and Their Effects on Wild Populations (2020).

124. *Alexis Cazorla*: Decreasing organic nitrogen concentrations in European water bodies - links to organic carbon trends and land cover (2020).

125. *Kharid Mwakoba*: Remote sensing analysis of land cover/use conditions of community-based wildlife conservation areas in Tanzania (2021).

126. *Chinatsu Endo*: Remote Sensing Based Pre-Season Yellow Rust Early Warning in Oromia, Ethiopia (2021).

127. *Berit Mohr*: Using remote sensing and land abandonment as a proxy for long-term human out-migration. A Case Study: Al-Hassakeh Governorate, Syria (2021).

128. *Kanchana Nirmali Bandaranayake*: Considering future precipitation in delineation locations for water storage systems - Case study Sri Lanka (2021).

129. *Emma Bylund*: Dynamics of net primary production and food availability in the aftermath of the 2004 and 2007 desert locust outbreaks in Niger and Yemen (2021).

130. *Shawn Pace*: Urban infrastructure inundation risk from permanent sea-level rise scenarios in London (UK), Bangkok (Thailand) and Mumbai (India): A comparative analysis (2021).

131. *Oskar Evert Johansson*: The hydrodynamic impacts of Estuarine Oyster reefs, and the application of drone technology to this study (2021).

132. *Pritam Kumarsingh*: A Case Study to develop and test GIS/SDSS methods to assess the production capacity of a Cocoa Site in Trinidad and Tobago (2021).

133. *Muhammad Imran Khan*: Property Tax Mapping and Assessment using GIS (2021).

134. *Domna Kanari*: Mining geosocial data from Flickr to explore tourism patterns: The case study of Athens (2021).

135. Mona Tykesson Klubien: Livestock-MRSA in Danish pig farms (2021).

136. *Ove Njøten*: Comparing radar satellites. Use of Sentinel-1 leads to an increase in oil spill alerts in Norwegian waters (2021).

137. *Panagiotis Patrinos*: Change of heating fuel consumption patterns produced by the economic crisis in Greece (2021).